NTNU – Trondheim
Norwegian University of
Science and Technology

Finite Control Set Model Predictive Control in Power Converters

Razieh Nejati Fard

Acknowledgement

I would also like to express my gratitude to my supervisor Prof. Lars Norum for giving me the opportunity to be involved with such an interesting subject and also for his encouragement and support through the learning process of this master thesis. Furthermore, I would like to thank Hamed Nademi (PhD. candidate) for his valuable comments and guidance during this work.

Finally, I would like to thank my loved ones; my parents and my husband for their invaluable love and support.

Razieh Nejati Fard

14th June 2013

Abstract

This study presents a detailed description of a cost function-based predictive control strategy called Finite Control Set Model Predictive Control (FCS-MPC) and its applications to the control of power electronics converters. The basic concepts, operating principles and general properties of this control technique have been explained. The analysis is performed on two different power converter topologies: traditional three-phase Voltage Source Inverter (VSI) and Modular Multilevel Converter (MMC). In order to verify its capabilities MATLAB (SIMULINK) simulations have been performed for both cases.

The design procedure of FCS-MPC is based on first, a discrete-time model of the system that is used to predict the behavior of the controlled variables for all the possible switching states of the converter and second, a cost function that should be defined according to the control requirements of the system. The switching state that minimizes the cost function will be selected to be applied to the converter at the next sampling time.

FCS-MPC is a powerful control technique that has several advantages such as high accuracy, flexibility and stability, easy implementation, simple and understandable concepts, but the most important and exclusive feature of this control strategy is the inclusion of nonlinearities and system constraints in the cost function. As a result, all the control requirements can be considered by one controller at the same time.

There are important factors, regarding FCS-MPC, that have been investigated in this study, such as:

- the effect of the cost function definition and the application of weighting factors
- the effect of discretization method and system model accuracy on the controller performance
- the effect of measurement errors on the controller robustness
- dynamic behavior of the controller and its response speed when a disturbance occurs in the system
- reference tracking capability of the controller

Contents

Chapter 1

Introduction

Model Predictive Control or MPC was first introduced in 1960s and found its industrial applications in 1970s. It has more complex calculations compared to classical linear controllers, while it provides faster controller with higher accuracy and stability. MPC was first applied to chemical process industry, where time constants are quite long to perform the required high amount of calculations. From 1980s, the idea of MPC in power electronics applications was introduced although lack of the fast processors at that time, limited its applications only to low switching frequencies. However, due to invention of fast and powerful processors such as DSP and FPGA, the power electronics industry could take the advantages of MPC strategy in practice.

While classical linear controllers try to neglect or simplify system nonlinearities, MPC is able to handle system nonlinearities and control constraints simultaneously with the main control requirements. In fact, the operating principle of Model Predictive Control strategy is based on a cost function that can contain different linear and nonlinear terms depending on the system needs; therefore, there is no need for additional controllers.

Furthermore, MPC can be applied easily in MIMO (Multiple Input Multiple Output) systems as well as SISO (Single Input Single Output) systems. Moreover, its design procedure is usually easy.

Sometimes future extensions and modifications are necessary for improving the system performance and it can be fulfilled easily by using MPC control scheme in contrast with classical linear controllers that need complete redesign.

However, an accurate system model is needed to have the MPC controller with good performance. Another disadvantage of this control strategy is its high number of calculations that should be repeated at each sampling time. Hence, it may have negative effect on the speed of controller in complicated systems.

In general, MPC uses discrete mathematical model of system to predict the system behavior in a predefined horizon of time (that is the integer multiple of the sampling time). An optimal of future actions is obtained repetitively by evaluating the predicted values and minimizing a cost function. At each sampling time, the first predicted value is the output of MPC controller which will be applied to the converter.

Based on MPC, three alternatives have been introduced in order to reduce its high amount of calculations; Generalized Predictive Control (GPC), Explicit MPC and Finite Control Set MPC (FCS-MPC). The focus of this study will be on FCS-MPC (the reader can refer to [1] to get more information regarding MPC and its alternatives in detail).

In chapter 2, the concepts of FCS-MPC, its advantages and disadvantages will be presented. The design procedure, system model discretization methods, cost function definition and the process of including system constraints with the help of weighting factors will be explained.

Chapter 3 contains the first design example of FCS-MPC for a three phase VSI that is connected to a typical load which can be either a motor or utility grid. The effect of different discretization methods, i.e. forward, backward and midpoint Euler, has also been investigated. Simulation tool is MATLAB/SIMULINK.

In chapter 4, Modular Multilevel Converter (MMC) has been introduced as a new and novel converter topology which is suitable especially for high voltage and high power applications.

In chapter 5, FCS-MPC has been designed to control MMC output currents and fulfill its specific control requirements such as keeping the capacitors voltages balanced and minimizing the circulating currents. Simulations have been done for a single phase three-level MMC connected to a simple RL load to check fundamental requirements. In the last section of this chapter, three-phase five-level MMC will be controlled by FCS-MPC control method. The robustness of the controller, its accuracy and stability have been investigated. Furthermore, by inserting separate disturbances, the dynamic response of the controller has

been verified. Finally, both conclusions and suggestions for future studies are presented in chapter 6.

Chapter 2

FCS-MPC operating principles and design procedure

Finite Control Set Model Predictive Control or FCS-MPC takes the advantage of the discrete nature of power converters to reduce the MPC calculations and processing time. As there is finite number of switching positions (states) in a converter, the prediction procedure will be limited only to these states and one should be selected due to cost function minimization process. The main elements of this control scheme are the system mathematical model and the predefined cost function.

In this chapter, the fundamental concept of FCS-MPC will be explained. In addition, the design procedure of this control scheme will be presented in general. In addition to different types of cost functions and their applications, the process of including system constraints with the help of weighting factors will be given as well.

2.1 FCS-MPC description

At the beginning, system model should be derived and discretized according to the controlled variable which can be current, voltage and/or motor speed. A cost function should also be defined according to the desired behavior of the system including controlled variables reference tracking (e.g. comparing the controlled variable with its reference value). The outstanding and exclusive feature of this control scheme is that the system constrains and nonlinearities can be included in the cost function. Therefore, all of the important patterns of system behavior from the control point of view can be simply written in a summation line called cost function.

In addition, the finite number of switching states should be found by considering the switches to have only two possible states; completely ON or completely OFF. Therefore, the short transient time of switching will be neglected.

At each sampling time, cost function results of the next time step are calculated for all of possible switching states, based on the measured values at the current state. Then, the switching state that minimizes the cost function will be selected and applied to the converter. Fig.2.1 displays the control block diagram of FCS-MPC.
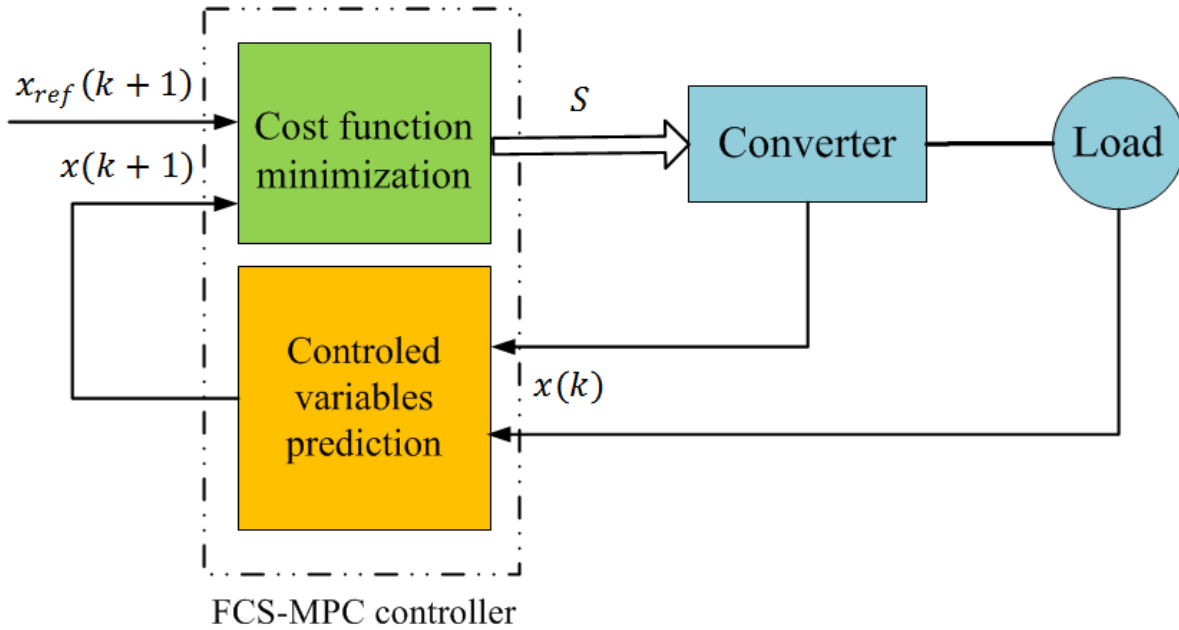

Fig. 2.1 The control block diagram of FCS-MPC

$x(.)$ is the controlled variables. Based on the discrete model of system (load and converter), the current values of the controlled variables (i.e., $x(k)$) are used to predict their future values $x(k+1)$ for all N possible switching states. All the predicted values of the controlled variables $x(k+1)$ are compared with their reference values $x_{ref}(k+1)$ in the cost function minimization block. Finally, the switching state (S) that minimizes the cost function will be selected as the next switching state and it will be applied to the converter. The procedure of switching state selection has been shown in Fig. 2.2.; $t=k$ is presenting the current state (now), $t=k+1$ and $t=k+2$ are the next time steps. The sampling time is T_s.

Assume that the FCS-MPC is applied to a converter with three possible switching states (S_1, S_2 and S_3) and the reference is constant in a short period of time. The cost function is defined as the distance between the controlled variable and its reference value that should be minimized in order to track the reference. The controlled variable at the next step time is

predicted for all the switching states, but choosing S_3 provides the least distance to the reference value x_{ref} ; as a result, it will be applied to the converter at time t_{k+1}. Subsequently, all the process will be shifted one step forward. By repeating the procedure once again for t_{k+2}, S_2 will be selected due to its minimum distance with x_{ref} . Thus, the whole procedure will be repeated again.
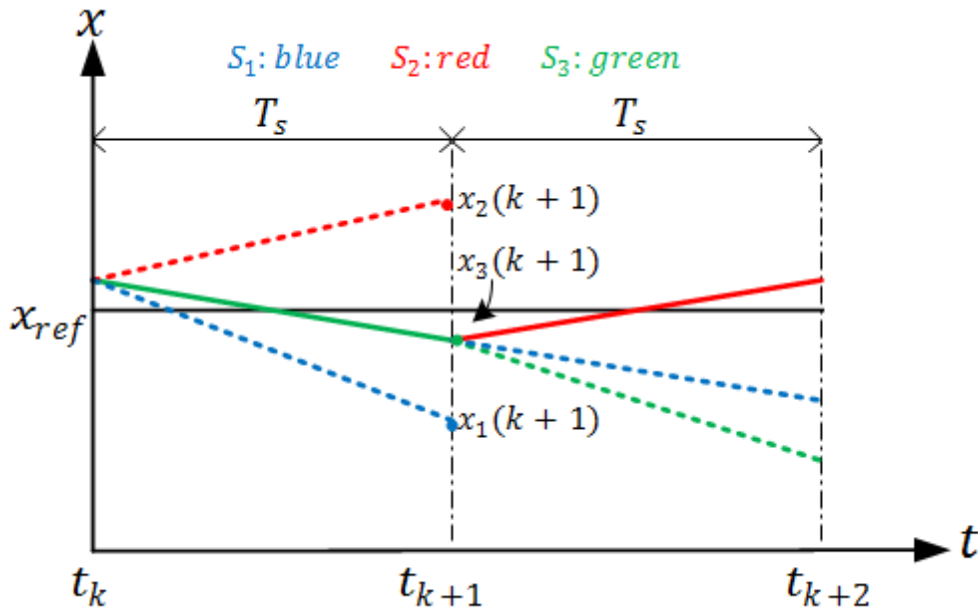

Fig 2.2: FCS-MPC operating principle

It is worth mentioning that x(k) can be measured or calculated directly by the system model and the reference current magnitude can be determined by another procedure, for example a linear PI controller. Two examples will be given in Chapter 3 and 4 in order to clarify the control strategy.

In summary, the FCS-MPC design has three main stages:

- Obtaining the discrete model of the system according to the controlled variable derivatives in order to be able to predict them in the future.

- Identifying all the possible switching states for the converter and their relation to the other variables such as voltage.

- Defining a cost function that represents the desired behavior of the system.

2.2 Mathematical model of system

In order to predict the controlled variables, the system model should be first derived and then discretized. At the first step, the discrete model of the system will be derived. A sample differential equation of a controlled variable x is:

$$\frac{dx}{dt} = f(u, x) \tag{2.1}$$

while x and u represent all controlled variables and inputs. In order to discretize Eq. 2.1, Euler methods are used due to their simplicity. They also give acceptable accuracy that is necessary for FCS-MPC good performance. According to this method, left side of Eq. 2.1 is written as:

$$\frac{dx}{dt} = \frac{x(k+1) - x(k)}{T_s} \tag{2.2}$$

where T_s is the time step or sampling time, $x(k+1)$ and $x(k)$ are the value of the controlled variable in the next sampling time and at the current state, respectively.

There are three Euler discretization methods that are different in the right-hand side of Eq. 2.2:

1. **Forward Euler method** [2]

Forward Euler method has been used in [3-5]. According to this approach, the current value of the system inputs is used to estimate the future value of controlled variables:

$$x(k+1) = x(k) + T_s f\big(x(k), u(k)\big) \tag{2.3}$$

where $u(k)$ is the current value of inputs. It has been stated in [4] that it is not accurate to use the current values f(x(k), u(k)) to estimate x(k+1). Due to microprocessor calculation time delay, the values at the beginning of sampling are not valid for the end of sampling period; therefore, it is necessary to make another step of prediction.

2. **Backward Euler method** [6]

Backward Euler method has been used in [7-13]. In this method, the future value of the system inputs is used in order to estimate the future value of the controlled variables:

$$x(k+1) = x(k) + T_s f(x(k+1), u(k+1)) \tag{2.4}$$

3. **Midpoint or Modified Euler method** [14]

In order to predict the controlled variable value in the future x(k+1), the average value of input current values f(x(k),u(k)) and future values f(x(k+1), u(k+1)) has been used:

$$x(k+1) = x(k) + \frac{T_s}{2}\left[f\big(x(k), u(k)\big) + f\big(x(k+1), u(k+1)\big)\right] \qquad (2.5)$$

Among these methods, forward Euler is the least accurate one, while it has been widely used due to its simplicity. Midpoint Euler is the most accurate and stable method although it has not been used in literature yet. This method is not more complicated than backward Euler, because the only difference between them is u(k) that is often measured and known.

In this study, the applicability of midpoint Euler method will be shown in chapter 3 and 4, while the accuracy of all Euler methods will be compared to each other chapter 3 to prove the mentioned claims.

2.3 Identifying possible switching states

At the second step of system modeling, all of the system possible switching states and their relations with input and controlled variables should be determined. Considering only two states for switches; ON or OFF, can simplify the calculation of possible switching states. As a result, the total number of switching states will be found by taking into account the configuration of converter. Some of the switching states are not permitted at all, such as those leading to dc-link short circuiting. For example, for an n-phase/m-level converter, total number of switches is $m \times n$, while it has $N = m^n$ possible switching states and for an (n+1)-level Modular Multilevel converter (MMC), it is $N = C_{2n}^{n}$. Therefore, the total possible switching states of a three-phase/two-level converter (used in chapter 3) and a 5-level MMC (used in chapter 4 and 5) are 8 and 70 respectively.

2.4 Cost function definition

Cost function is the main distinction of MPC with the other predictive control strategies. It is basically a sum function that contains different sub-functions representing the system requirements.

Cost functions contains at least one controlled variable reference tracking part that can be current, voltage, torque or speed. As the additional terms, nonlinearities and system

constraints can also be added to the cost function in order to be considered at the same time and optimize the system operation. These constraints can be, for example switching frequency minimization, switching loss minimization or defining maximum allowed current. In order to clarify the cost function structure in different cases, the main body of it will be described first and then additional system constraints will be explained.

2.4.1 Single-term cost functions

In the case of having only one controlled variable, the cost function can be expressed as:

$$J = \left\| x_{ref}(k+1) - x(k+1) \right\|$$
(2.6)

while $x_{ref}(k+1)$ is the reference value and $x(k+1)$ is the predicted value of the controlled variable calculated from the discretized system model. The norm $\|.\|$ is a measure of distance between x_{ref} and x and it can be written as an absolute value (Eq.2.7), square value (Eq.2.8), or integral value of the error between them (Eq.2.9) in one sampling period [3]:

$$J = |x^* - x^p|$$
(2.7)

$$J = (x^* - x^p)^2$$
(2.8)

$$J = \frac{1}{T_s} \int^{T_s} |x^*(t) - x^p(t)| dt$$
(2.9)

The difference between Eq.2.7 and Eq.2.8 is that the latter produces an over proportional cost in power of two making the error bigger in the case of $error > 1$ and make it smaller when $error < 1$.

- In the first case, which is often the case in power electronics, controller sensitivity increases and it can react to the changes faster; however, a faster controller will be needed and switching frequency increases [7] as negative effects.
- The controller sensitivity in the second case may be reduced and as a result, it may not track the reference value properly.

However, the absolute and squared error give similar results when a single-term cost function is used [3]; while, squared error presents a better reference following when cost function includes additional terms.

The integral form of error Eq.2.9 considers the whole predicted values during T_s, not only its value at t_{k+1}. Therefore, the mean value of the error will be minimized, leading to more accurate reference tracking although it is more complicated and also the computational time will increase. Considering fast sampling, as is usual in power converters applications, the three cost functions have almost the same effect [7].

2.4.2 Multi-term cost functions

If the main controlled variables of the system are more than one, there are two different options for cost function:

- If all of the controlled variables have the same nature or unit, for example d-axis and q-axis current of an induction motor, the resulting cost function will be the sum of their errors between their predicted value and their reference value:

$$J = |i_{refd} - i_d^p| + |i_{refq} - i_q^p| \qquad (2.10)$$

where i^p is the predicted value of current in the next sampling time. It can also be defined in the squared format of error as follows:

$$J = (i_{refd} - i_d^p)^2 + (i_{refq} - i_q^p)^2 \qquad (2.11)$$

- If the controlled variables have different natures a weighing factor λ is used to adjust their units for the controller. In fact, weighting factor is a positive constant coefficient that fixes the controlled variables importance for the controller. For instance, torque and flux can be defined as the controlled variables in an induction machine:

$$J = |T_{ref} - T^p| + \lambda|\Psi_{ref} - \Psi^p| \qquad (2.12)$$

The method of finding weighting factor λ is only empirical (i.e. try and error) that will be explained later in this chapter. Another approach for compensating the unit difference is normalizing the sub-functions (per unit values) in order to eliminate their unit effects:

$$J = \frac{(T_{ref} - T^p)^2}{T_n^2} + \frac{(\Psi_{ref} - \Psi^p)^2}{\Psi_n^2} \qquad (2.13)$$

There is usually no need for weighting factor when using the above method, while sometimes adding a weighting factor close to one ($\lambda \approx 1$) can improve the controller performance.

2.4.3 Adding system constraints to cost function

Adding system constraints is a remarkable feature of MPC. These constraints can be added simply to the cost function with their specific weighting factors that allow the level of compromise to be adjusted between all of the cost function terms. Consequently, all the control requirements will be observed by the controller simultaneously without need for additional controller which is the case when using classical controllers. However, adding additional terms to cost function reduces the influence of the main terms to some extent. An optimization should be done in order to find the best solution for control problems.

In the following sections, some of the important constraints that can be added to the cost function will be explained:

2.4.3.1 Switching frequency minimization

The amount of switch states that are changed at each sampling time will be minimized by adding a component (n) multiplied by a proper weighting factor:

$$J = (i_{refd} - i_d^p)^2 + (i_{refq} - i_q^p)^2 + \lambda.n \tag{2.14}$$

where n is the number of switches, that change their position from ON to OFF or vice versa, when a new switching state S(k+1) is applied.

If the switching vector S is defined as:

$$S = (S_1, S_2, S_3, .., S_N) \tag{2.15}$$

S_i is the state of the switch number i which can be 0 , when the switch is OFF, or 1 when it is ON. Therefore, changing state of all switches (n) can be calculated from:

$$n = \sum_{i=1}^{N} |S_i(k+1) - S_i(k)| \tag{2.16}$$

where $S_i(k+1)$ is the state of switch number i at the next sampling period and $S_i(k)$ is the state of switch i at the current state.

2.4.3.2 Voltage and current ripple minimization

It can be implemented by an additional term to the cost function as the distance between the measured value of voltage at the current state and the future state (e.g. one step time forward).

The general form of adding this constraint is:

$$J = \|x_{ref} - x^p\| + \lambda \|v(k+1) - v(k)\| \tag{2.17}$$

The same procedure should be done for the current ripple minimization case.

2.4.3.3 Defining maximum allowed current and voltage

This constraint is applied simply by adding a nonlinear term that is active only when the value of specified variables exceeds the limitations [3]. In the other words, it results zero in normal conditions and a very large value if current or voltage exceeds the defined maximum or minimum values. Therefore, the switching state causing very high cost function result will not be surely selected.

$$J = \frac{(T_{ref} - T^p)^2}{T_n^2} + \frac{(\Psi_{ref} - \Psi^p)^2}{\Psi_n^2} + f_{lim}(i^p) \tag{2.18}$$

where i is the current that should be limited to protect equipment and $f_{lim}(i^p)$ is a nonlinear function:

$$f_{lim}(i^p) = \begin{cases} \infty & if\,|i^p| > I_{max} \\ 0 & if\,|i^p| \le I_{max} \end{cases} \tag{2.19}$$

It can also be applied for limiting voltage level.

2.4.4 Weighting factor determination

According to [3], there is no analytical or numerical methods to adjust the weighting factors. They can be determined simply by empirical methods. However, there are some guide lines to determine the range of weighting factors in different cases. There are two main categories of cost functions:

- **Cost Functions without additional terms (system constraints)**

There is no need for weighting factor when working with single term cost functions and also multi-term cost functions with the same nature (unit). One example of this case will be given in chapter 3 when controlling a three phase inverter.

However, the cost function terms are usually different in nature and importance from the control point of view. Therefore, the existence of weighting factors would be inevitable to achieve the appropriate result. When the cost function is written in per unit structure (for example Eq. 2.20), the value of weighting factor will be one or close to one.

$$J = \frac{(T_e^* - T_e^p)^2}{T_n^2} + \lambda.\frac{(|\Psi_s^*| - |\Psi_s^p|)^2}{\Psi_{sn}^2} \tag{2.20}$$

While without using per unit expressions (Eq. 2.21), the necessity of weighting factor is obvious.

$$J = |T_e^* - T_e^p| + \lambda.||\Psi_s^*| - |\Psi_s^p|| \tag{2.21}$$

Although there is no general rule to find the value of weighting factor in this case, [3] and [15] have suggested applying try and error method for λ equal to zero, 1, 10, 100 and 1000. Then according to the result, the values between them should be tested to find the best value of weighting factor.

- **Cost Functions with additional terms (system constraints)**

The additional terms most likely have different natures and they can be considered as the second control priority, like switching frequency, switching loss, output voltage ripple; as a result, the presence of weighting factor λ is needed. If the per unit values of components are used, the weighting factor value will be surely between zero and one, because the reference tracking expression is more important in the control point of view. Otherwise, the value of weighting factor can be any positive value [15].

Chapter 3

FCS-MPC in three-phase VSI inverter

In this chapter, Finite Control Set Model Predictive Control will be applied to a simple three-phase voltage source inverter (VSI) which is connected to a typical R-L-e load. The designed controller capabilities are verified by simulating the system in MATLAB/SIMULINK. The discretization methods; forward, backward and midpoint (modified) Euler methods will be exerted to make a good comparison between them and find the most accurate one.

3.1 Inverter Topology

Three-phase/two-level voltage source inverter is a very well-known topology in power electronics. It has six power switch-diode combinations. The circuit diagram of the three-phase inverter connected to an RLe load has been illustrated in Fig. 3.1.
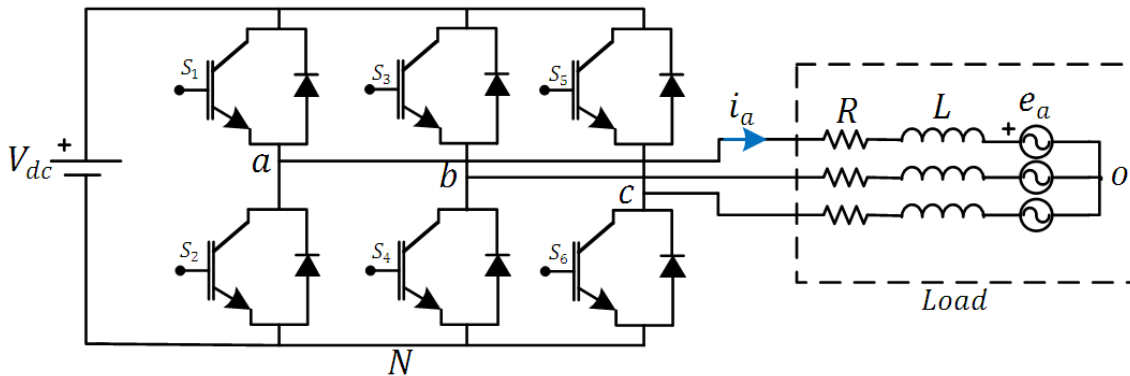
Fig.3.1 Voltage source inverter power circuit

IGBT has been selected to be power switches. The transient switching time will be neglected and only two possible states for each IGBT is going to be assumed that are completely ON or completely OFF. These switching states are not acceptable:

- both of switches in each phase are ON at the same time (short circuiting the dc link)
- both of switches in each phase are OFF at the same time (no power transfer)

Consequently, eight (2^3) possible switching states can be found (Table. 3.1).

The load consists of three branches of a resistor (R), an inductor (L) and a voltage source (e) that have been connected together in star shape. This voltage source can be a representation of motor back emf.

As space vector analysis is a good method in order to simplify three phase equations to a single equation, the mathematical equation of the load will be:

$$v = L\frac{di}{dt} + Ri + e \tag{3.1}$$

where v, i and e are the representations of the inverter terminal voltage, phase currents and load back emf space vectors, respectively. They can be found by the following equations based on the space vector theorem.

$$i = \frac{2}{3}(i_a + ai_b + a^2i_c) \tag{3.2}$$

$$e = \frac{2}{3}(e_a + ae_b + a^2e_c) \tag{3.3}$$

$$v = \frac{2}{3}(v_{aN} + av_{bN} + a^2v_{cN}) \tag{3.4}$$

$$a = e^{j\frac{2\pi}{3}} = -\frac{1}{2} + j\frac{\sqrt{3}}{2} \tag{3.5}$$

Based on this approach and the inverter topology depicted in Fig. 3.1, the relation between switching states and terminal voltage can be found (Table. 3.1)

S_1	S_2	S_3	S_4	S_5	S_6	Inverter terminal voltage space vector v
0	1	0	1	0	1	$v_0 = 0$
1	0	0	1	0	1	$v_1 = \frac{2}{3}\,V_{dc}$
0	1	1	0	0	1	$v_2 = \frac{1}{3}(-1 + j\sqrt{3})V_{dc}$
0	1	0	1	1	0	$v_3 = \frac{1}{3}(-1 - j\sqrt{3})V_{dc}$
1	0	1	0	0	1	$v_4 = \frac{1}{3}(1 + j\sqrt{3})V_{dc}$
1	0	0	1	1	0	$v_5 = \frac{1}{3}(1 - j\sqrt{3})V_{dc}$
0	1	1	0	1	0	$v_6 = -\frac{2}{3}V_{dc}$
1	0	1	0	1	0	$v_7 = 0$

Table 3.1 Switching states and voltage vectors

3.2 System modeling

At the beginning of the controller design, the system model should be discretized with T_s as sampling period and one of Euler methods; forward, backward or midpoint. Then, a cost function based on the control requirements will be defined.

1. Forward Euler method

By applying this method on Eq. 3.1, the system model will be found as follows:

$$i(k + 1) = \left(1 - \frac{T_s R}{L}\right) i(k) + \frac{T_s}{L} (v(k) - e(k)) \tag{3.6}$$

where k is the presentation of the instant that the last switching state has been applied to the inverter (it is very close to now) and k+1 represents the next sampling instant. $i(k)$ is measured, $v(k)$ is assumed to be approximately equal to $v(k + 1)$ that is the future value of the inverter terminal voltage. There are 7 different values related to $v(k + 1)$ depending on the switching states (Table. 3.1). Finally, $e(k)$ can be simply measured or estimated by $e(k - 1)$, if the sampling frequency is high enough. In the other words, it can be approximated constant $(e(k) \approx e(k - 1))$ in one sampling time. By rewriting Eq. 3.6 based on the previous step time, $e(k - 1)$ can be found:

$$e(k) \approx v(k - 1) - \frac{L}{T_s} i(k) + \frac{L - RT_s}{T_s} i(k - 1) \tag{3.7}$$

[3] has used this method.

2. Backward Euler method

The system model by backward Euler method is given in the following Equation.

$$i(k + 1) = \frac{T_s}{L + RT_s} [v(k + 1) - e(k + 1)] + \frac{L}{L + RT_s} i(k) \tag{3.8}$$

Knowing the values of variables in the next time step is necessary while discretizing by backward Euler method. As a result, this method is more complicated that forward Euler method because predicting the values is a challenge. However, in this case it is not as difficult as it seems.

$v(k+1)$ can be seven different values depending on the switching states (Table. 3.1). $e(k+1)$ can be assumed to be constant in one sampling period (if sampling frequency is high enough) and $e(k)$ can be measured or calculated by Eq. 3.8 in the previous step time.

$$e(k) \approx v(k) - \left(R + \frac{L}{T_s}\right)i(k) + \frac{L}{T_s}i(k-1) \tag{3.9}$$

The finalized version of the system model that is the basis of further calculations is:

$$i(k+1) = \frac{1}{L+RT_s}\left[T_s\big(v(k+1)-v(k)\big) + (2L+RT_s)i(k) - Li(k-1)\right] \tag{3.10}$$

Therefore, backward Euler is also applicable and all the variables can be calculated or estimated easily even if their future value is needed.

3. Midpoint Euler method

This method has not been used in the reviewed literature regarding model predictive controllers, while it uses both current and future state values in order to predict the controlled variable. It is more accurate than the other two methods and this claim will be proved by simulation results.

The system model will be as Eq. 3.11.

$$i(k+1) = \frac{2-RT_s}{2+RT_s}i(k) + \frac{T_s}{2+RT_s}[v(k)+v(k+1)-e(k)-e(k+1)] \tag{3.11}$$

where $i(k)$ can be measured and $v(k)$ is known because the inverter is in a specific switching state and knowing that switching state is enough to find $v(k)$ according to Table. 3.1. $e(k-1)$ is assumed to be equal to $e(k)$ and $e(k)$ can be both measured or estimated by the same equation at previous time step.

$$e(k) \approx 0.5[v(k-1)+v(k)] - \left(\frac{2L+RT_s}{2T_s}\right)i(k) + \frac{2L-RT_s}{2T_s}i(k-1) \tag{3.12}$$

Therefore, the main system model based on midpoint Euler will be:

$$i(k+1) = \frac{2-RT_s}{2+RT_s}i(k) + \frac{T_s}{2+RT_s}[v(k)+v(k+1)-2e(k)] \tag{3.13}$$

3.3 Cost function definition

According to the system model, the cost function can be defined as:

$$J = |i_\alpha^*(k+1) - i_\alpha(k+1)| + |i_\beta^*(k+1) - i_\beta(k+1)| \tag{3.14}$$

where $i_\alpha(k+1)$ and $i_\beta(k+1)$ are the real and imaginary parts of the load currents that are predicted by mathematical system model and $(.)^*$ is the presentation of the controlled variables reference value. In high sampling frequency, the reference current can be approximated to be constant during a step time for simplification purposes.

$$J = |i_\alpha^*(k) - i_\alpha(k+1)| + |i_\beta^*(k) - i_\beta(k+1)| \tag{3.15}$$

Since the cost function in this case has two parts with the same unit, the weighting factor is not needed.

The FCS-MPC controller repeats the control algorithm at each time step in order to find the switching state that minimizes the predefined cost function. The selected switching state will be applied to IGBTs' gates. It is worth mentioning that there is no need for pulse width modulation. In addition, the switching frequency is not fixed in contrast with an ordinary PWM controller and it can be minimized by additional terms to the cost function.

3.4 Simulation results

The proposed control scheme with three different discretization methods has been simulated in MATLAB/SIMULINK. The inverter is assumed to be connected to a utility grid load. Table 3.2 contains the inverter and load parameter as well as sampling frequency.

V_{dc}	6.6 kV	R	0.3 Ω
$e_{line-line}$	3.3 kV (rms)	L	2.5 mH
F	50 Hz	T_S	100 µs
$I_{nominal}$	3.5 kA (peak)	f_s	10 kHz

Table 3.2 parameters of the study system illustrated in Fig. 3.1

Fig. 3.2 illustrates the schematic of the system depicted in SIMULINK. The reference currents are fixed sinusoidal waveforms with amplitude equal to nominal current (3500 A) and 50 Hz frequency. The inverter and load have been shown in Fig. 3.3.
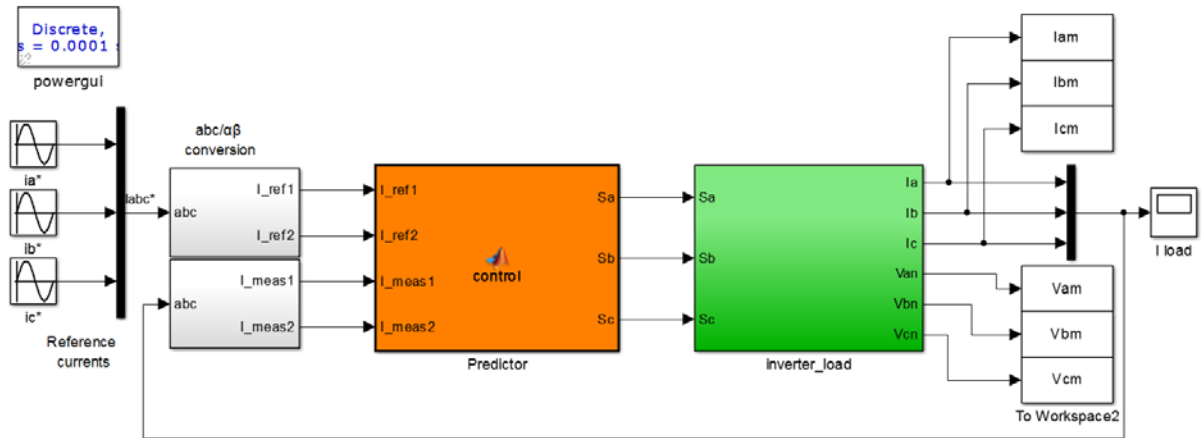
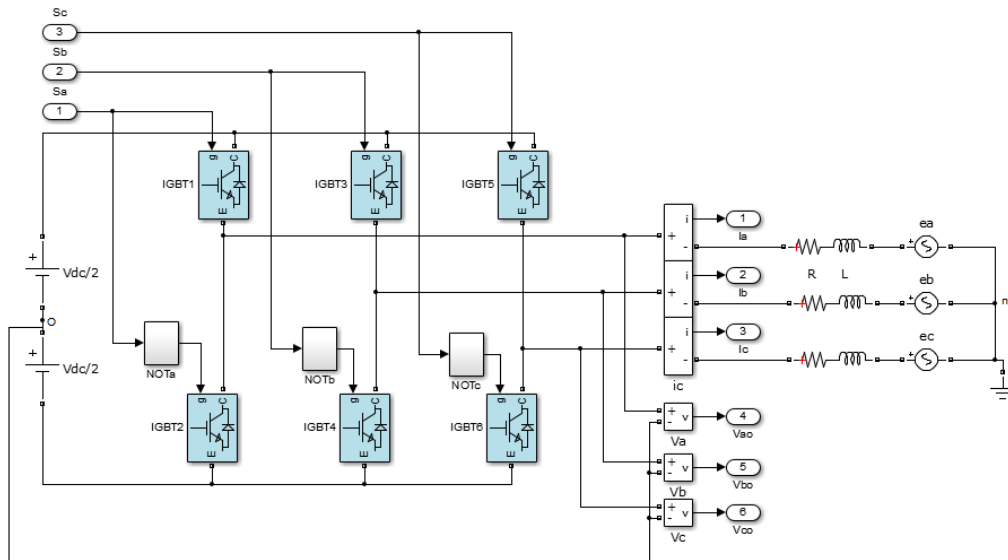Fig. 3.2 The system model in SIMULINK

Fig. 3.3 Circuit model built in SIMULINK

The output currents have been illustrated in Fig. 3.4 when all the Euler methods are used (Eq.3.6, 3.10 and 3.13). It can be seen that the proposed FCS-MPC control method is very successful in reference tracking. All Euler methods provide satisfying performance although midpoint Euler method establishes more accurate currents with the least ripple. Fig. 3.5 illustrates the currents ripple of phase-a more clearly.
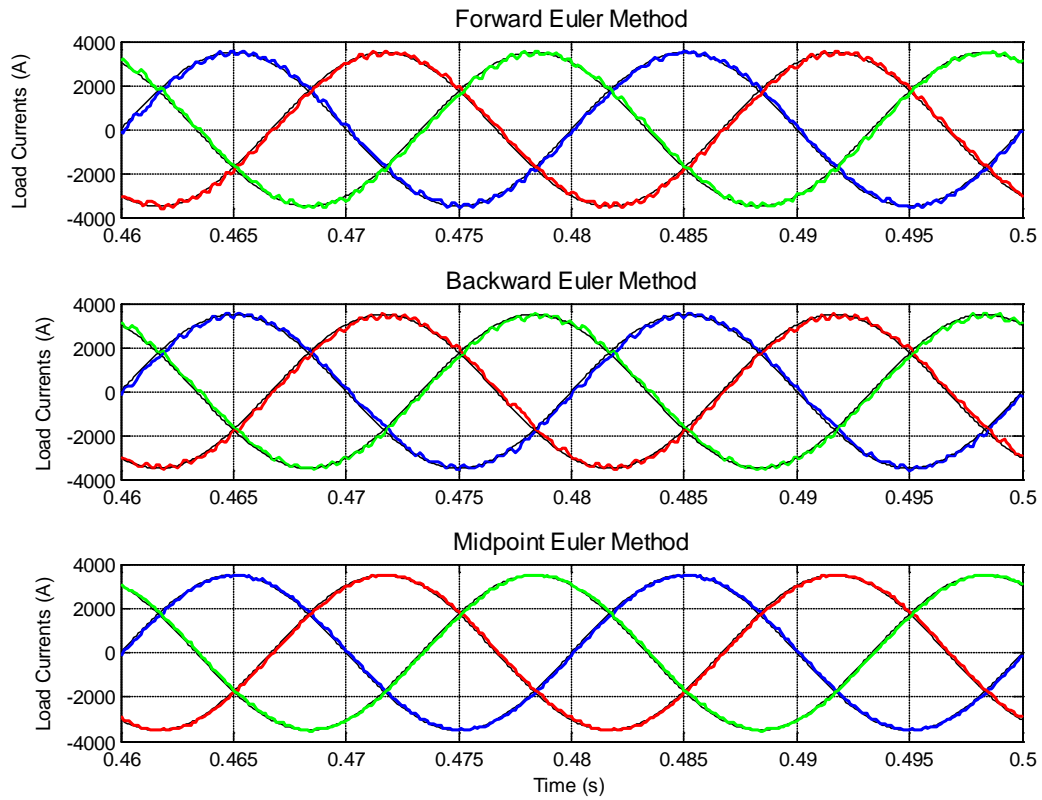
Fig. 3.4 The three-phase load currents using Euler methods
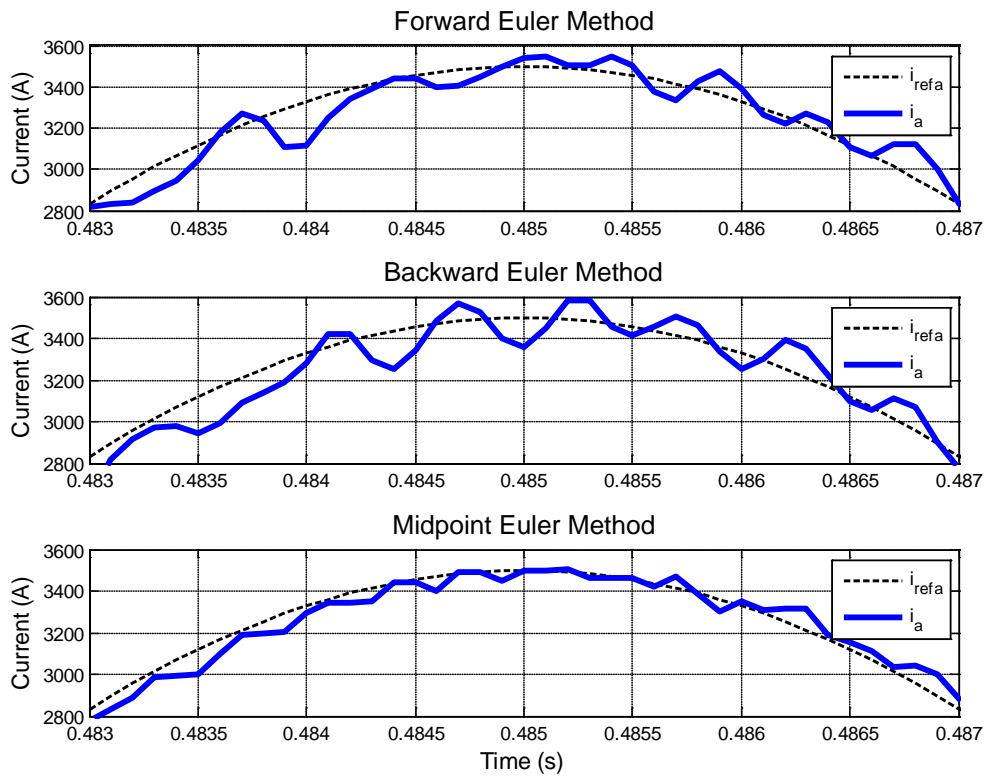
Fig. 3.5 The focused view of phase-a current using Euler methods

19

Another interesting figure is the current frequency spectrum has been shown in Fig. 3.6. Note that the magnitude is depicted in logarithmic scale.
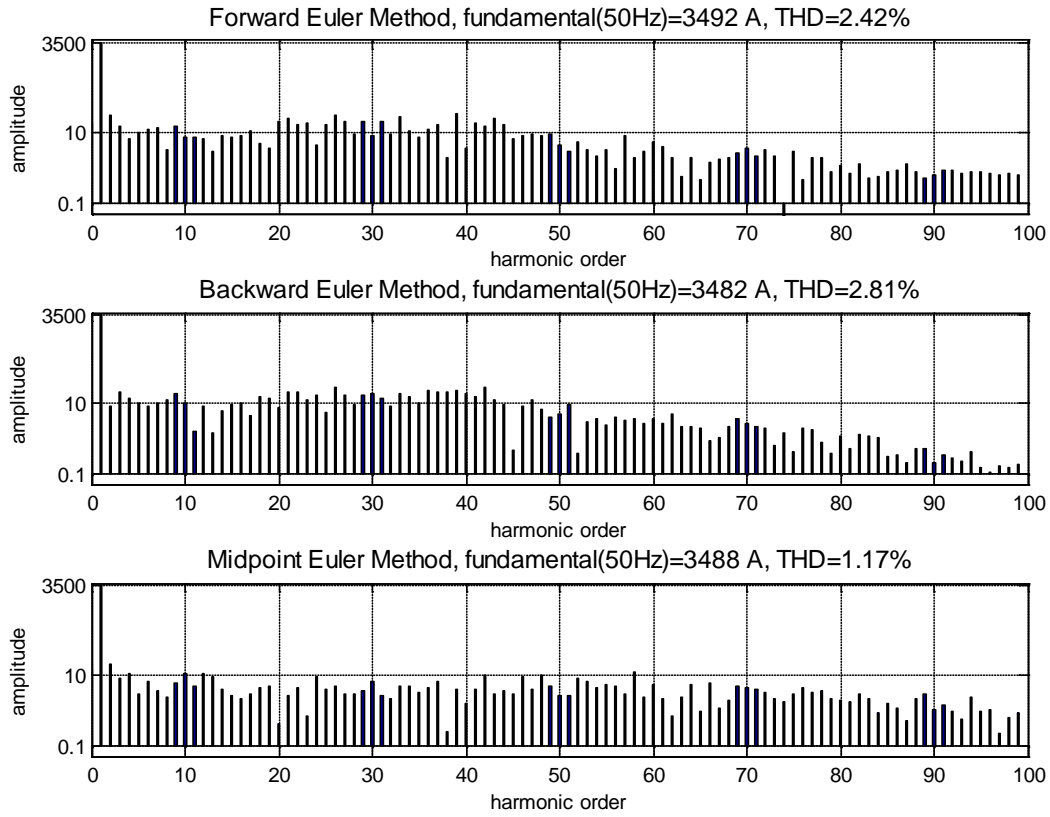
Fig. 3.6 frequency spectrum of phase-a load using Euler methods

Total Harmonic Distortion (THD) of a signal (x) is a good scale to observe its closeness to a pure sinusoidal signal. It is defined as Eq.3.15 [16].

$$THD = \frac{\sqrt{x_2^2 + x_3^2 + \cdots + x_\infty^2}}{x_1} \tag{3.16}$$

While x_1 is the magnitude of fundamental frequency component and x_j j=2, 3,… is the magnitude of jth harmonic order. In order to get an accurate value, it is better to limit the infinity to the Nyquist frequency which is half of sampling frequency [17].

As a result, the THD of all output currents are calculated up to 5000 Hz (100th harmonic order) and they are very small. This is another reason to prove the capabilities of the proposed control scheme. In addition, the value of THD is almost half when using midpoint Euler discretization method, as expected.

One of the inverter terminal (pole) voltages, when DC source middle point is the reference, is presented in Fig. 3.7 for different Euler methods. Terminal voltages V_{ao} oscillate between 3.3 kV and -3.3 kV, however their first order amplitude and switching frequencies are different.
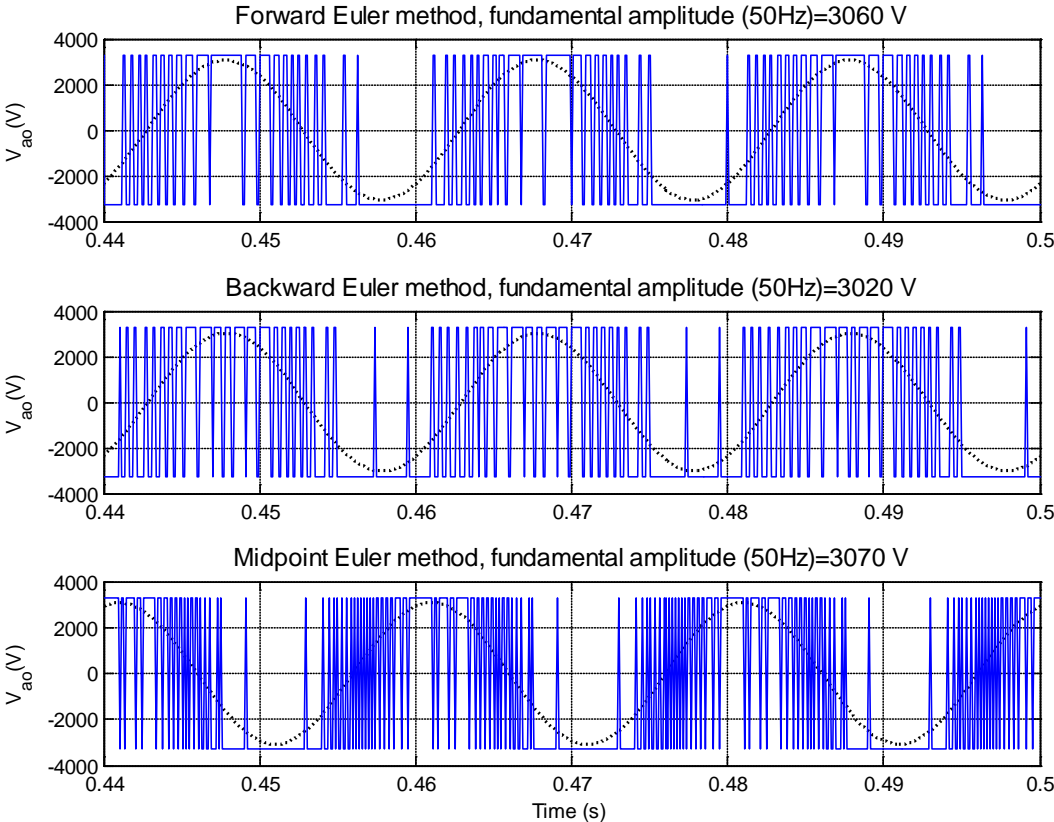
Fig. 3.7 The inverter phase-a pole voltage (V_{ao}) using Euler methods

Although midpoint Euler method provide the largest voltage amplitude at 50 Hz, its higher switching frequency is a disadvantage compared the other methods, because higher switching frequency will lead to higher switching loss that is undesirable. It is worth mentioning that by adding switching frequency minimization to the cost function, it can be considered as a system constraint by the controller, but it is beyond the scope of this chapter.

Line-to-line terminal voltage has been shown in Fig.3.8.

21
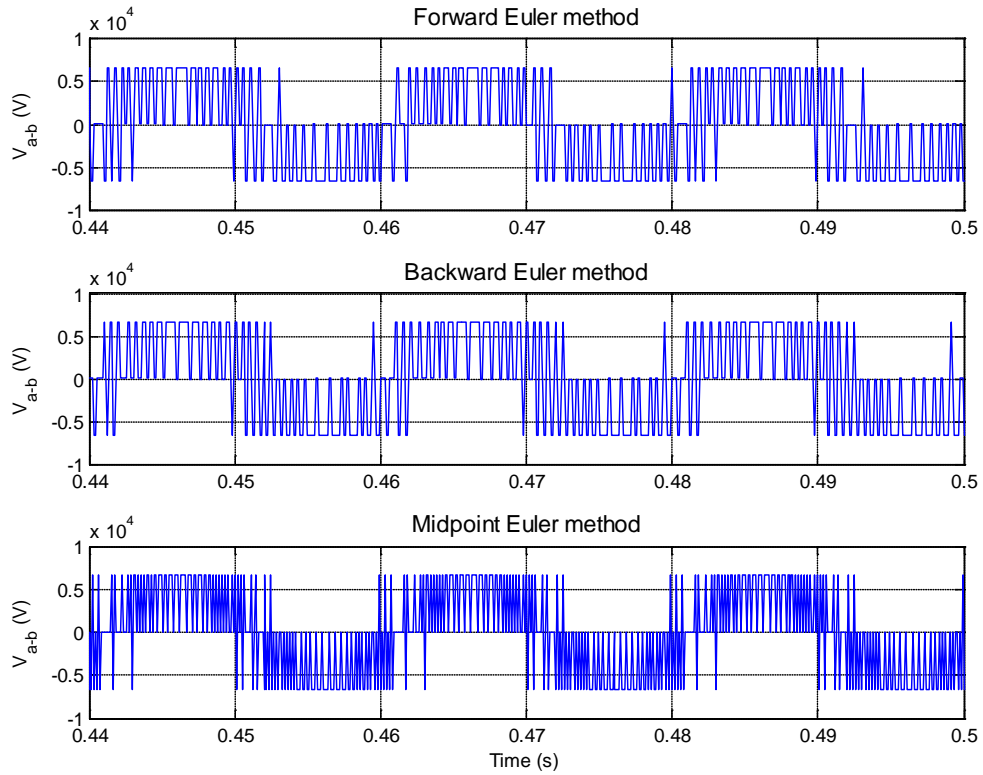
Fig. 3.8 line-to-line output voltage using Euler methods
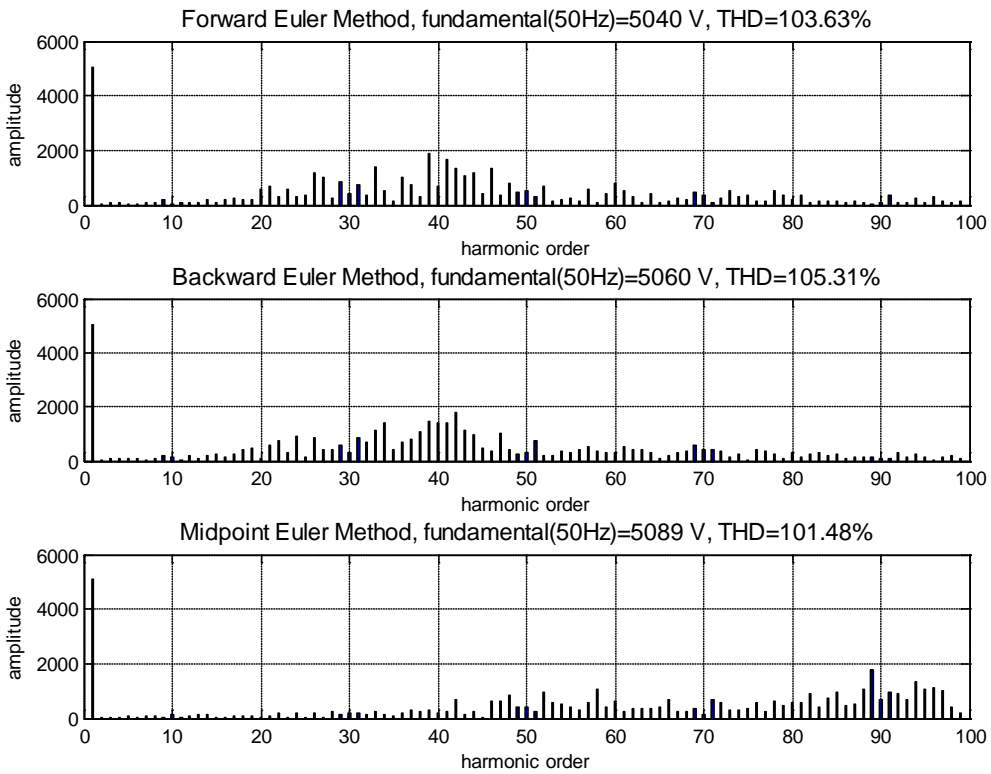
Fig. 3.9 Frequency spectrum of terminal voltage (line-to-line) using Euler methods

Fig. 3.9 gives frequency domain information of the line-to-line voltages while all the Euler methods have been considered to discretize the system model.

It can be observed that applying midpoint Euler method provides the largest voltage value at 50 Hz with least THD. In addition, the harmonics orders less than 20 (1000Hz) have smaller magnitude; therefore, design of high pass filter will be easier. The concentration of higher harmonics magnitudes can be an interpretation of switching frequency that has been worked with. Thus, the switching frequency is the highest when applying midpoint Euler method. The switching frequency is mostly around 2 kHz using forward and backward Euler methods, while it is concentrated around 4.5 kHz by applying midpoint Euler method.

In conclusion, the simulation results prove the accurate and fast performance of the proposed FCS-MPC applied on a three-phase voltage source inverter. The controlled variables (load currents) are forced to follow their reference signals by the controller. All the Euler methods for discretizing the load equation provide acceptable results. However, there are two main differences between them in concern with accuracy and switching frequency.

- The most accurate discretization method is midpoint Euler and the load current has the least ripple when using this method. In addition, in this case THD is the almost half of the other two methods and the fundamental component of current (50Hz) has the largest amplitude.
- On the other hand, the cost of the accuracy increase is the increase in switching frequency. As a result, the backward and forward Euler methods give smaller switching frequency which results in power loss reduction.

Chapter 4

Modular Multilevel Converter (MMC)

Modular Multilevel Converter (MMC) is an AC to DC converter topology that was first introduced in 2003 [18]. It is very suitable for high power-high voltage applications especially High Voltage Direct Current (HVDC) systems. In this chapter, a brief description of MMC topology and its operation principles will be presented.

4.1 MMC configuration

In this section, MMC topology (Fig. 4.1) will be explained as well as its advantages and disadvantages comparing it with high power Voltage Source Converters (VSC) shown in Fig. 4.2.
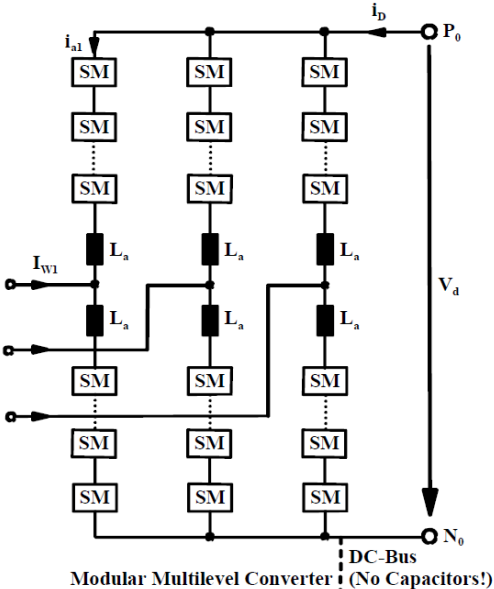
Fig. 4.1 HVDC-transmission using a Modular Multilevel Converter [19]
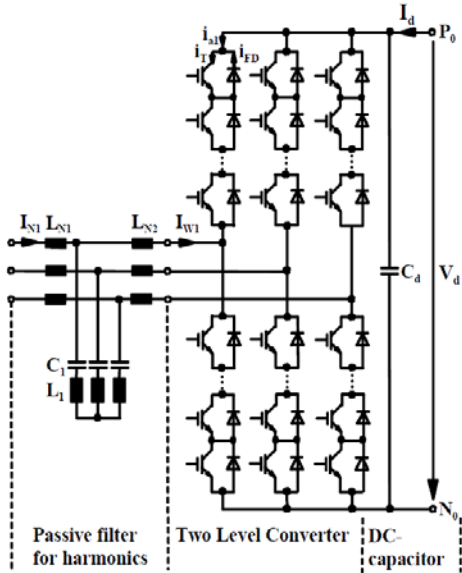
Fig. 4.2 HVDC-transmission with a Two Level Converter [19]

A three-phase (n+1)-level MMC has three upper and three lower arms that are all identical (Fig. 4.1). Each arm has been made of a specific number (n) of units named Sub-modules (SMs) and a small inductor (L_a) which is called arm inductor. Each SM has been made of a

series connected of two IGBT/diode parallel combinations and a pre-charged capacitor in parallel with them (Fig. 4.3).

$$V_C = \frac{V_{dc}}{n}$$
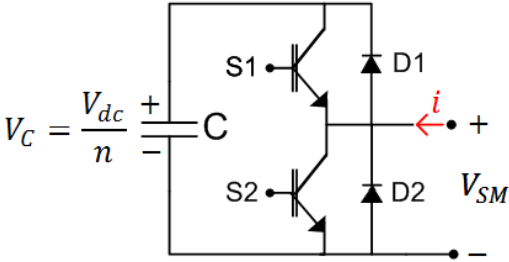
Fig 4.3 Sub-module circuit

In contrast, the VSC (Fig. 4.2) has a certain number of simple IGBT/diode in series in order to share high voltage. In addition, there is no arm inductor in this configuration.

The main purpose of using arm inductor is limiting AC current when a short circuit occurs at the DC-line [19]. Hence, high *di/dt* which is dangerous for equipment can be controlled and minimized by this inductor. Although it is very useful during fault, it does not contribute to the normal operation of MMC because the internal arm currents are flowing continuously. The smoothness of current is another outstanding feature of MMC compared to VSC. Fig. 4.4 and 4.5 illustrate the arm currents using VSC and MMC as the converter. Currents are chopped in VSC case because if one of the IGBTs is turned off the arm current goes to zero. On the other hand in MMC topology, when an SM is turned off the current is still flowing. Therefore, MMC makes less current harmonics than VSC.
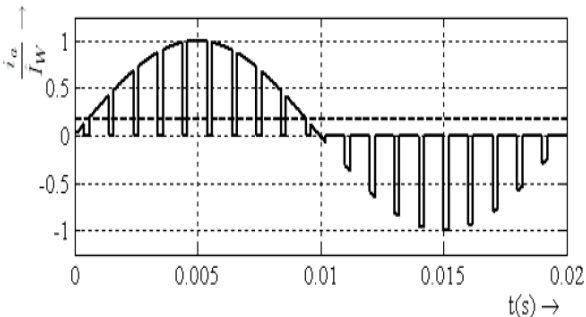
Fig 4.4 The arm currents of the Two level converter (Solid line: Arm current i_a, Dashed line: DC-Bus current component (Idc/3) [19]

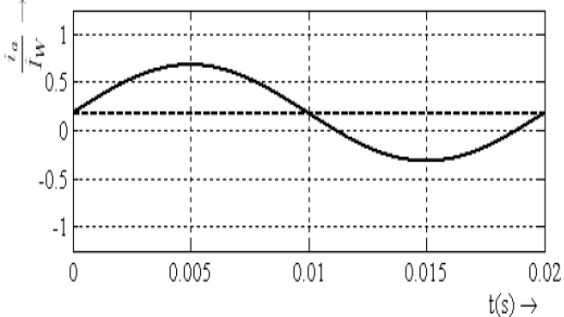Fig 4.5 The arm current of the MMC (Solid line: Arm current i_a, Dashed line: DC-Bus current component (Idc/3) [19]

Voltage sharing between switches is important for high voltage converters. Sometimes especially during the switching time, harmful high voltages may destroy the power switches

or at least shorten their life time. The SMs' capacitors have solved this problem by maintaining the voltage level across the switches to a certain value.

Moreover, MMC provides the advantage of scalability, modularity and high power quality. Another remarkable feature of using MMC in high power applications is that there is no need of input transformer to adjust the voltage in contrast with the conventional converters. As a result, the elimination of the transformer itself and its cooling equipment that are usually large in size and weight will lead to saving money and space. Furthermore, the input filter installations, which are necessary for classical converters, are not needed when using MMC. When using VSC, a DC-line capacitor is needed to keep the voltage constant and the stored energy in this capacitor may result in extremely high surge currents during short circuit occurrence [19]. There is no need for this capacitor in MMC installations.

MMC operates in lower switching frequency than VSC. Therefore, switching power loss is less. This feature makes MMC an appropriate converter for high power applications. It is worth mentioning that, total loss and efficiency of MMC and 2-level VSC have been calculated and compared carefully regarding the switching loss and conductance loss of diodes and switches in [19]. The results illustrate the remarkable feature of MMC in high power applications due to their very low total loss compared to 2-level VSC. It has been shown that the efficiency of VSC in high power (more than 25 MW) is about 98% while it is 99.5% for MMC.
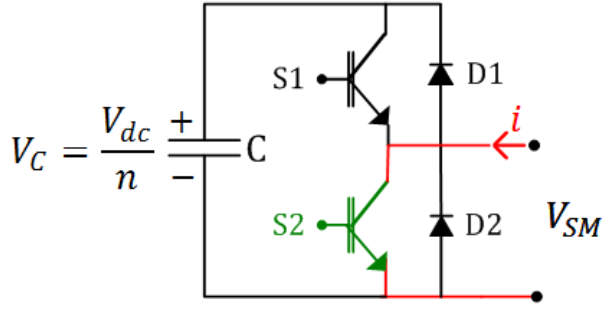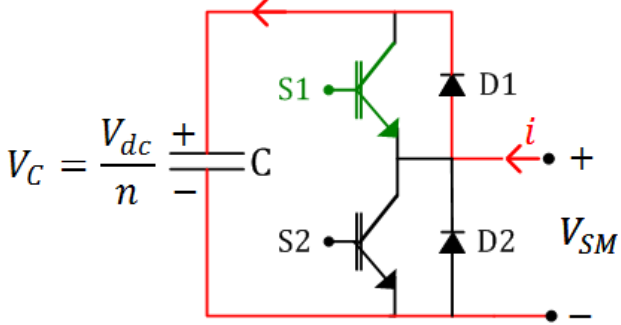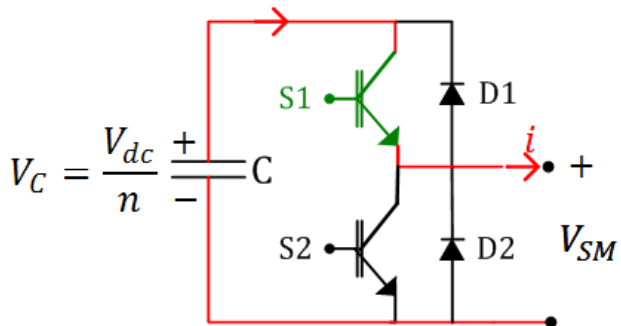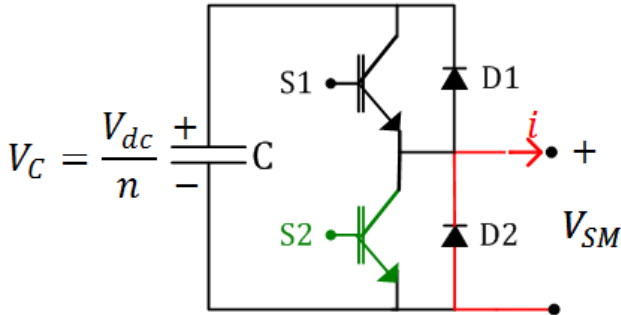
However, MMCs are more expensive and complicated than VSCs and controlling them is more difficult. A big challenge regarding MMC controlling is how to keep the capacitor voltages around the initial value that is equal to $\frac{V_{dc}}{n}$.

4.2 Sub-Module operating principles

In order to create the desired output voltage at the MMC terminals, the controller command the switches in SMs to be turned on or off. Regarding SM circuit in Fig. 4.3, there are two complementary switching states:

- S1 is on and S2 is off
- S2 is on and S1 is off

It is not allowed to turn on both switches simultaneously, because the capacitor voltage will be totally discharged and afterward it becomes useless. By considering the switching states, four different working states can be made based on the current direction:

S1 is OFF and S2 is ON The current (i) will pass through S2 , V_{SM} will be zero (IGBT on-state voltage drop is assumed to be zero) and the capacitor is bypassed.	$V_C = \dfrac{V_{dc}}{n}$
S1 is ON and S2 is OFF In this case the current (i) will pass through D1 and capacitor will be charged and $V_{SM}=V_C$. The voltage of the arm, in which the SM is placed, will increase one step.	$V_C = \dfrac{V_{dc}}{n}$
S1 is ON and S2 is OFF The controller will turn on S1 in order to connect the capacitor to the circuit and increase the arm voltage on step. In this state, the capacitor is discharged and $V_{SM}=V_C$.	$V_C = \dfrac{V_{dc}}{n}$
S1 is OFF and S2 is ON In this state, D2 is turned on and i will pass through it. The capacitor will be bypassed and $V_{SM}=0$.	$V_C = \dfrac{V_{dc}}{n}$

In this report, the term "turned on" SM means that its capacitor is connected and the term "turned off" SM means a bypassed capacitor. Charging and discharging of capacitors depend on the currents direction.

4.3 How does MMC works?

In normal operation of MMC, all of the capacitors are charged up to its nominal value $\frac{V_{dc}}{n}$. In order to reach this value, [18] has proposed to turn on one SM of a leg and turn off the rest of SMs in that leg that are 2n-1 SMs. When the capacitor is charged up, it should be turned off by the controller command and the next SM should be turned on. All of the capacitors will be energized individually one after another. This process has been shown in Fig. 4.6.
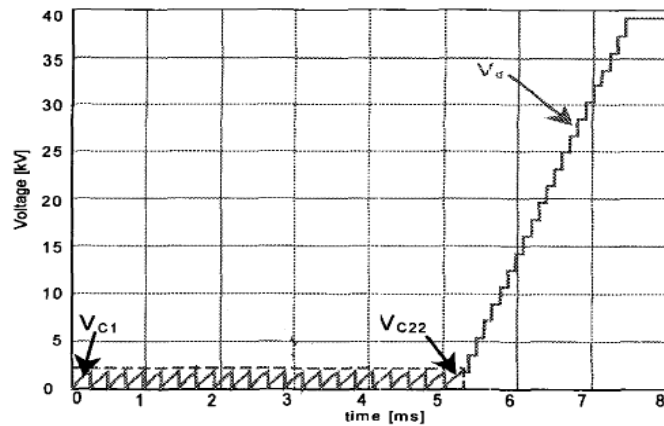
Fig.4.6 Process of charge per inverter arm [18]

However, it is not possible to charge them by the main voltage source, because applying a high step voltage to the capacitors will lead to extremely high currents. As a consequence, an external voltage source with lower DC voltage level is needed [20].

As a better charging method, adding a resistor to the arms has been proposed by [21]. By using this method, there will be no need for any external voltage source and there is no loss due to the resistors in the normal operation, since they will be bypassed by a switch. The controller should only provide the connection and disconnection of the resistors when needed.

When all of the capacitors have been charged, the controller sends turning on and off signals to SMs to create an AC voltage from a DC source or vice versa. At each sampling time, only half of the total number of SMs in each phase is on (n SMs).Therefore, the total number of the connected capacitors from upper arm and lower arm together is equal to n at

28

any instant. For example, if all of the n upper SMs are on, all of the lower arm SMs should be off. So, the AC-line voltage level will be minimum:

$$v_{ac} = n.\left(-\frac{V_{dc}}{n}\right) + \frac{V_{dc}}{2} = -\frac{V_{dc}}{2} \tag{4.1}$$

And reversely, if all of the lower arm SMs are on, the AC-line voltage level will be maximum:

$$v_{ac} = 0.\left(-\frac{V_{dc}}{n}\right) + \frac{V_{dc}}{2} = \frac{V_{dc}}{2} \tag{4.2}$$

Therefore, AC-bus voltage can vary between $\frac{-V_{dc}}{2}$ and $\frac{+V_{dc}}{2}$ with the steps of $\frac{+V_{dc}}{n}$. Each arm of MMC represents a controllable voltage source. AC-line voltage increases by turning off upper arm SMs and simultaneously turning on the same number of SMs in the lower arm. However, it is better to increase and decrease the voltage one step at each switching time to have a smooth voltage waveform. Charging or discharging of the capacitors depends on the current direction as explained in section 4.2

4.4 MMC control requirements

The following aspects from control point of view are very important to transfer desired power with maximum efficiency and minimum voltage and current harmonics:

1. Controlled variable reference tracking

    Depending on the main controlled variable(s) that can be output voltage or current, the control scheme should be able to create the turning on and turning off signals to make the required output voltage and current with minimum error with their reference signals.

2. Keeping the capacitor voltages balanced

    As mentioned earlier, if SM is going to be turned on or off, depending on the current direction, its capacitor will be charged or discharged; so, it will be more or less than $\frac{V_{dc}}{n}$. The value of voltage variation obviously depends on the capacitance value and the on-time duration of SM. In high switching frequency, on-time duration of Sub-Modules is short; therefore, voltage balancing is not critical. By the way, the control

scheme should consider it carefully to stabilize the voltage of capacitors in its limitations especially in low switching frequencies.

3. Circulating current minimization

During the operation of MMC, in addition to the AC side and DC side currents there are three pure AC high frequency circulating currents [22].The main reason behind these currents is the voltage variation (ripple) of capacitors during charging and discharging period [22]. These circulating currents have no effect on the DC or AC side of MMC and no power transfer occurs due to them. However, they have a significant impact on the rating values of the MMC components, SMs capacitor ripples and converter loss [22]. Hence, the circulating current should be minimized by the controller as much as possible.

In the next chapter, FSC-MPC will be applied to MMC and it will be proved that it can handle all of the above control challenges.

Chapter 5

Applying FCS-MPC to MMC

In this chapter, a control scheme based on FCS-MPC for controlling Modular Multilevel Converter will be proposed to fulfill its control requirements; controlled variables (current or voltage) reference tracking, keeping the capacitor voltages balanced and minimizing the circulating currents. In order to verify its capabilities, simulation has been done in MATLAB/SIMULINK and the results will be presented at the end of this chapter.
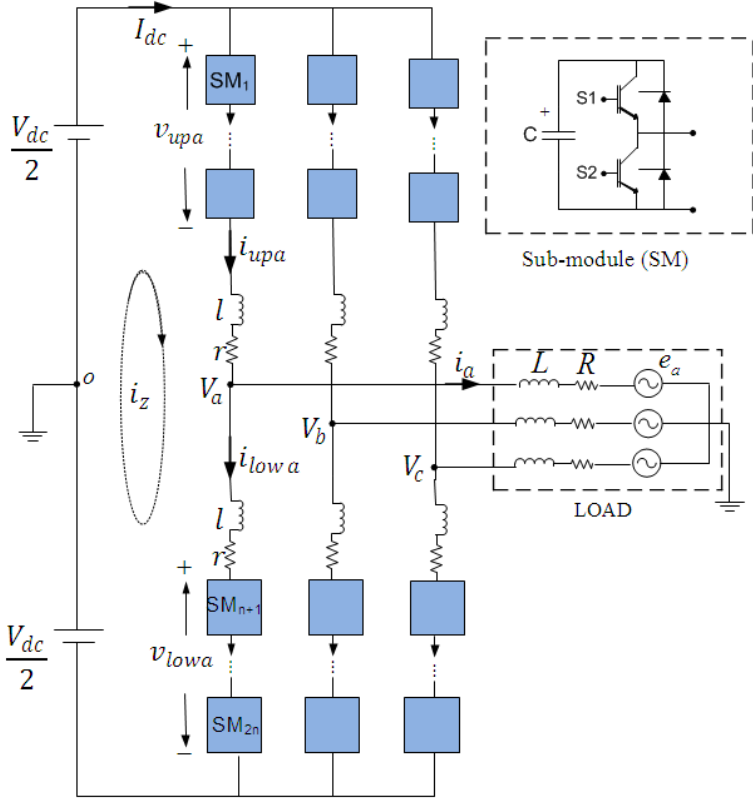
5.1 Basic equations for MMC modeling

Fig. 5.1 Topology of the (n+1)-level MMC connected to a typical load.

The circuit model of a three-phase DC-AC MMC has been demonstrated in Fig. 5.1. It is connected to the utility grid or motor as a load. In this study, the loss in Sub Modules and arm

inductors has been modeled with a small resistor (r) connected in series with them [5, 22]. In contrast with this model, [13] has proposed to add an equivalent resistor in parallel with the MMC legs in order to model the loss of SMs. The resistivity of DC source and DC line has been neglected.

The load is three sets of series-connected inductor (L), resistor (R) and voltage source (e) in star shape. The voltage source has 50 Hz frequency.

According to Chapter 4, each arm of MMC represents a controllable voltage source called v_{upj} and v_{lowj}, which are the sum of SMs output voltages (V_{SM})of upper arm and lower arm in phase j (a, b or c). As shown in Fig. 5.1, v_{tj} is the representation of pole voltages with respect to point O. By assuming that each capacitor voltage is ideally equal to $\frac{V_{dc}}{n}$ and neglecting the voltage drop across arm inductor and resistor, v_{tj} can be calculated by:

$$v_{tj} = \frac{n_{lowj} - n_{upj}}{2n} V_{dc} \tag{5.1}$$

where n_{upj} and n_{lowj} are the number of upper and lower SMs that have been turned on. Total number of on SMs in each phase of MMC is:

$$n = n_{upj} + n_{lowj} \tag{5.2}$$

According to [13, 22 and 23], the upper and lower arm currents ($i_{upj}$and i_{lowj}) can be calculated by:

$$i_{upj} = \frac{I_{dc}}{3} + \frac{i_j}{2} + i_{zj} \tag{5.3}$$

$$i_{lowj} = \frac{I_{dc}}{3} - \frac{i_j}{2} + i_{zj} \tag{5.4}$$

where I_{dc} is the dc component of the dc line current, i_j is the output phase current and i_{zj} is the circulating current flowing through phase j. These equations mean that the arm currents consist of three main components with different frequencies:

1. zero frequency current (I_{dc}) that is its dc offset
2. 50 Hz current (i_j) that is transferring power to the load
3. 100 Hz circulating current (if capacitor voltages are balanced and the circulating current is minimized very well)

According to Fig. 5.1 and by applying KVL law, the mathematical equations can be described as follows.

$$\frac{V_{dc}}{2} = v_{upj} + l\frac{di_{upj}}{dt} + ri_{upj} + Ri_j + L\frac{di_j}{dt} + e_j \tag{5.5}$$

$$\frac{V_{dc}}{2} = v_{lowj} + l\frac{di_{lowj}}{dt} + ri_{lowj} - Ri_j - L\frac{di_j}{dt} - e_j \tag{5.6}$$

Phase currents i_j can be calculated by subtracting Eq.5.4 from Eq.5.3 and the circulating currents i_{zj} can be found by adding Eq.5.3 and Eq.5.4.

$$i_j = i_{upj} - i_{lowj} \tag{5.7}$$

$$i_{zj} = \frac{1}{2}\left(i_{upj} + i_{lowj} - \frac{2I_{dc}}{3}\right) \tag{5.8}$$

By subtracting Eq.5.6 from Eq.5.5 and replacing Eq.5.7, the main first order differential equation (Eq.5.10) that can be used to predict the phase currents will appear:

$$v_{upj} - v_{lowj} + l\frac{d(i_{upj} - i_{lowj})}{dt} + r.(i_{upj} - i_{lowj}) + 2Ri_j + 2L\frac{di_j}{dt} + 2e_j = 0 \tag{5.9}$$

$$\frac{di_j}{dt} = \frac{1}{(l + 2L)}\left[v_{lowj} - v_{upj} - (r + 2R)i_j - 2e_j\right] \tag{5.10}$$

In order to predict the second controlled variable, i.e. the circulating current, Eq.5.5 and Eq.5.6 should be added.

$$V_{dc} = v_{upj} + v_{lowj} + l\frac{d(i_{upj} + i_{lowj})}{dt} + r.(i_{upj} + i_{lowj}) \tag{5.11}$$

And Eq.5.8 should be replaced into the above equation:

$$\frac{di_{zj}}{dt} = \frac{1}{2l}[V_{dc} - v_{upj} - v_{lowj} - 2ri_{zj} - \frac{2}{3}r I_{dc}] \tag{5.12}$$

For simplification, the DC line current is assumed to be constant ($\frac{dI_{dc}}{dt} = 0$).

The third and last controlled variable is the capacitor voltages that can be calculated by

$$\frac{dv_{Cij}}{dt} = \frac{i_{mj}}{C} \tag{5.13}$$

where i=1,2,..,2n is the SM number and i_{mj} can be zero if SM is off, or i_{upj} if SM is located in the upper arm or i_{lowj} if SM is located in the lower arm.

5.2 System modeling

FCS-MPC can fulfill all the MMC control requirements simultaneously and very well. By defining a proper cost function, it can make the output currents to follow their references, keep the capacitor voltages in a balanced position around $\frac{V_{dc}}{n}$ and minimize the circulating currents as much as possible.

In a single-phase (n+1)-level MMC, the total possible switching states are:

$$N = C_{2n}^{n} = \binom{2n}{n} = \frac{2n!}{n!\,(2n-n)!} \tag{5.14}$$

Consequently, for a three-phase one it will be equal to N^3. For example, a 3-level MMC has totally $6^3 = 216$ switching states. This number is important because the controller speed depends directly to it. Cost function calculation process repeats for all the switching states and then, the one that minimizes the cost function will be selected to be applied at the next switching instant.

As mentioned earlier, there are three controlled variables regarding MMC; output AC currents, capacitor voltages and circulating currents. In order to predict the one-step ahead value of the controlled variables, Eq5.10, 5.12 and 5.13 should be discretized by one of the Euler methods. As the system model accuracy is very important for the controller performance, midpoint Euler method is selected. However, the system model based on both backward and forward Euler methods will be calculated and used for a single phase 3-level MMC.

- Midpoint Euler discretization method (with T_s as sampling time)

$$i_j(k+1) = A.i_j(k) + B.\left[v_{lowj}(k+1) + v_{lowj}(k) - \left[v_{upj}(k+1) + v_{upj}(k)\right]\right. \tag{5.15}$$
$$\left. - 2\left[e_j(k+1) + e_j(k)\right]\right]$$

$$A = \frac{2(l+2L) - T_s(r+2R)}{2(l+2L) + T_s(r+2R)}$$

$$B = \frac{T_s}{2(l+2L) + T_s(r+2R)}$$

For simplification, e_j is assumed to be constant during a sampling period ($e_j(k+1) \approx e_j(k)$). Therefore, the phase currents can be calculated by:

$$i_j(k+1) = A.i_j(k) + B.\left[v_{lowj}(k+1) + v_{lowj}(k) - v_{upj}(k+1) - v_{upj}(k) - 4e_j(k)\right] \quad (5.16)$$

Another controlled variable that should be predicted is the circulating currents that can be found by Eq.5.17.

$$i_{zj}(k+1) = C.i_{zj}(k) + \quad\quad\quad (5.17)$$
$$+D.\left[2V_{dc} - v_{upj}(k+1) - v_{upj}(k) - v_{lowj}(k+1) - v_{lowj}(k) - \frac{2r}{3}\left(I_{dc}(k+1) + I_{dc}(k)\right)\right]$$

$$C = \frac{2l - rT_s}{2l + rT_s}$$

$$D = \frac{T_s}{4l + 2rT_s}$$

where v_{upj} and v_{lowj} can be found by adding voltage of the connected upper and lower arm capacitors.

$$v_{upj}(k+1) = n_{upj}(k+1).\frac{V_{dc}}{2n} \quad\quad\quad (5.18)$$

$$v_{lowj}(k+1) = n_{lowj}(k+1).\frac{V_{dc}}{2n} \quad\quad\quad (5.19)$$

Also in this case, the DC line current can be assumed to be constant in one sampling period to simplify the calculations ($I_{dc}(k+1) \approx I_{dc}(k)$).

$$i_{zj}(k+1) = C.i_{zj}(k) + \quad\quad\quad (5.20)$$
$$+D.\left[2V_{dc} - \left(v_{upj}(k+1) + v_{upj}(k)\right) - \left(v_{lowj}(k+1) + v_{lowj}(k)\right) - \frac{4r}{3}\left(I_{dc}(k)\right)\right]$$

And capacitors voltages are predicted by

$$v_{Cij}(k+1) = v_{Cij}(k) + \frac{T_s}{2C}\left[i_{mj}(k+1) + i_{mj}(k)\right] \quad\quad\quad (5.21)$$

$$v_{Cij}(k+1) = \begin{cases} v_{Cij}(k) & SM\ is\ OFF \\ v_{Cij}(k) + \frac{T_s}{2C}\left[i_{upj}(k+1) + i_{upj}(k)\right] & Upper\ arm\ SM \\ v_{Cij}(k) + \frac{T_s}{2C}\left[i_{lowj}(k+1) + i_{lowj}(k)\right] & Lower\ arm\ SM \end{cases} \quad (5.22)$$

- Backward Euler discretization method

$$i_j(k+1) = A.i_j(k) + B.\left[v_{lowj}(k+1) - v_{upj}(k+1) - 2e_j(k+1)\right] \quad\quad\quad (5.23)$$

$$A = \frac{l + 2L}{l + 2L + T_s(r + 2R)}$$

$$B = \frac{T_s}{l + 2L + T_s(r + 2R)}$$

$$i_{zj}(k+1) = C.i_{zj}(k) + D.\left[V_{dc} - v_{upj}(k+1) - v_{lowj}(k+1) - \frac{2r}{3}I_{dc}(k+1)\right] \quad (5.24)$$

$$C = \frac{l}{l + rT_s}$$

$$D = \frac{T_s}{2(l + rT_s)}$$

$$v_{Cij}(k+1) = v_{Cij}(k) + \frac{T_s}{C}\left[i_{mj}(k+1)\right] \quad (5.25)$$

- Forward Euler discretization method

$$i_j(k+1) = A.i_j(k) + B.\left[v_{lowj}(k) - v_{upj}(k) - 2e_j(k)\right] \quad (5.26)$$

$$A = \frac{l + 2L - T_s(r + 2R)}{l + 2L}$$

$$B = \frac{T_s}{l + 2L}$$

$$i_{zj}(k+1) = C.i_{zj}(k) + D.\left[V_{dc} - v_{upj}(k) - v_{lowj}(k) - \frac{2r}{3}I_{dc}(k)\right] \quad (5.27)$$

$$C = \frac{l - rT_s}{l}$$

$$D = \frac{T_s}{2l}$$

$$v_{Cij}(k+1) = v_{Cij}(k) + \frac{T_s}{C}\left[i_{mj}(k)\right] \quad (5.28)$$

5.3 Cost function definition

In the next step of designing FCS-MPC, a cost function should be defined in order to force the output AC currents to track their references, keep the capacitor voltages balanced (i.e. around the nominal value $\frac{V_{dc}}{n}$) and minimize the circulating currents.

It should be mentioned that the total switching states $[N = (C_{2n}^n)^3]$ of a three-phase MMC are three identical sets. Therefore, it is better and simpler to design three identical controller' codes to work in parallel instead of writing one code for considering all of them;

therefore, each phase is controlled by their own cost function separately and at the same time with the other two phases.

$$g = \left|i_{jref}(k+1) - i_j(k+1)\right| + \lambda_1 . \sum_{i=1}^{2n} \left|v_{Cij}(k+1) - \frac{V_{dc}}{n}\right| + \lambda_2 . \left|i_{zj}(k+1)\right| \qquad (5.29)$$

where $i_{jref}(k+1)$ is the predicted reference current, $i_j(k+1)$, $v_{Cij}(k+1)$, and $i_{zj}(k+1)$ are the predicted values of the load currents, capacitor voltages and circulating currents that can be found by the equations presented in section 5.3. This cost function has three components with different units and importance; hence, λ_1 and λ_2 are necessary to adjust the differences. They can be found by empirical methods, i.e. try and error.

For simplicity, $i_{jref}(k+1)$ is approximated with $i_{jref}(k)$ in high sampling frequency. It can be easily set to be sinusoidal 50 Hz signals with certain amplitude in the simulations, while it can also be made by another controller (for example a PI controller). The latter method can be complicated but it makes the whole control strategy useful for real life implementation as well. In this study, at first the capabilities of FCS-MPC controller on a 3-level MMC have been investigated by using fixed current references and then, a PI controller has been designed to build the references for a 5-level MMC.

5.4 Simulation results of a single-phase 3-level MMC

In this section, FCS-MPC will be applied to a single phase 3-level MMC to observe its performance. At first, a cost fucntion with all the required terms (reference current tracking, capacitor voltages balancing and circulating current minimization) will be employed as the basis of the control strategy. Then, the circulating current minimization term will be removed in order to observe its impact on the system performance. Table5.1 contains both converter and load parameters. The load is a simple R-L load. Furthurmore, the reference current signal is a fixed 50Hz sinusoidal one. Fig.5.2 shows the circuit model used in the simulation.
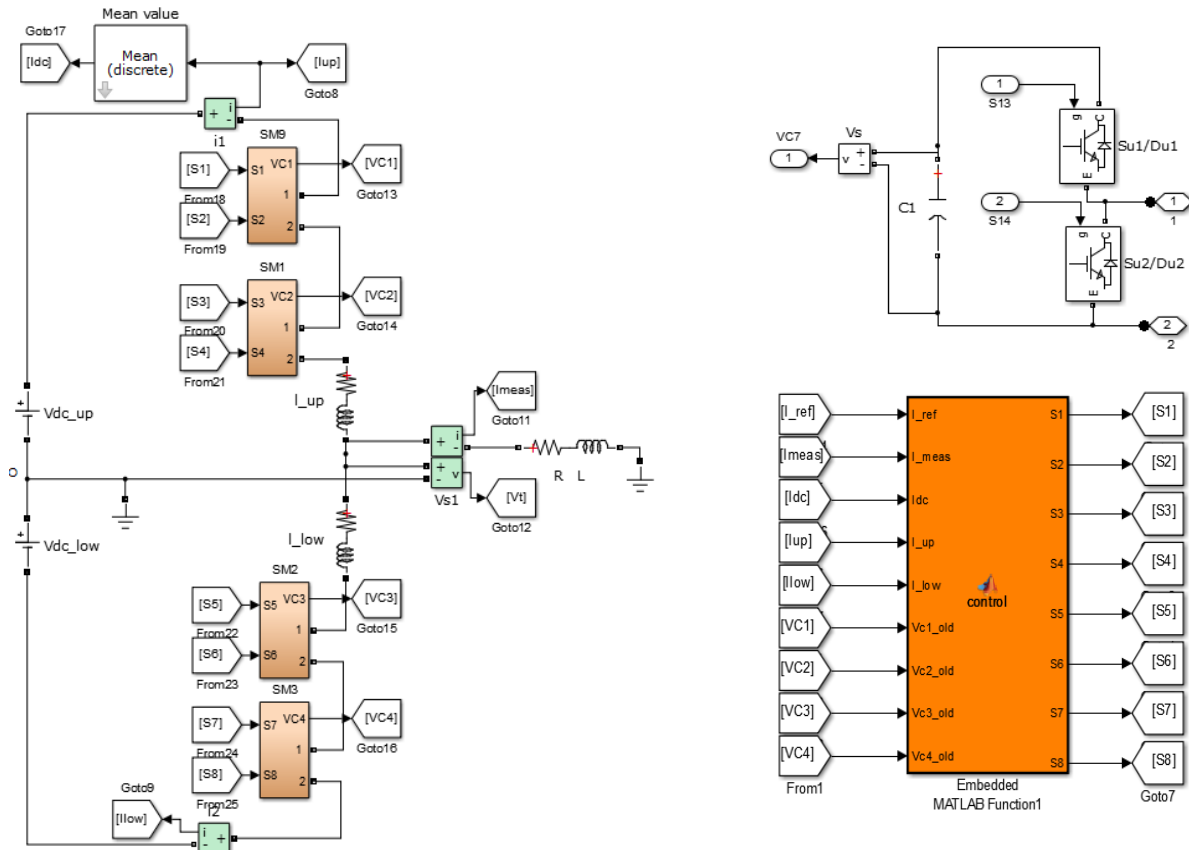
Fig.5.2 the system model depicted in SIMULINK

Parameter	Symbol	Value
Number of SMs per arm	n	2
SM capacitor	C	3.6 mF
Arm inductance	l	5 mH
Arm resistance	r	30 mΩ
DC link voltage	V_{dc}	400 V
Load resistance	R	11.9 Ω
Load inductance	L	8.4 mH
Reference current	I_{ref}	15 A
Rated frequency	f	50 Hz
Sampling time	T_s	100 µs

Table5.1 Parameters of the study system illustrated in Fig.5.1

The system model has been made based on midpoint Euler method (Eq.5.16 and Eq.5.22). For predicting the circulating current, a change should be made in Eq.5.20 because it has been written for a three-phase MMC. For a single phase MMC the new equation will be:

$$i_{zj}(k + 1) = C . i_{zj}(k) + \tag{5.30}$$
$$+D . \left[2V_{dc} - \left(v_{upj}(k + 1) + v_{upj}(k) \right) - \left(v_{lowj}(k + 1) + v_{lowj}(k) \right) - 4r \left(I_{dc}(k) \right) \right]$$

By inserting the parameters values of Table5.1, the main system equations are:

$$i(k + 1) = 0.8963 i(k) + 0.0022 \left[v_{low}(k + 1) + v_{low}(k) - v_{up}(k + 1) - v_{up}(k) \right] \tag{5.31}$$
$$i_z(k + 1) = i_z(k) + \tag{5.32}$$
$$+0.005 \left[2V_{dc} - v_{low}(k + 1) - v_{low}(k) - v_{up}(k + 1) - v_{up}(k) + 0.12 I_{dc} \right]$$

The used cost function is exactly like Eq.5.29 and $\lambda_1 = 1$ and $\lambda_2 = 0.5$ are determined by try and error. There are some points regarding the weighting factors selection:

1. In the beginning it would be simpler if λ_2 is set to zero. The first selected value for λ_1 is optional (it can be for example 1).

2. The output current is the first variable to be observed. If it is not following its reference, it means that λ_1 is too high and should be reduced; otherwise, the capacitor voltages, as the second important variable, should be watched. If it is not in order around $\frac{V_{dc}}{n}$, for example some of them are continuously increasing or decreasing, λ_1 is too small and should increase.

3. After finding an acceptable value for λ_1, the second weighting factor should be discovered in order to make the variables similar to their ideal waveforms. A visible change can be noticed in circulating current, while its ideal waveform is an almost pure sinusoidal current that has double frequency (100 Hz). If λ_2 is selected too high, capacitors voltages and/or output current will be deformed and if it is too small, it would have had other harmonics.

5.4.1 Cost function with circulating current minimization term (λ_2=1)

The simulation has been done for 5 seconds. The steady state has been reached after 0.4 sec. Fig.5.3 displays the load and circulating currents in the first 0.7seconds. After the transient time, the circulating current is 1.4 A (peak-to-peak) which is 4.6% output current. The output current, arm currents and circulating current has been illustrated in Fig.5.4.
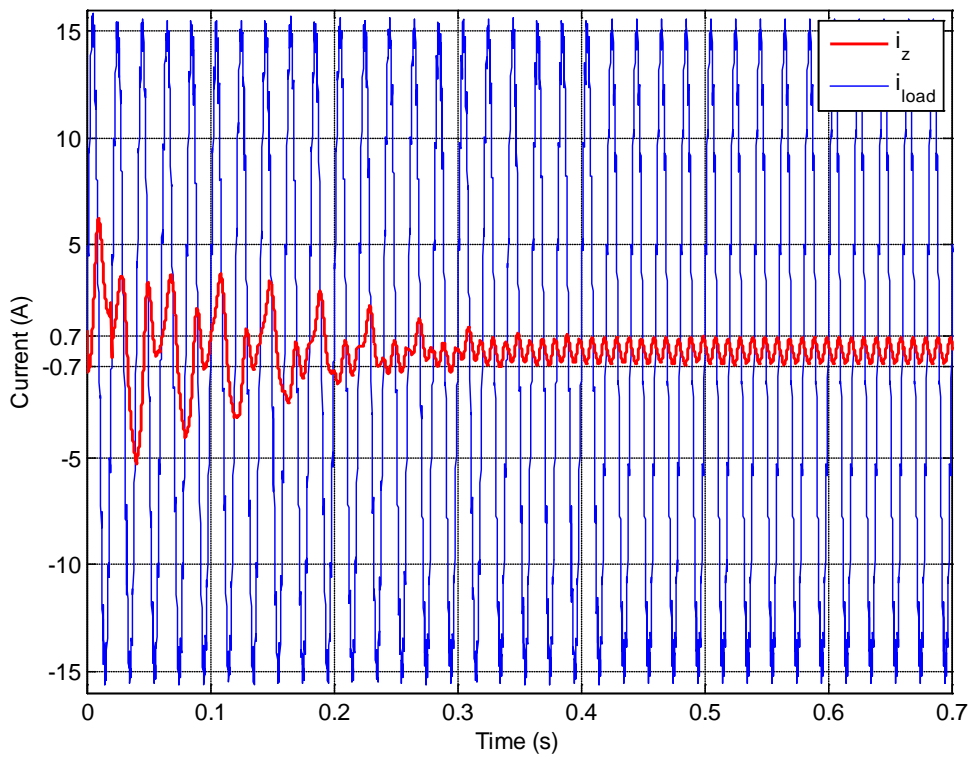
Fig.5.3 Phase-a load current and circulating current
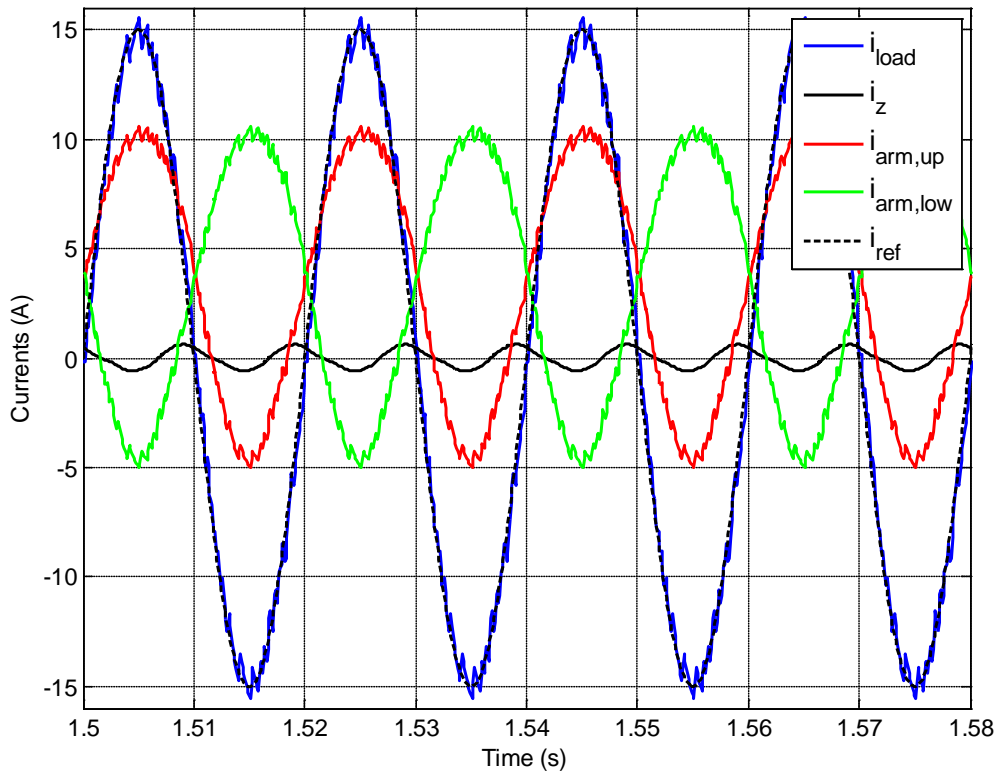
Fig.5.4 The arm currents, circulating and load current of phase-a

According to Fig.5.4, the controller forces the load current to follow its reference very well and its ripple is small and acceptable. The largest ripples occur in the peaks (Fig.5.5). The upper arm and lower arm currents have 180° phase shift that is correct.
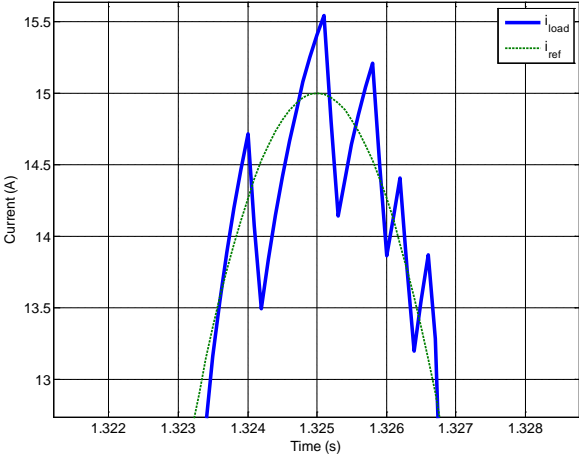
Fig.5.5 A focused view of phase-a current ripple

The capacitors voltages are shown in Fig.5.6 and 5.7. During the transient time (0.5 s),the maximum voltage is 213 V; therefore its overshoot is 6.5% which is acceptable. In steady state, they are completely in order and kept balanced around 200 V, while the peak-to-peak voltage is roughly equal to 8 V. The charging and discharging process can be clearly seen in Fig.5.7.
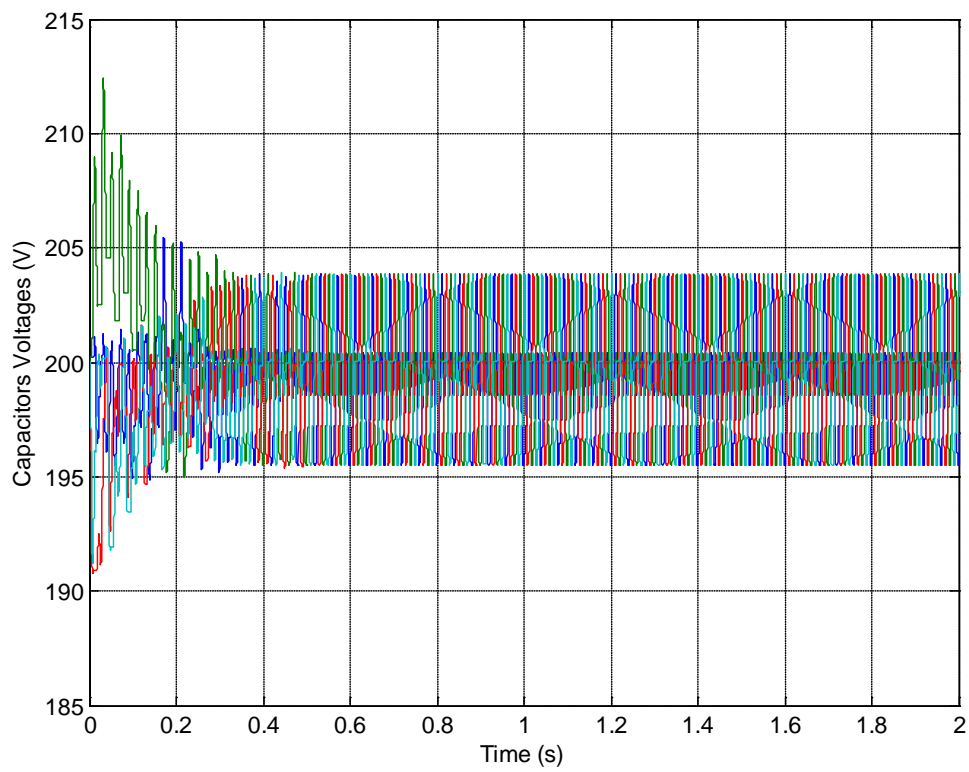
Fig.5.6 The capacitor voltages in the first 2 seconds
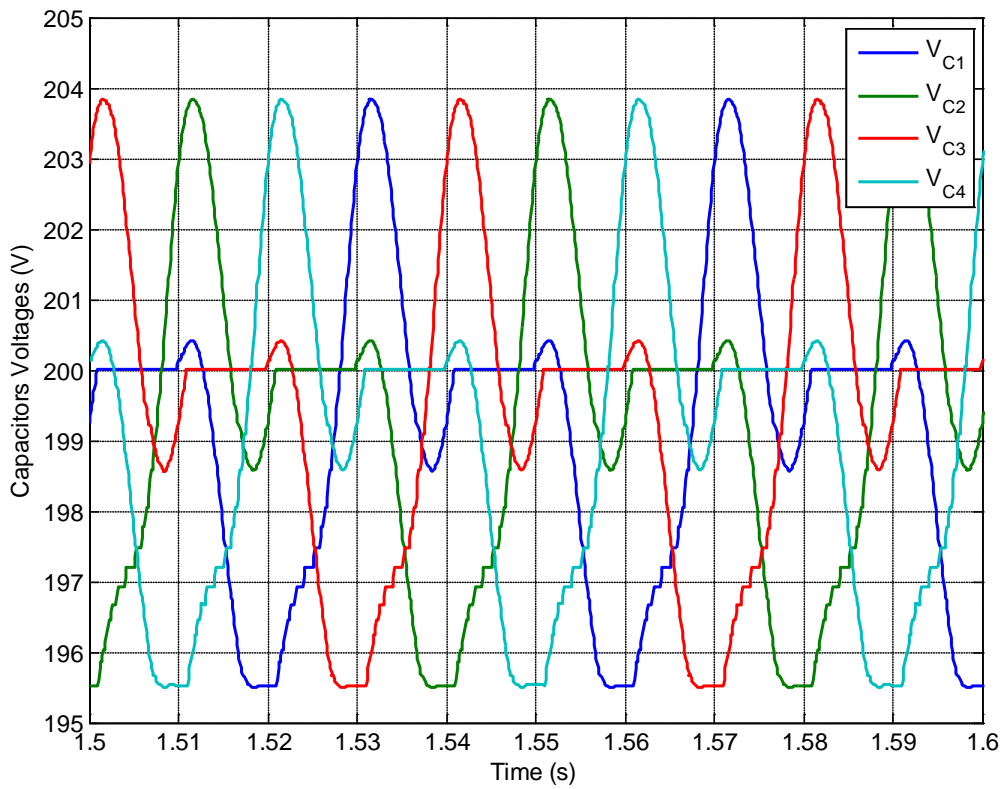
Fig.5.7 The capacitor voltages in steady state

42

The next figure (Fig.5.8) presents the terminal voltage of phase-a with reference to the midpoint of dc source. As expected, it has three main voltage levels (-200, 0 and +200), while its maximum voltage jump is almost 150 V during switching time.
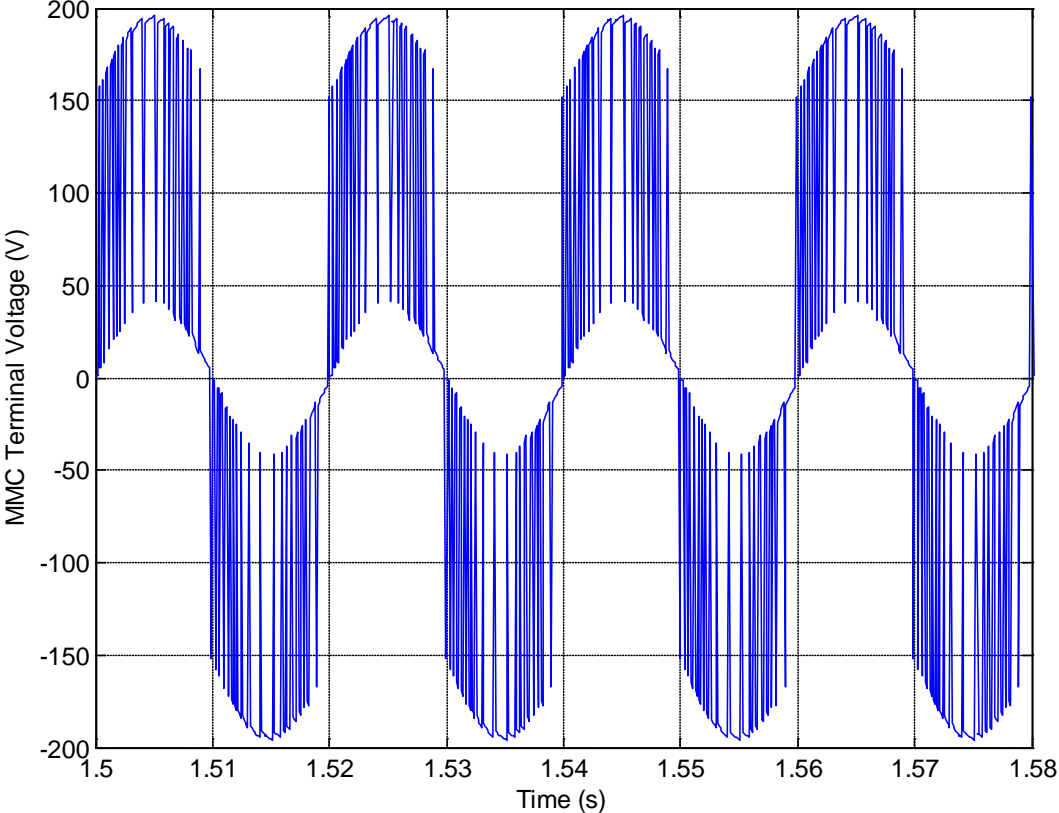
Fig.5.8 The MMC terminal (pole) voltage of phase-a

The upper and lower arm voltages have been depicted in the following figure. They have 180° phase shift oscillating between 0 and 400 V.
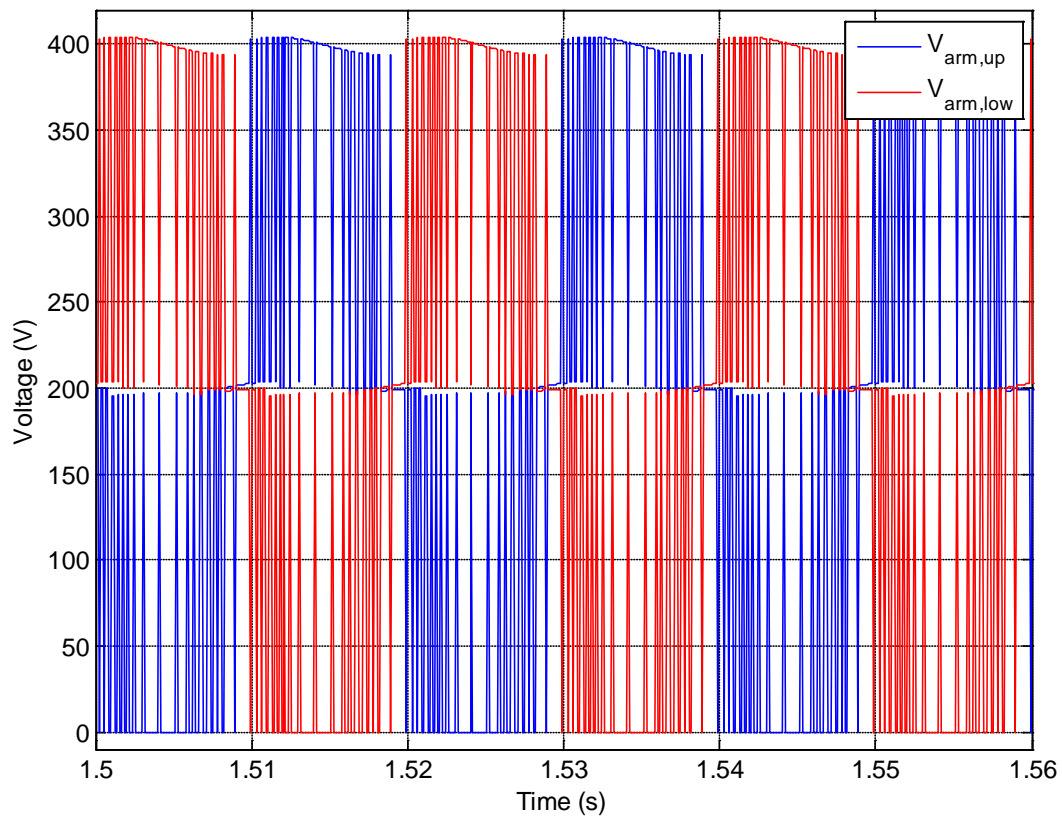
Fig.5.9 The upper and lower arm voltages of phase-a

The following figures show the frequency spectrum of the output current (logarithmic scale), the terminal voltage and the circulating current. Total Harmonic Distortion (THD) has been calculated by FFT analysis of SIMULINK. The load current's THD is small and equal to 4.43% and its fundamental frequency amplitude is 14.9A. However, the pole voltage THD is 48.10% that is relatively high. According to Fig.5.11, the largest harmonics occur around 3kHz; as a result, the switching frequency is mostly around 3 kHz (order of 60).
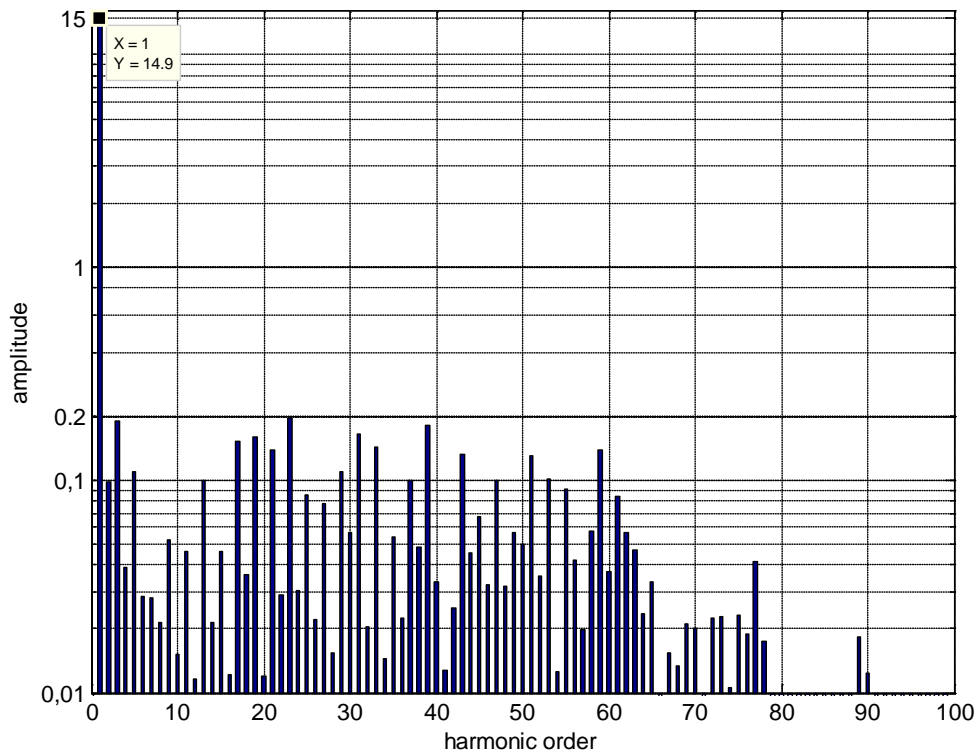
Fig.5.10 The load current frequency spectrum (logarithmic scale)
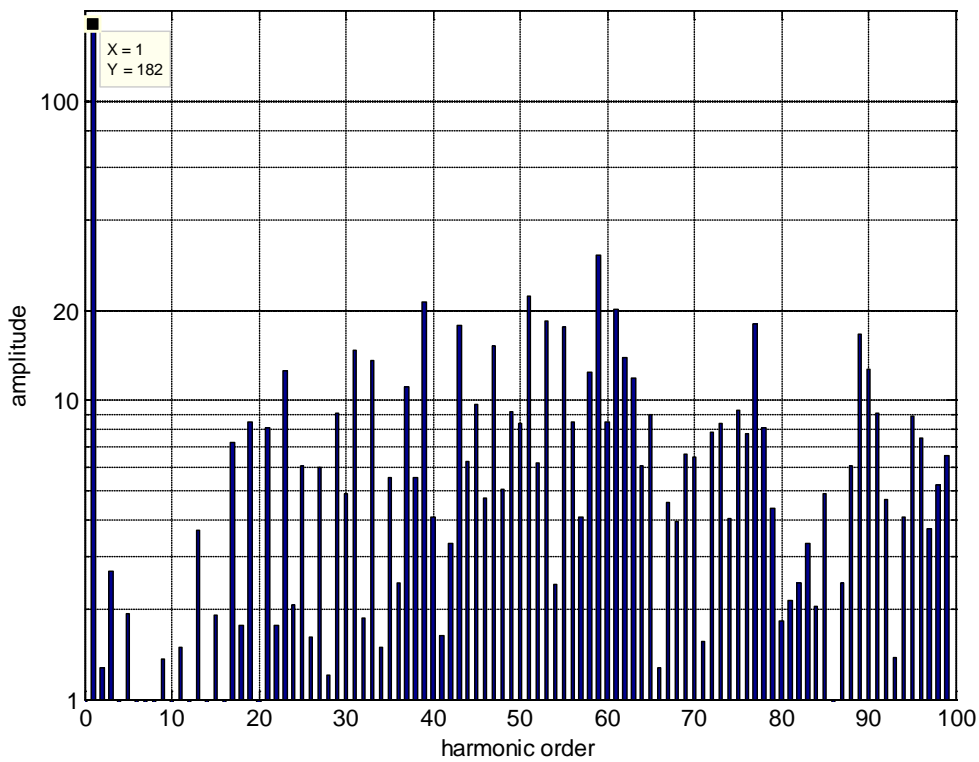
Fig.5.11 The pole voltage frequency spectrum (logarithmic scale)

As explained earlier, the ideal waveform of the circulating current is a pure sinusoidal with double frequency of system and according to Fig.5.12, the controller has been designed appropriately to minimize the circulating current. In the next section, the circulating current minimization term will be removed from the cost function in order to observe its effect clearly.
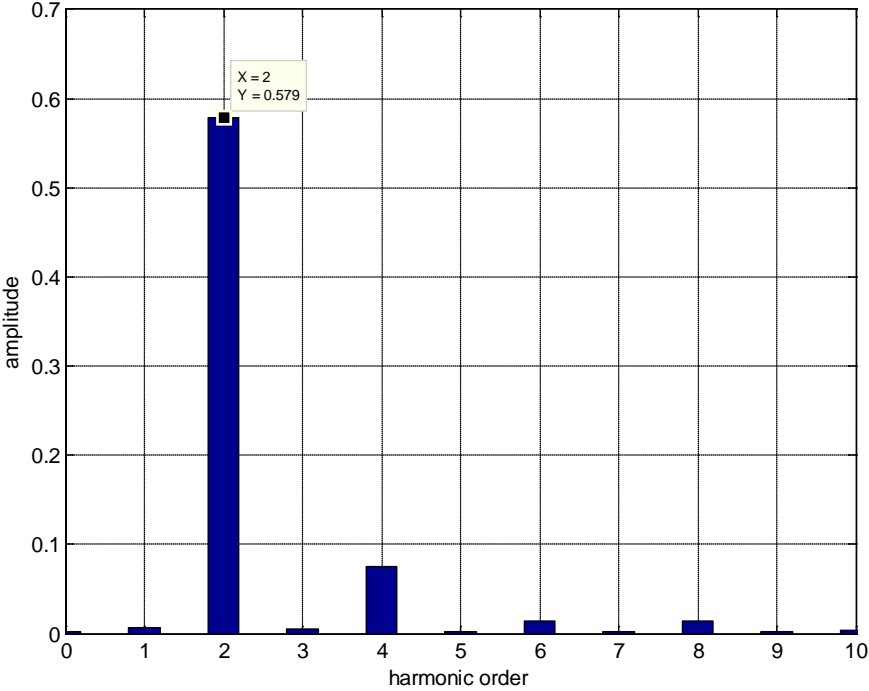
Fig.5.12 the circulating current frequency spectrum

5.4.2 Cost function without circulating current minimization term (λ_2=0)

It would be interesting to know the result of eliminating circulating current part ($\lambda_2 = 0$) from the cost function of Eq.5.29. If so, the load current follows its reference as well, but the circulating current has harmonics and its peak-to-peak value is 5 A (Fig.5.13) which is much higher than 1.4 A in previous section. MMC loss will increase and as a result, the system efficiency will decrease that is undesirable.

The frequency spectrum of circulating current has been given in Fig.5.14. It is clearly seen that it is not a 100 Hz sinusoidal signal which is its ideal waveform.

46
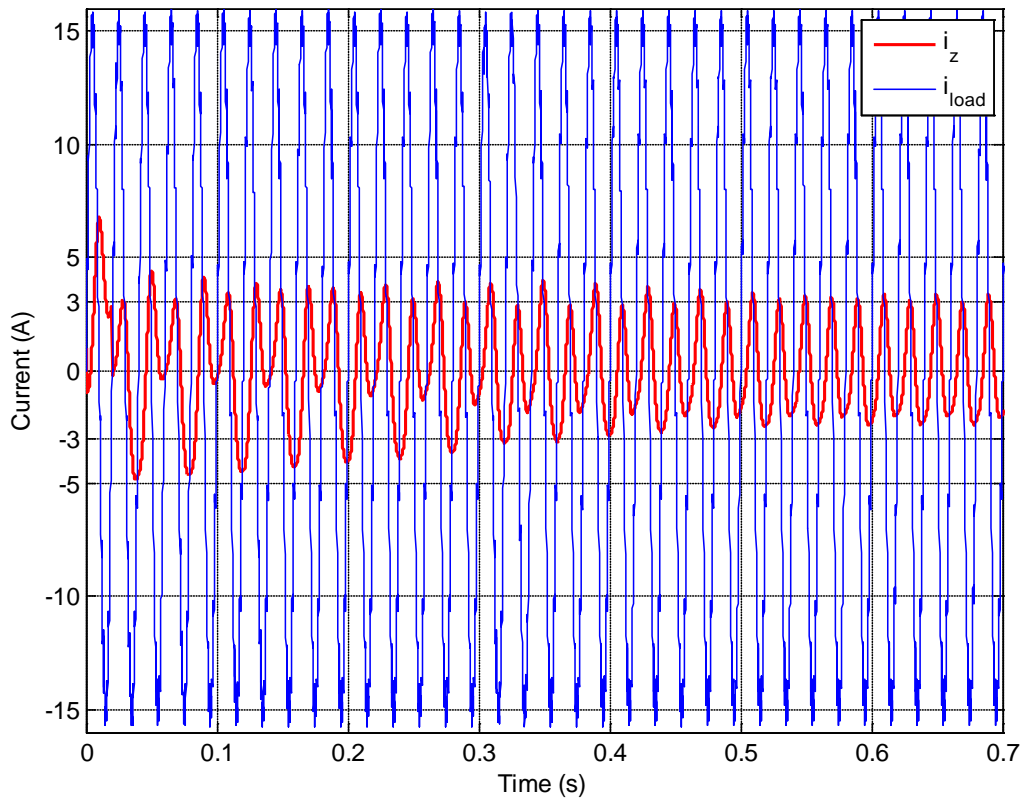
Fig.5.13 The phase-a load current and circulating current ($\lambda_2=0$)
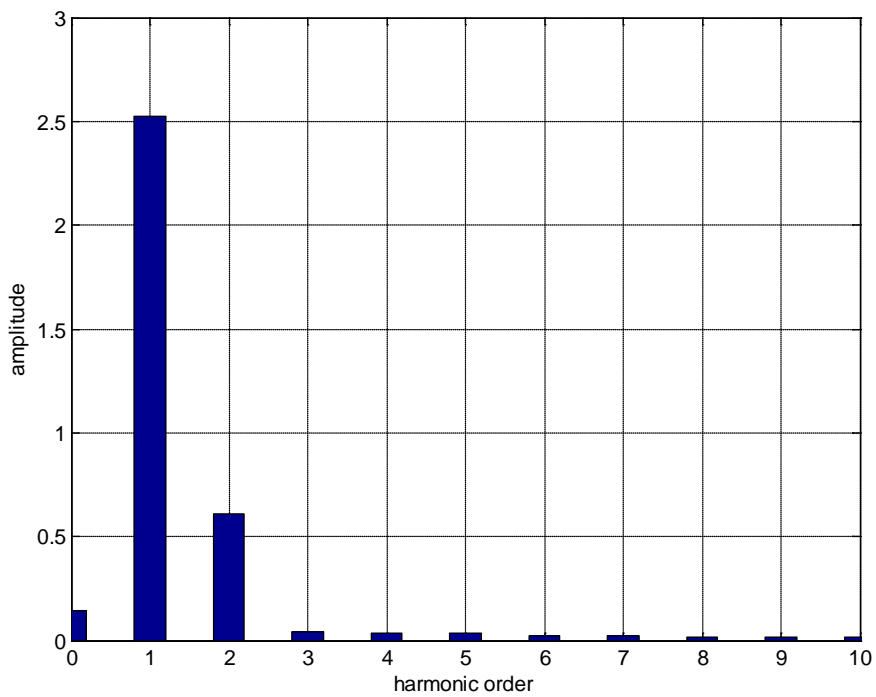
Fig.5.14 Frequency spectrum of circulating current ($\lambda_2=0$)

Moreover, the capacitor voltages will not be precisely in order (Fig.5.15 and 5.16) and it may affect the MMC performance in long term.
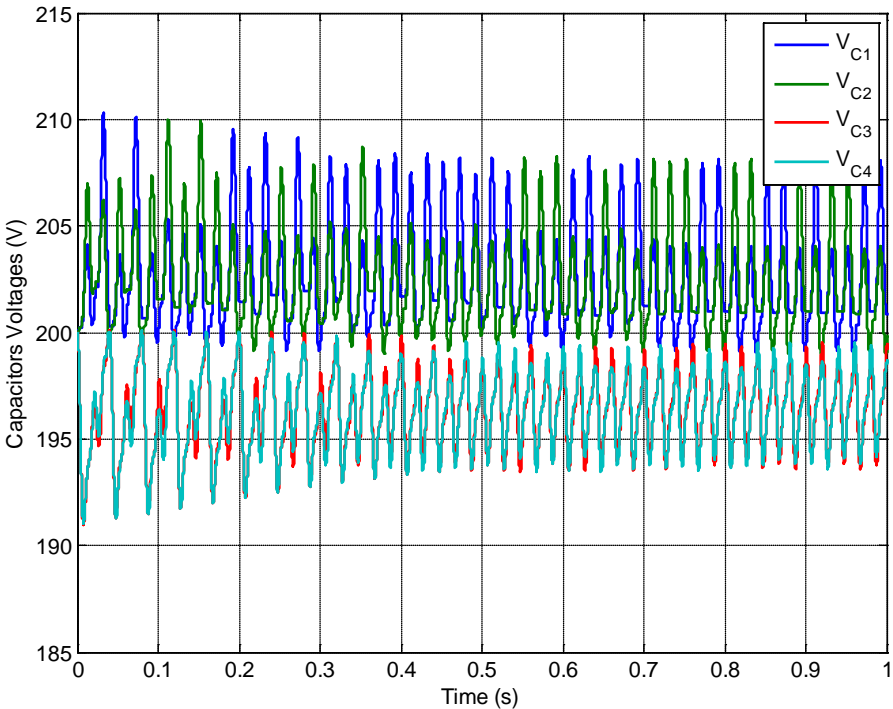
Fig.5.15 Capacitors voltages in the first second of simulation ($\lambda_2=0$)
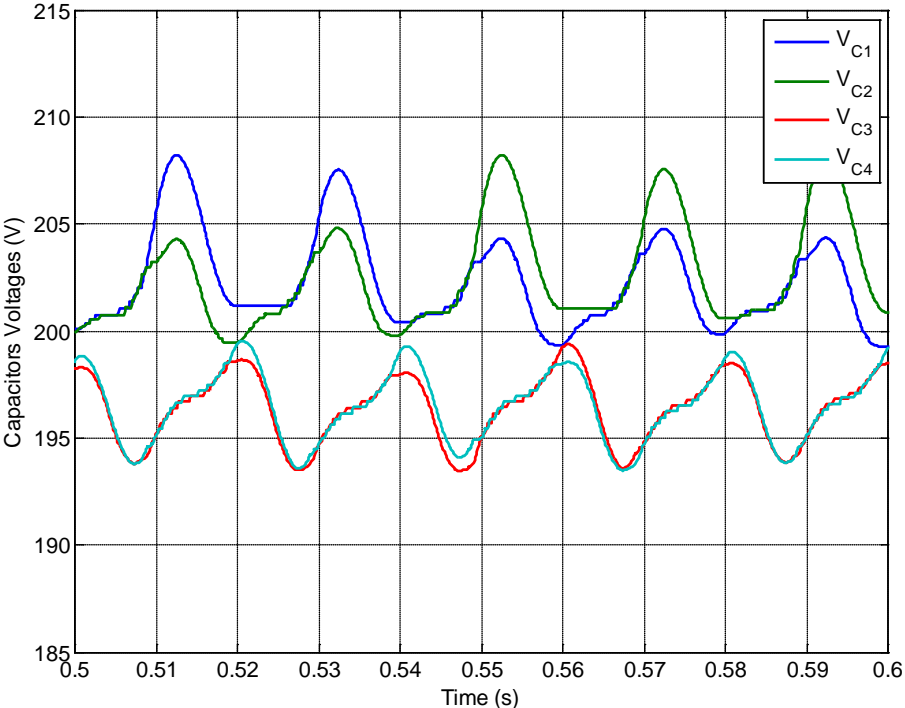
Fig.5.16 Capacitors voltages in steady state ($\lambda_2=0$)

However, adding the circulating current minimization part to the cost function reduces the reference current tracking significance to some extent. Consequently, the load current THD will increase from 4.32% to 4.43% and the terminal voltage THD will also increase from 46.49% to 48.10%. As the advantages of adding circulating current minimization to the cost function are more than its disadvantages, it is recommended to do consider this term in the cost function.

5.4.3 Applying backward and forward Euler methods

In order to observe the results of using the other discretization methods, new simulations have been done based on Eq.5.23-28, but no proper weighting factors have been found to get good results as previous sections. Fig.5.17 and 5.18 illustrate the load current, circulating current and capacitor voltages waveforms applying backward Euler method.
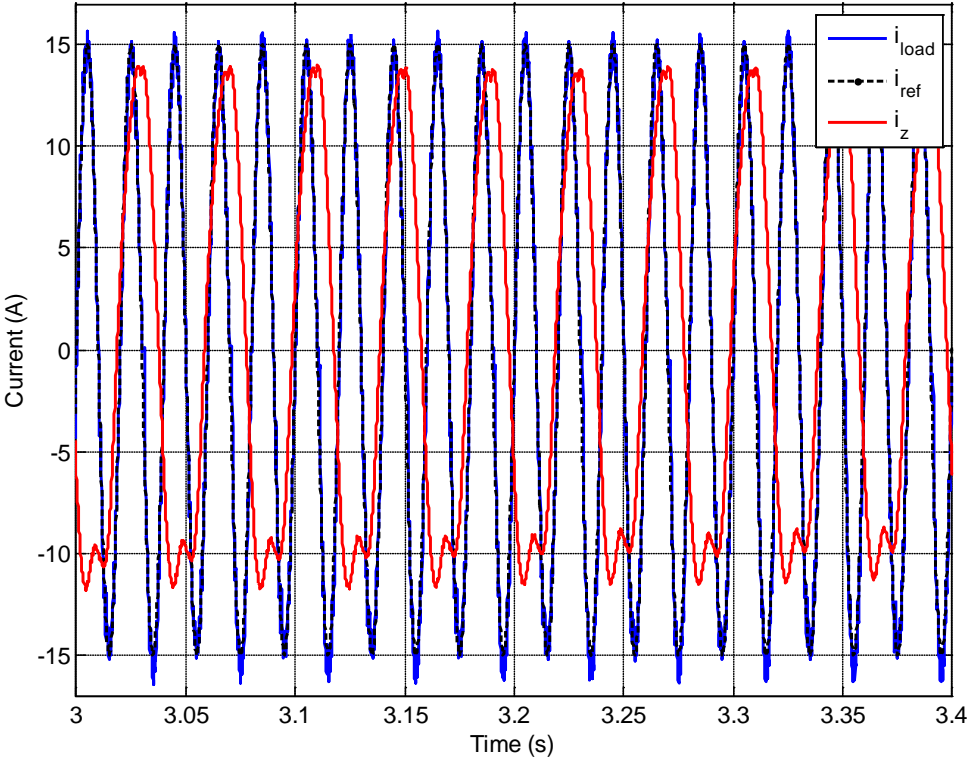
Fig.5.17 The phase-a load current and circulating current (backward Euler)
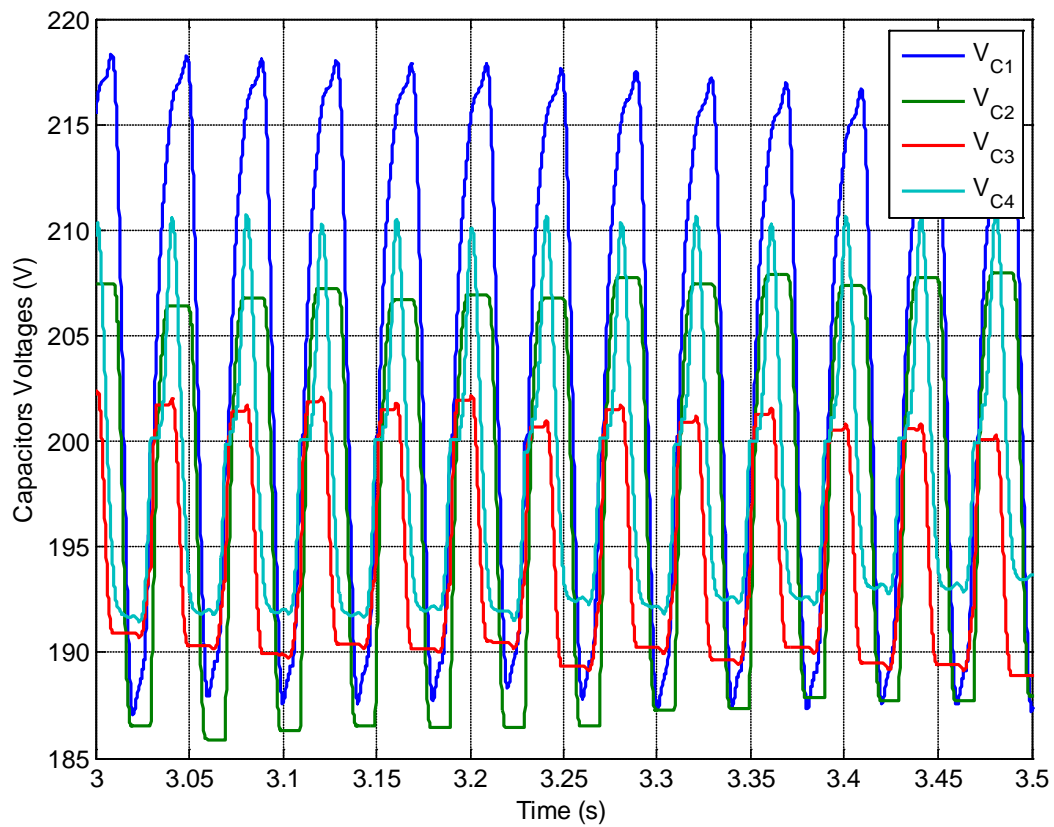
Fig.5.18 Capacitors voltages (backward Euler)

The results of forward Euler method are quite similar to the above waveforms with the best selected weighting factors. Hence, it can be concluded that the accuracy of system model plays an important role when designing an FCS-MPC for MMC and midpoint Euler discretization method is the best, because it provides the most accurate system model to predict the controlled variables.

5.5 Simulation results of a three-phase 5-level MMC

In this section, the proposed FCS-MPC will be applied to a three-phase 5-level MMC connected to an R-L-e load. The load can be motor or utility grid. Different fixed reference current signals will be applied to the controller to observe its performance. At first, identical sinusoidal reference signals will be used to observe normal operation of MMC and find the best weighting factors to overcome the challenges. Then, unbalanced sinusoidal signals, sinusoidal signals with additional third harmonic and trapezoidal signals will be applied to the controller to verify the reference tracking capability of it.

In addition, dynamic performance of the control system has been investigated by inserting disturbance to the system like DC source and load voltage source step change. Furthermore, the robustness of FCS-MPC control strategy has been investigated by including 20% measurement errors in load parameters.

The following figures illustrate the system model made in SIMULINK. The 5-level converter has 24 SMs (48 power switches).

Parameter	Symbol	Value
Number of SMs per arm	n	4
SM capacitor	C	6.6 mF
Arm inductance	l	1.2 mH
Arm resistance	r	44 mΩ
DC link voltage	V_{dc}	10 kV
Load resistance	R	5.9 Ω
Load inductance	L	9 mH
Rated line-line voltage	e_{l-l}	6.6 kV
Rated load current	I_n	200 A
Rated frequency	f	50 Hz

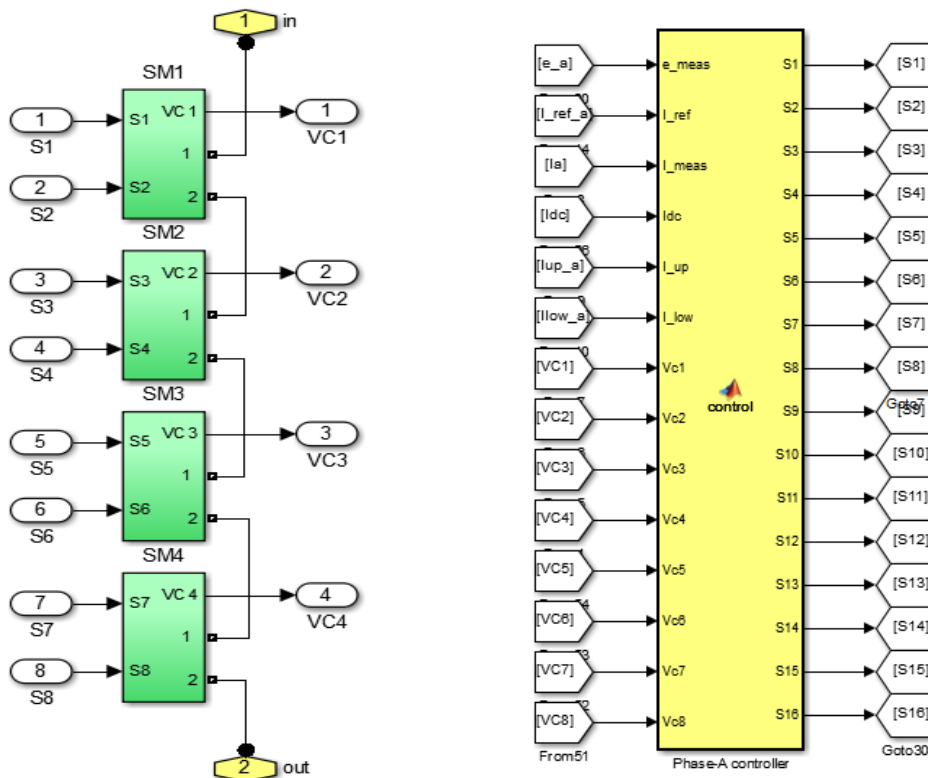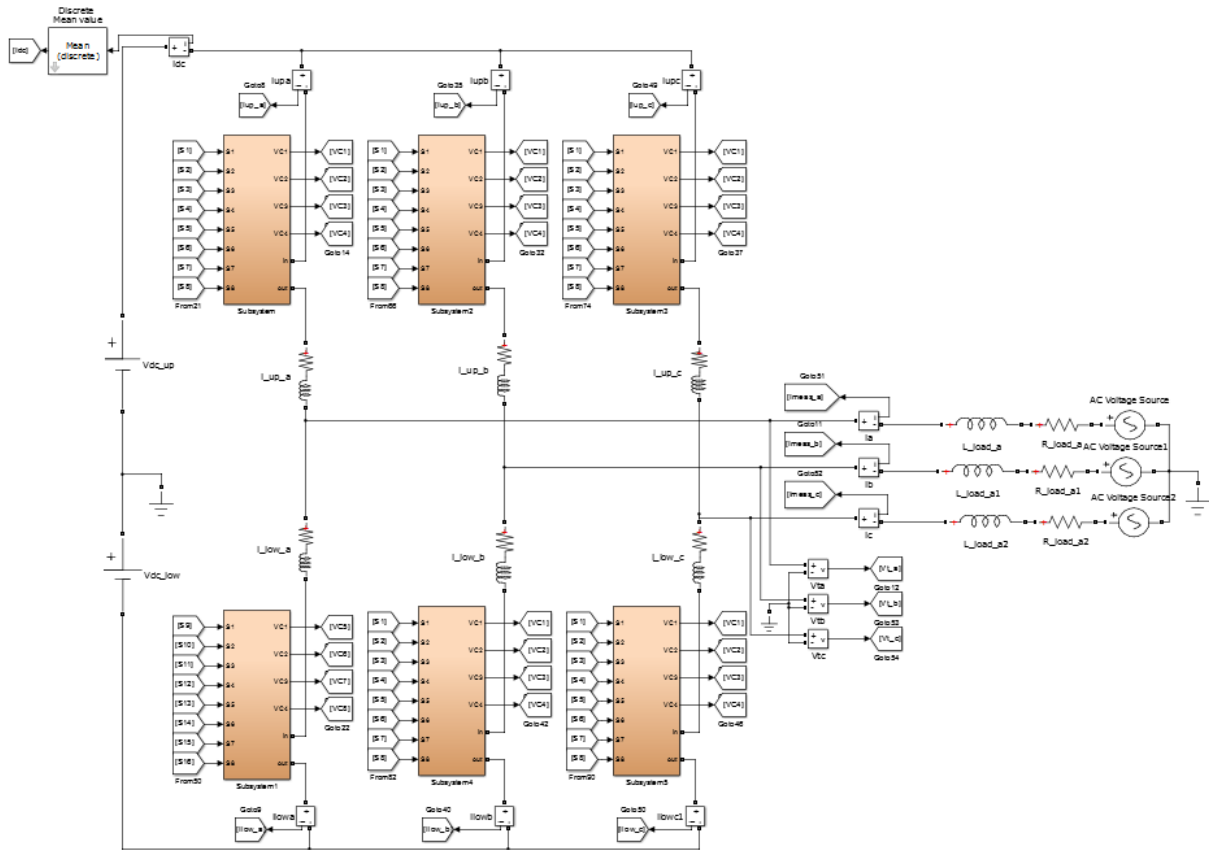Table5.2 Parameters of the system illustrated in Fig.5.19

Fig.5.19 The modeled MMC and its controllers in SIMULINK

The controller has two main parts: FCS-MPC controller and PI controller. The first one that is responsible for commanding the switches to be turned on or off in order to build the

load currents similar to their reference signals, keep the capacitor voltages balanced and minimize the circulating currents based on the predefined cost function (Eq.5.29). Midpoint Euler discretization method has been selected due to its high accuracy. There are three identical FCS-MPC controllers for each phase and they work in parallel. The control block diagram of the system has been displayed in Fig.5.20.
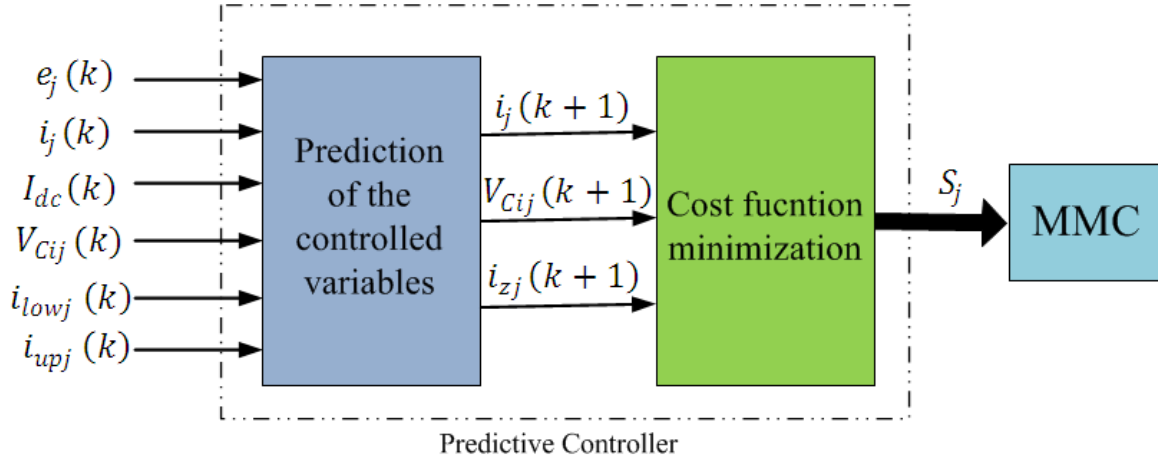
Fig.5.20 The system control block diagram

The load and converter parameters have been given in Table5.2. According to these parameters, the main equations for predicting the controlled variables are as follows:

$$i_j(k + 1) = 0.9402 i_j(k)$$
$$+0.0025 \left[v_{lowj}(k + 1) + v_{lowj}(k) - v_{upj}(k + 1) - v_{upj}(k) - 4e_j(k) \right] \quad (5.33)$$

$$i_{zj}(k + 1) = 0.9963 i_{zj}(k) \quad (5.34)$$
$$+0.0208 \left[2V_{dc} - v_{upj}(k + 1) - v_{upj}(k) - v_{lowj}(k + 1) - v_{lowj}(k) - \frac{4r}{3} I_{dc}(k) \right]$$

$$v_{Cij}(k + 1) = \begin{cases} v_{Cij}(k) & SM\ is\ OFF \\ v_{Cij}(k) + 0.0152 \left[i_{upj}(k) \right] & Upper\ arm\ SM \\ v_{Cij}(k) + 0.0152 \left[i_{lowj}(k) \right] & Lower\ arm\ SM \end{cases} \quad (5.35)$$

For predicting the capacitors voltages, forward Euler equation (Eq.5.28) has been selected. Its simplicity is the main reason for this selection, while its accuracy is high enough and acceptable. In contrast with the other methods, there is no need for calculating $i_{upj}(k + 1)$ and $i_{lowj}(k + 1)$ which is an advantage.

The cost function has been defined as follows ($\lambda_1 = 2, \lambda_2 = 1$):

$$g = \left| i_{jref}(k) - i_j(k+1) \right| + 2. \sum_{i=1}^{8} \left| v_{Cij}(k+1) - \frac{V_{dc}}{4} \right| + 1. \left| i_{zj}(k+1) \right| \qquad (5.36)$$

5.5.1 Verifying the performance of the proposed controller in steady state

In the beginning of this section, three identical pure sinusoidal reference signals will be applied to the controller to verify its performance. Their amplitude is equal to 200 with 50 Hz frequency. Sampling time is 100μs. The load currents and their references have been illustrated in Fig.5.21.
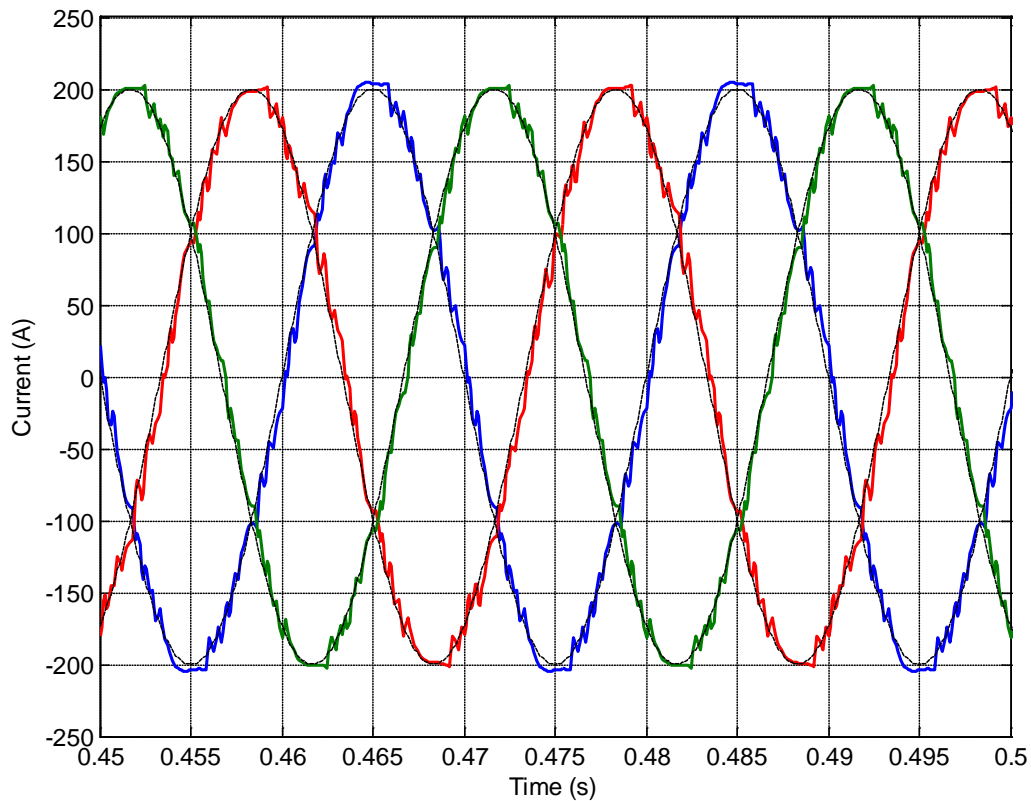
Fig. 5.21 The load Currents in steady state
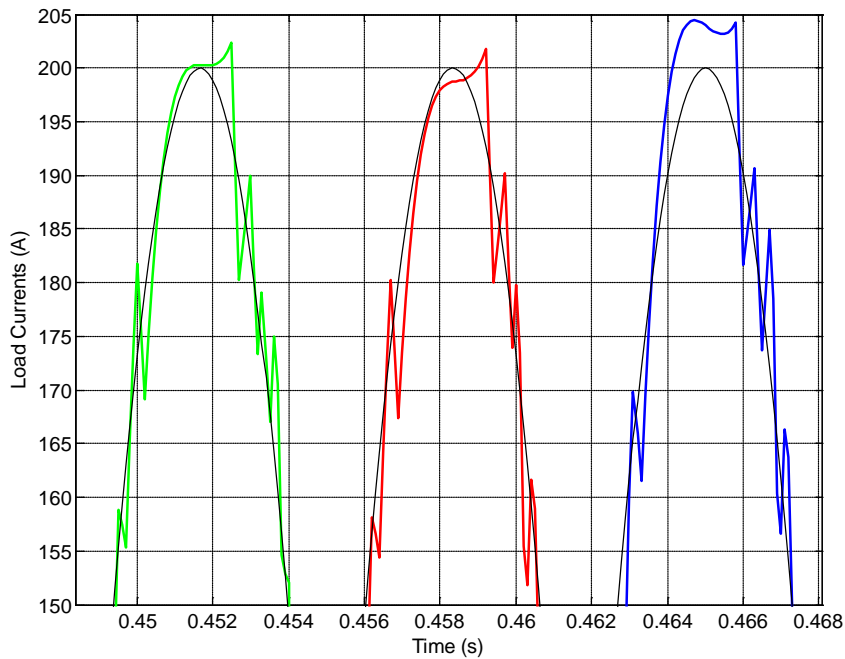
Fig. 5.22 The focused view of load currents and the ripples

The load currents are tracking their references very well, while small ripples can be observed in the measured load currents and they have been focused in Fig.5.22. The controller has done its reference tracking responsibility very well.

In order to find out the harmonics contribution of the load currents, its frequency spectrum would be helpful. Because of the 10kHz sampling frequency, the frequency spectrum has been depicted up to 5kHz (Fig.5.23). According to this figure, the 50Hz current amplitude is 199A and the THD of the load current is small (3.4%). As the observation of harmonics magnitude is very important to find the switching frequency, Fig.5.23 gives a focused view of them in ordinary (not logarithmic) scale. Their magnitude reaches 2A in the worst case and they are mostly concentrated in the frequencies less than 2500 Hz. Consequently, it seems that the switching frequency is variable but less than 2500 Hz (one fourth of sampling frequency) which is acceptable in practice.

Figure 5.24 contains the arm currents, load current and circulating current of phase-a. The upper arm and lower arm currents have 180° phase difference that is correct. They mainly have three frequency components; ac component that has 50 Hz frequency and it transfers power to the load, dc component (zero frequency) and second order harmonic (100 Hz) that is the circulating current. In this case, its amplitude is roughly 80 A.
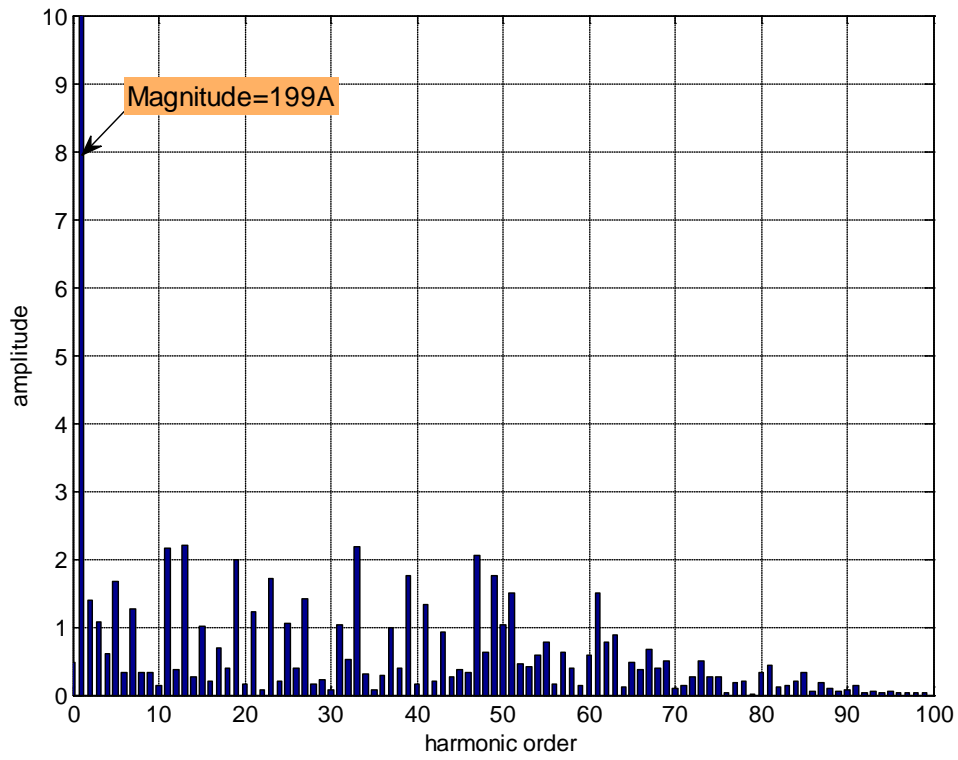
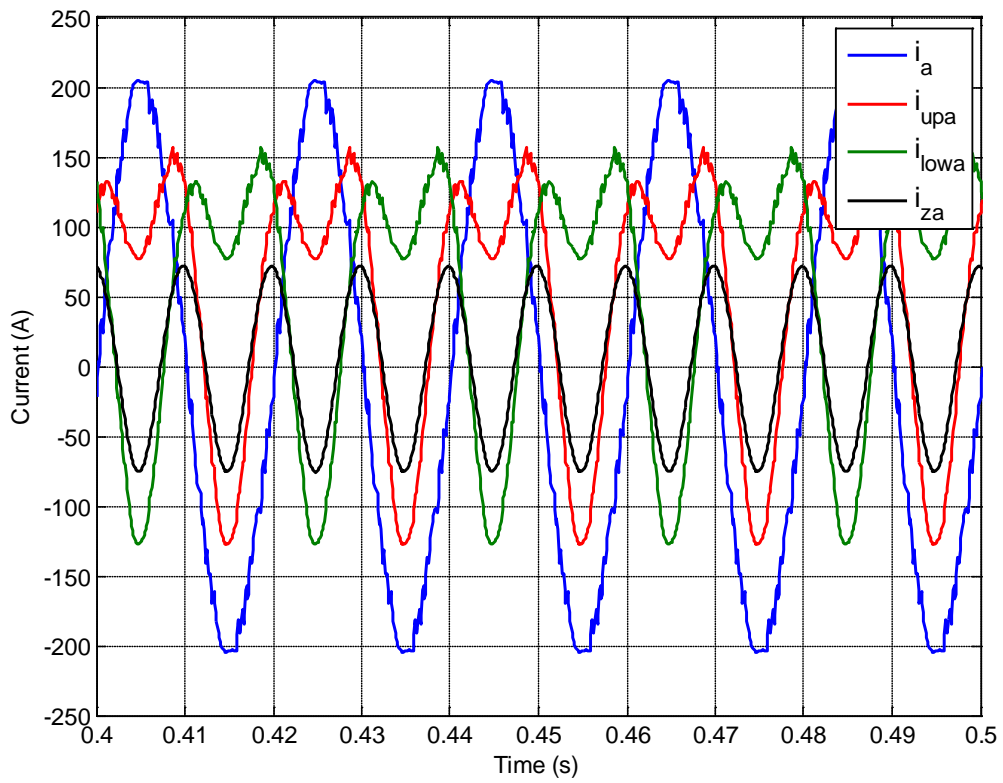Fig. 5.23 The frequency spectrum of the load currents (one phase)

Fig. 5.24 The load, circulating and arm currents of phase-a in steady state

56

As mentioned earlier, the circulating currents are necessary for the MMC operation and their existence is due to capacitors charging and discharging process that leads to change in the upper and lower arm voltage level. The circulating current waveform is dependent on its weighting factor in the cost function. Their ideal waveform is pure 100 Hz sinusoidal and if this waveform is achieved by selecting the best weighting factors, the amplitude cannot be reduced anymore. In the other words, the circulating current is minimized whenever its waveform gets close to a pure 100 Hz sinusoidal one and this is the sign of appropriate weighting factors selection. However, without considering them in the cost function or by a poor weighting factor selection, their waveforms contain a lot of harmonics with much higher amplitude that increase the converter loss and power switches ratings.

Fig.5.25 shows the frequency spectrum of the phase-a circulating current that is an evidence of the proposed FCS-MPC success in circulating current minimization.
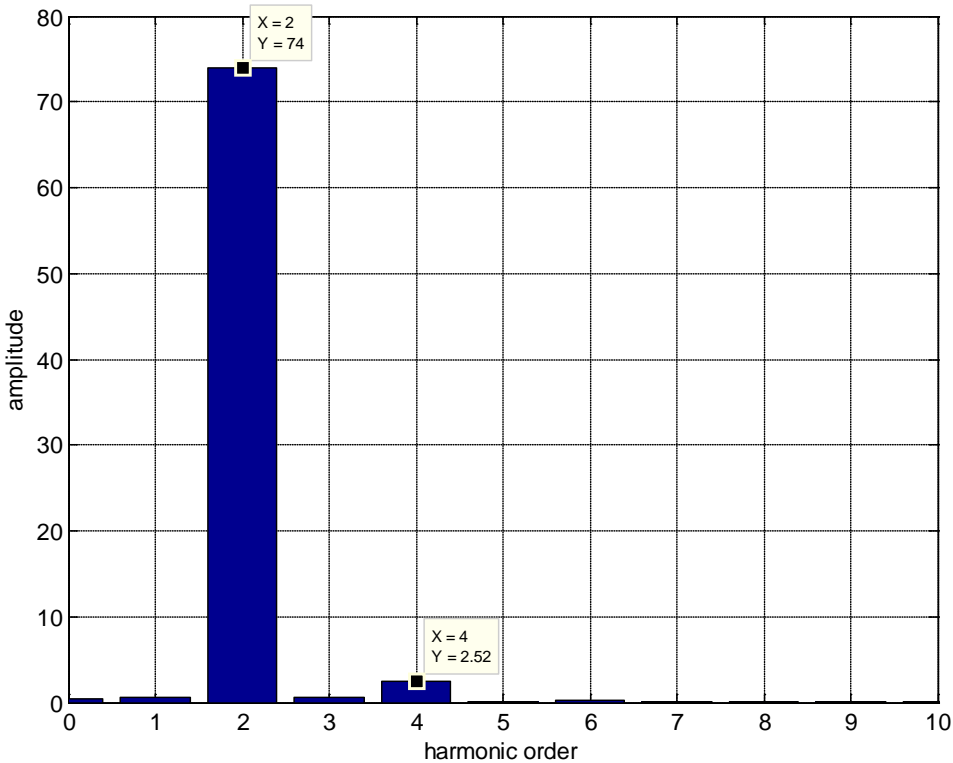
Fig.5.25 The circulating current frequency spectrum (phase-a)

The MMC pole (terminal) voltages in steady state have been illustrated in Fig.5.26. While the terminal voltages are varying from -5kV and +5kV, they have five voltage levels roughly equal to 2.5kV as expected. Moreover, the fundamental components amplitude is 5030V.
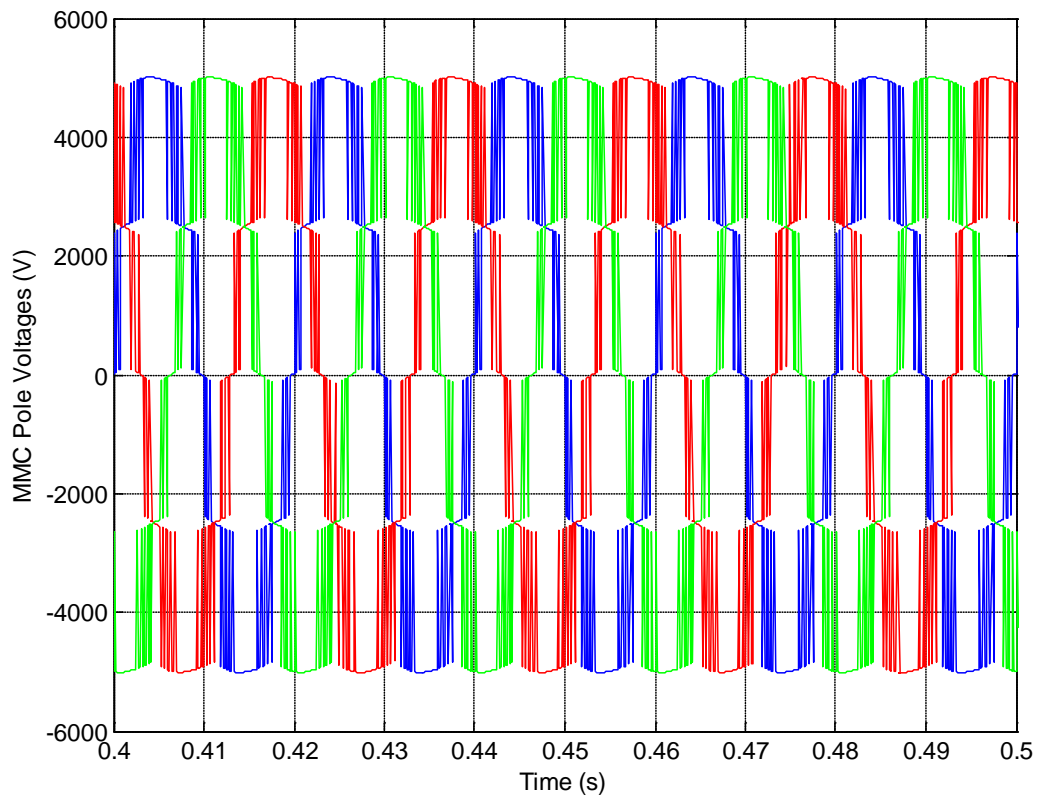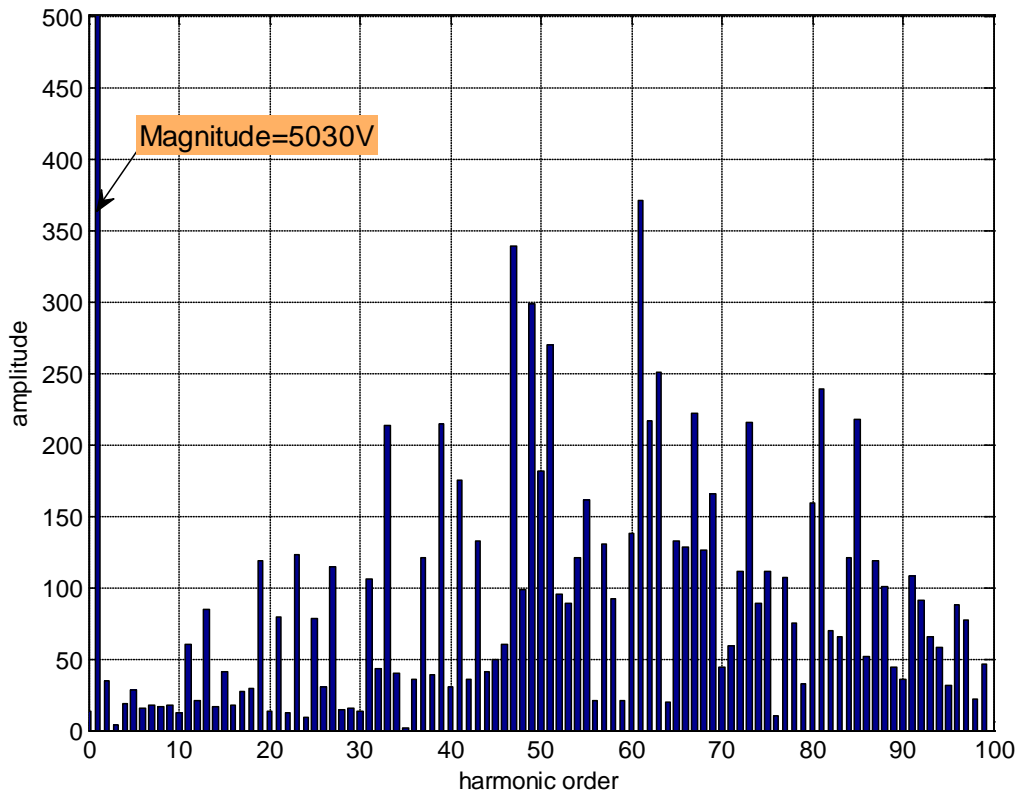
Fig.5.26 MMC pole Voltages

Fig.5.27 The frequency spectrum of pole voltage (one phase)

58

The frequency spectrum of MMC pole voltage (phase-a) has been given in Fig.5.27. THD is calculated by FFT analysis of SIMULINK and is equal to 23.4%. As the concentration of harmonics with larger magnitude is higher between 1500 Hz and 3000 Hz, the switching frequency is mostly in this range. In addition, the low order harmonics are relatively small and acceptable and this is another advantage of the FCS-MPC control strategy.

The capacitor voltages waveforms are the next important and interesting ones shown in Fig.5.28. They are completely in order and oscillating between 2465V and 2535V (i.e. is 70V peak to peak) and they have been kept around the nominal value ($V_{dc}/4=2.5$kV). The upper arm (lower arm) capacitors of one phase are charging and discharging at the same time, while their voltages have 180° phase shift with lower arm (upper arm) capacitors. Therefore, the FCS-MPC can be counted as a powerful control strategy for keeping the capacitors voltages balanced.

The voltage of upper arms capacitors have been shown in solid lines while the voltage of lower arm capacitors have been depicted in dotted lines and each phase has a specific color.
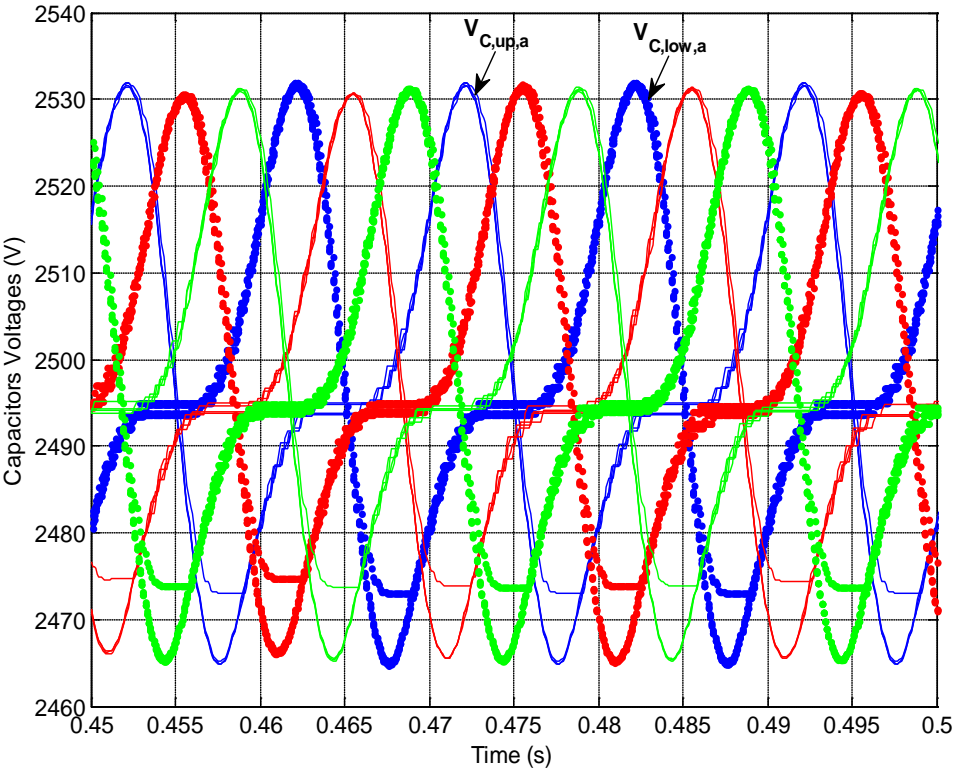

Fig.5.28 The capacitors voltages

59

According to the above simulation results, it can be concluded that the proposed control strategy is capable of controlling MMC output currents in addition to keeping the capacitors voltages balanced and minimizing the circulating currents at the same time.

However, the accuracy of the control scheme in current reference tracking depends on the sampling frequency directly. Higher sampling frequency reasonably leads to less output current error with its reference and less ripple as a result. As mentioned earlier, the switching frequency of MMC is mainly one fourth to one third of sampling frequency; therefore, there is a tradeoff between having high accuracy and low switching frequency which is directly related to the switching loss.

It would be interesting to see the controller performance in lower sampling frequencies. In this part, the sampling frequency is halved (5kHz). The following figures are the output currents and capacitors voltages in time domain and the frequency spectrum of the load current and pole voltage of phase-a.
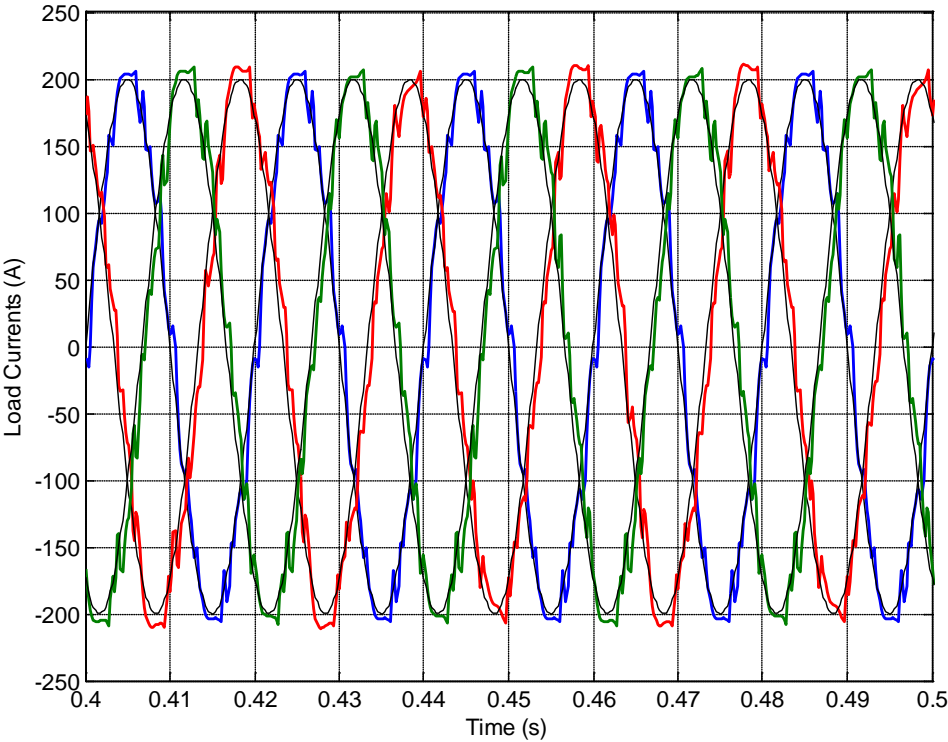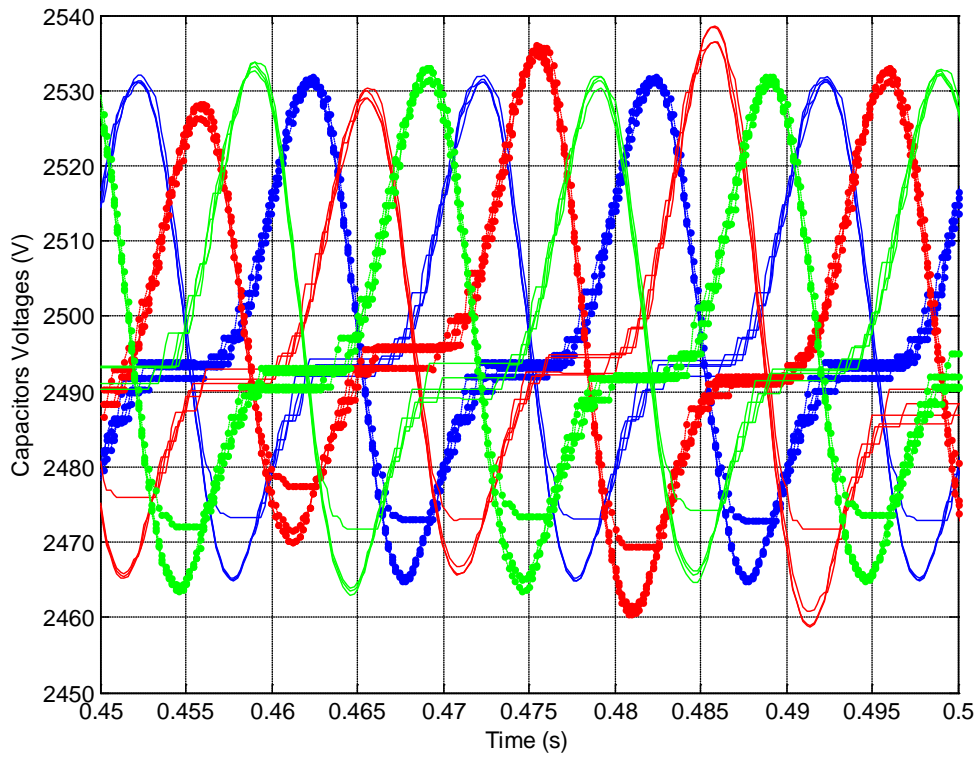

Fig.5.29 The load currents (Ts=200us)

60

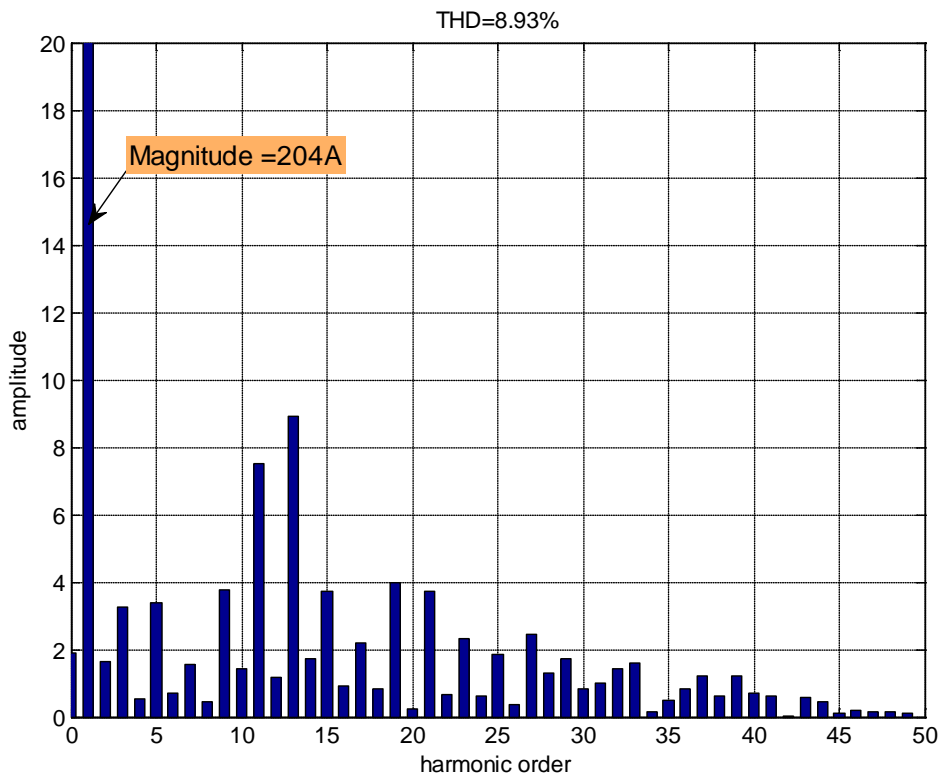Fig.5.30 The capacitors voltages (Ts=200us)

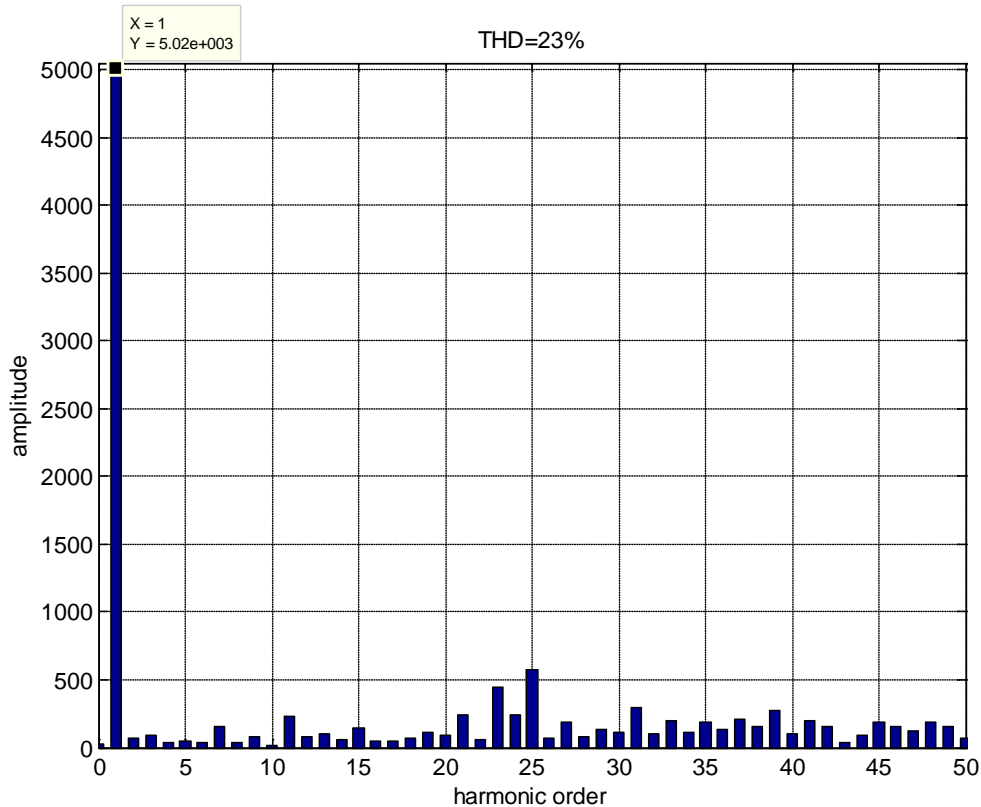Fig.5.31 The frequency spectrum of load current (A)

61

Fig.5.32 The frequency spectrum of pole voltage (V)

Although the output currents are not following the references as accurate as before, the ripple is in an acceptable range. The capacitors voltages have been remained balanced while the peak to peak value has increased a little which is inevitable due to the switching frequency decrease. The worthy result of decreasing the sampling frequency is reducing the switching frequency (mostly 1.5kHz) as expected. If the sampling frequency is reduced to less than 3kHz, the load currents harmonics increase that leads to have a THD higher than 10%.

5.5.2 Current reference tracking verification

1) Applying unequal sinusoidal reference signals

The reference currents have been set to be unequal (210A, 190A and 170A). The following figures illustrate the load currents and capacitors voltages that are important and can be the proofs of the controller performance.
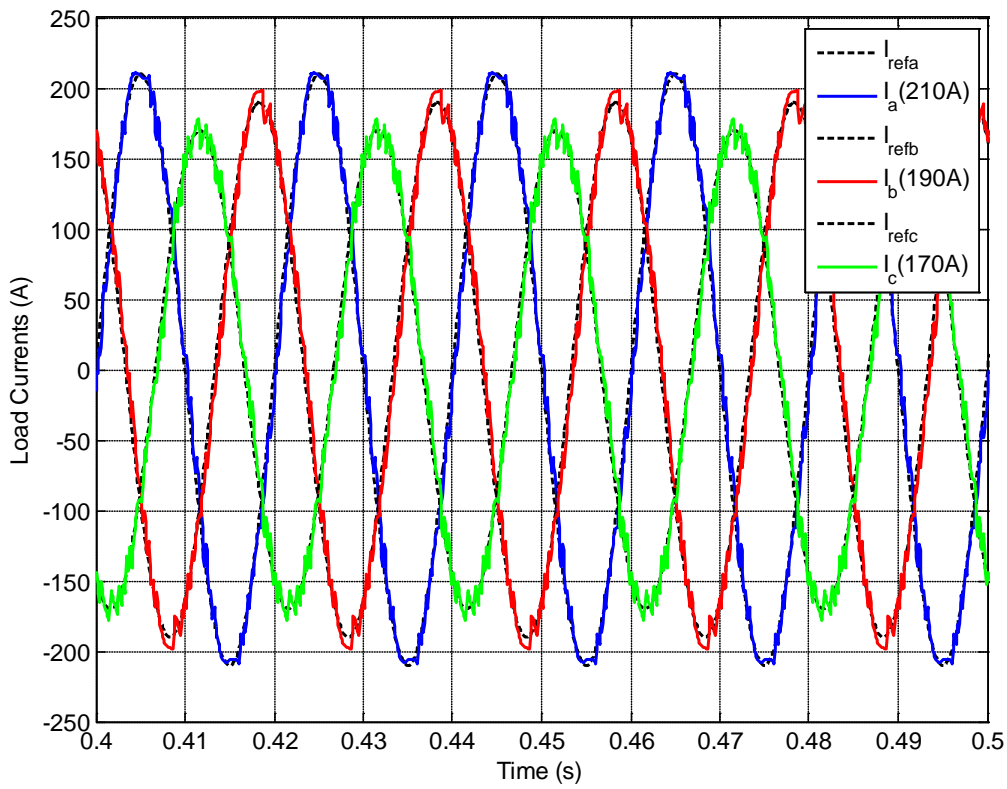
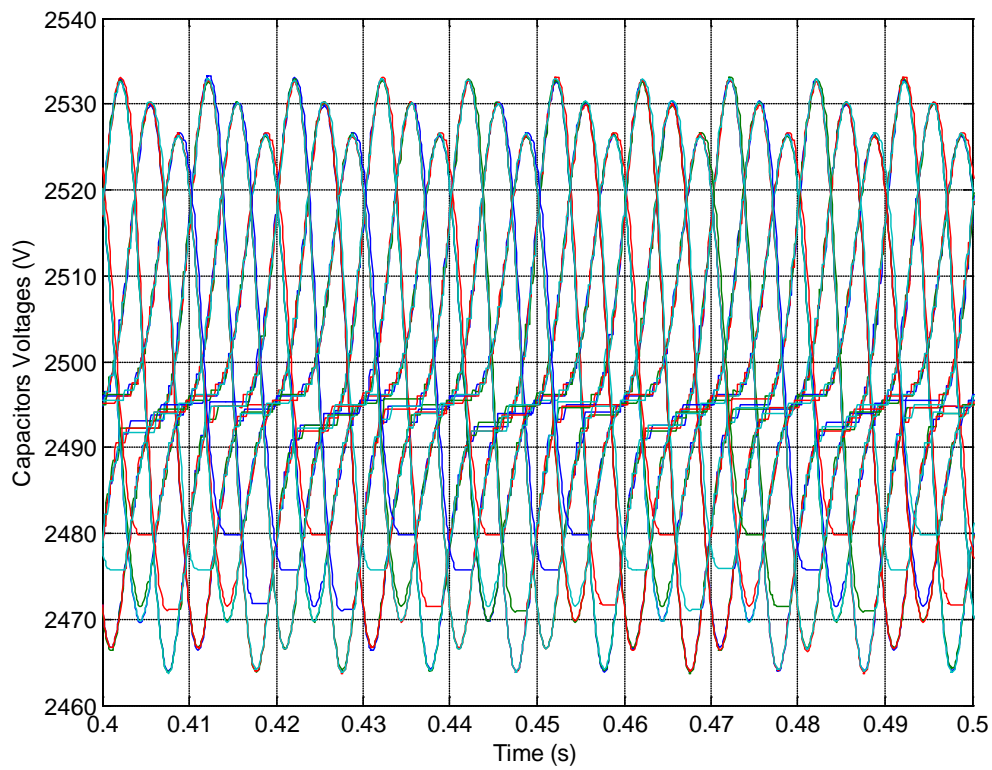Fig.5.33 The load currents with variable amplitudes

Fig.5.34 The capacitors voltages

63

According to the above figures, the controller is able to handle this situation as well. The load currents follow their references very well and the capacitors voltages have been kept around 2.5kV. However, the peak to peak value of the capacitors voltages are different that is reasonable due to the difference in current amplitude.

2) Adding third order harmonic to the reference signals

In some applications such as Shunt Active Power Filters (SAPF), there is need for the other types of reference signals. Therefore, in this section two different reference signals will be applied to the controller to observe the result of reference tracking.

At first, third harmonic component with the same amplitude (200A) has been added to the reference current signals. Fig.5.35 demonstrates the load currents.
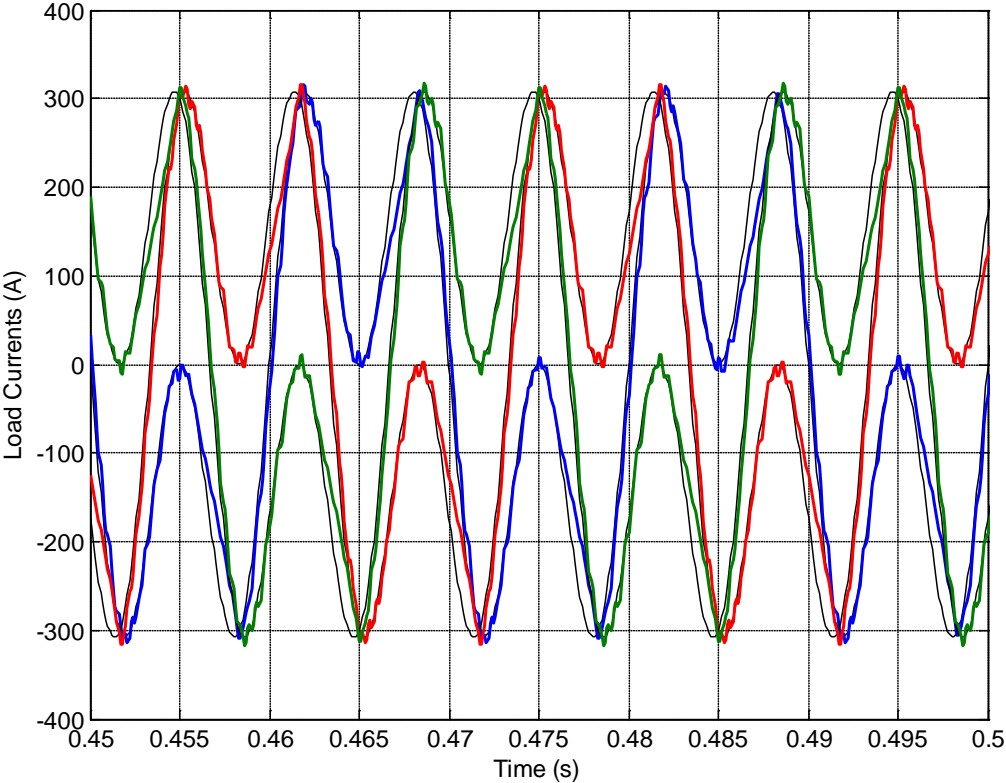

Fig.5.35 The load currents

The error between the reference signals and the measured currents is small. The following figure presents the capacitors voltages as the second task of the controller.
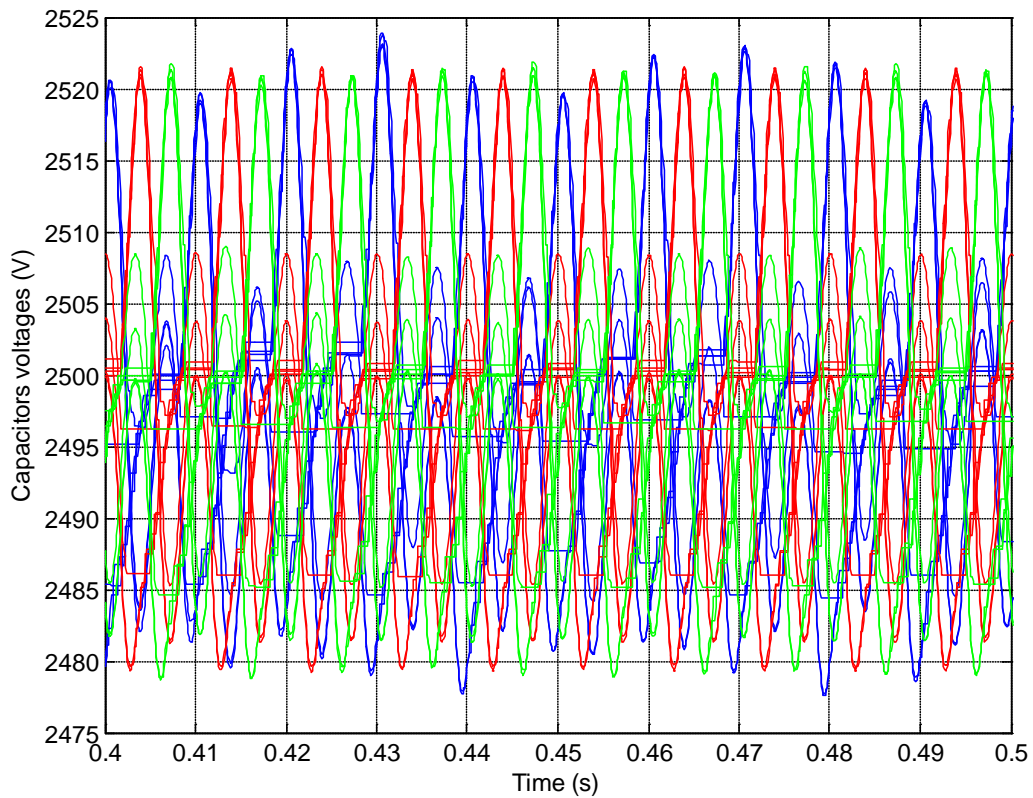
64

Fig.5.36 The capacitors voltages

As a result, the proposed control strategy can also manage this situation.

3) Applying trapezoidal signals as the reference

Fig.5.37 and 5.38 are presenting the load currents and capacitors voltages when trapezoidal signals are the references.

According to Fig.5.38, it takes time to reach steady state for the capacitors voltages due to the change in reference currents that have high order harmonics, but the whole procedure is less than 2 s.
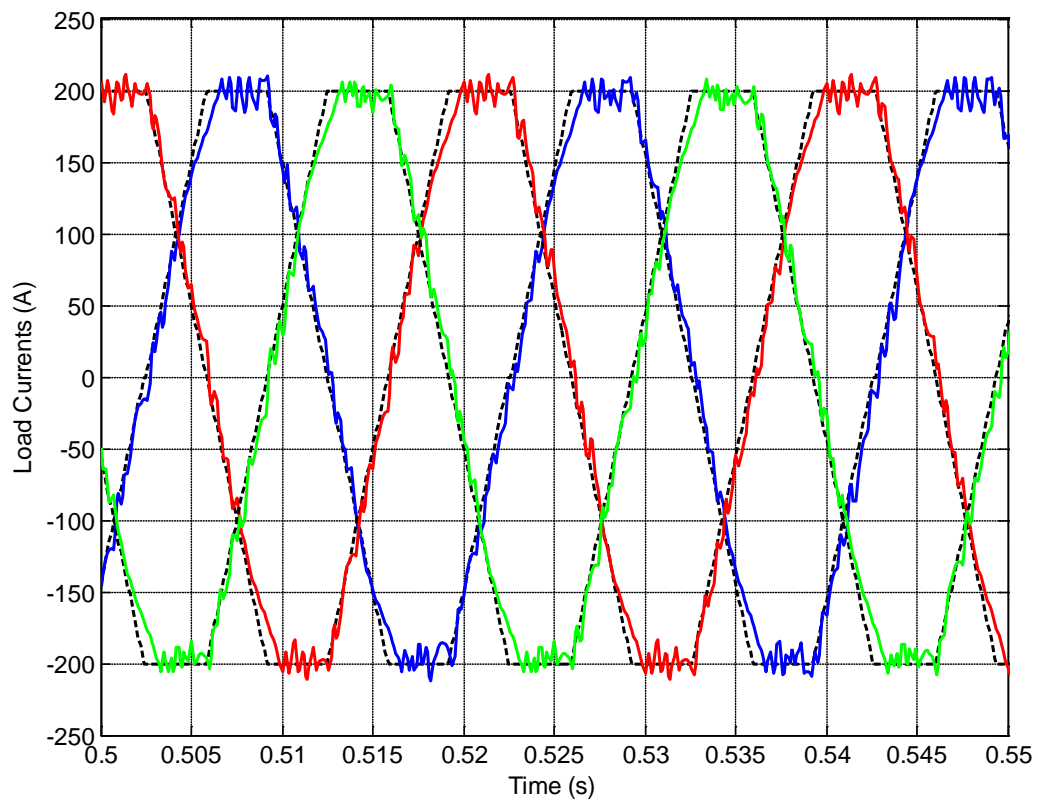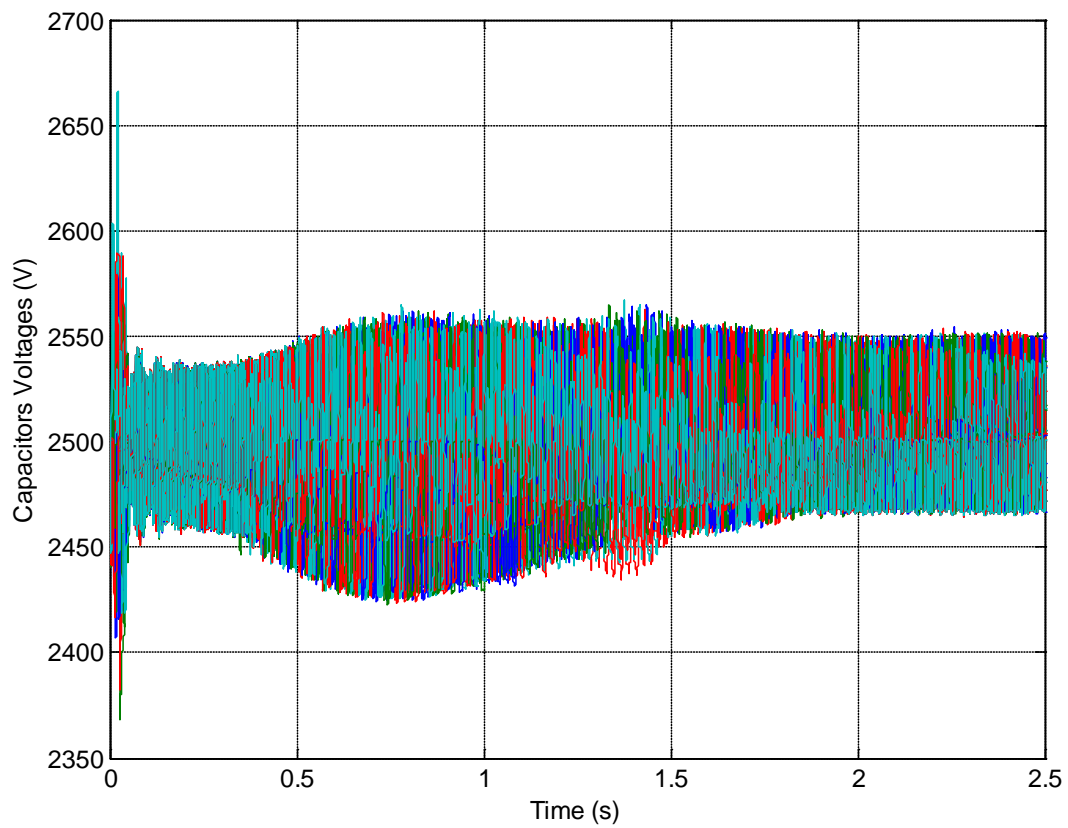
Fig.5.37 The load currents

Fig.5.38 The capacitors voltages

66

5.5.3 Including measurement errors

All measurements are exposed to some uncertainty as a wide range of errors and inaccuracies that might happen during the measuring process. Therefore, they should be considered in the system verification specially for verifying the robustness of the proposed controller. A robust controller should be able to perform its tasks properly in an acceptable range of measurement errors. In this section, the robustness of the proposed FCS-MPC controller will be tested by applying ±20% of measurement error to the load parameters.

The load inductor (L) and resistor (R) shown in Fig.5.1 are the presentations of the line and load inductance and resistance and it is very likely to measure these parameters inaccurately. The new system model equations will have R±ΔR.R and L±ΔL instead of R and L. In order to make a good comparison, it is useful to change the load parameters by two step function. The initial state is the contribution of ¬20% measurement error to the load parameters and then at t=0.45s, the parameters become ideally measured (0% error) and finally at t=0.5s, +20% measurement error will be considered in the system model of the controller. Fig.5.39 presents the load currents and their references.

It can be seen that there is almost no difference between the load currents and their ripples in different states. Fig.5.40 and Fig.5.41 show a focused view of phase-a current, as a sample, before and after t=0.45s.
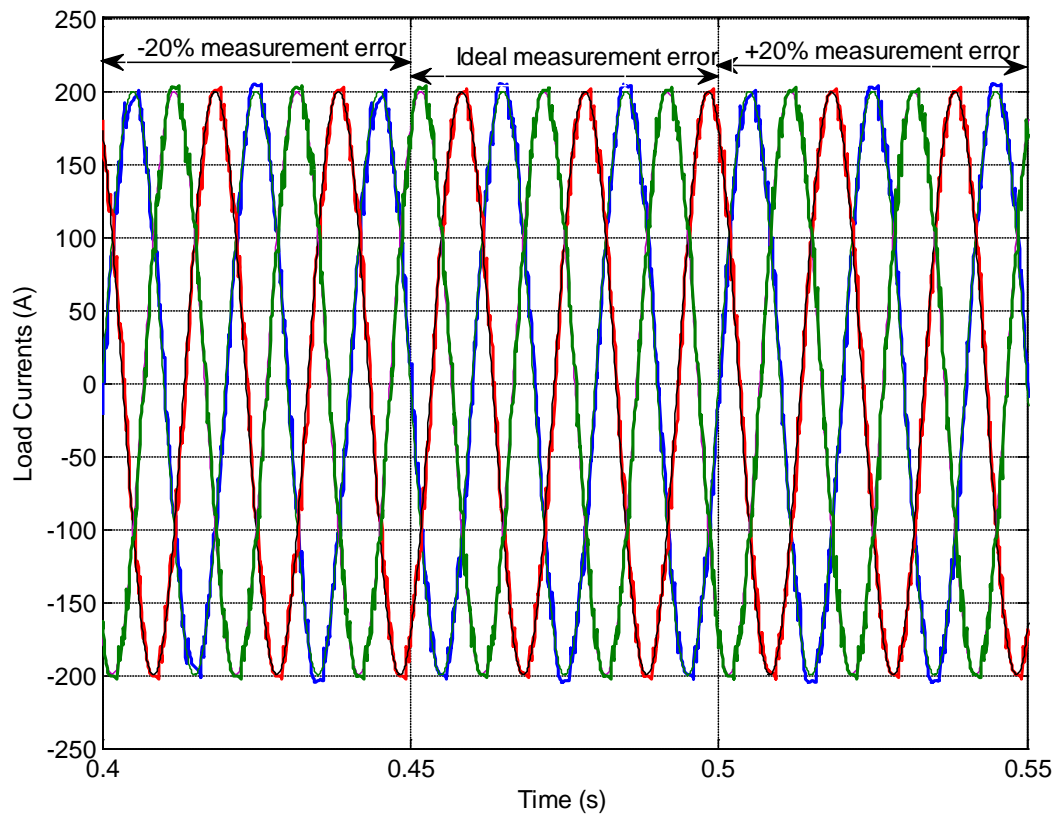
Fig.5.39 The load currents when measurement errors are present in load parameters
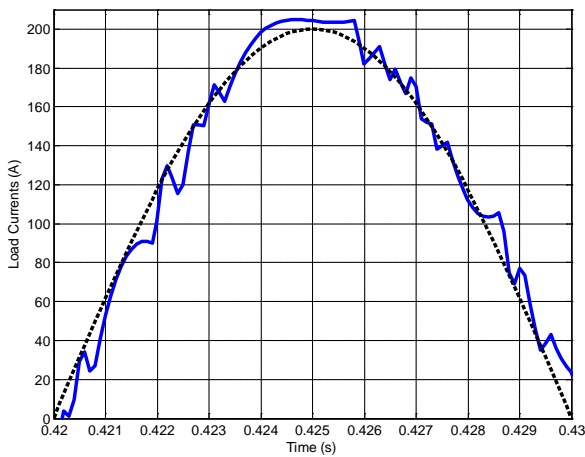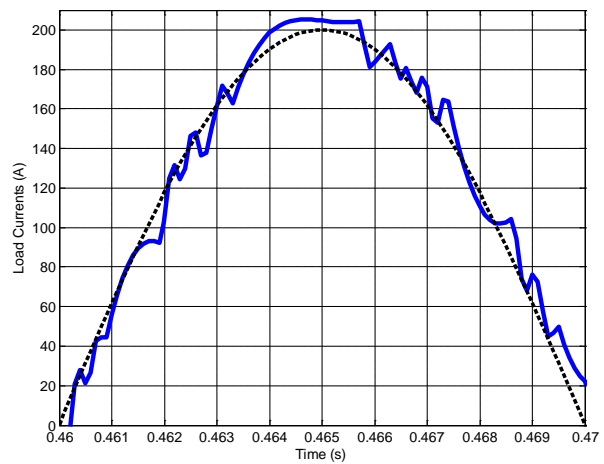

Fig.5.40 Phase-a current (¬20% error)

Fig.5.41 Phase-a current (0% error)

The MMC terminal voltages and capacitors voltages have been demonstrated in the following figures and again no considerable change can be observed when the measurement errors have been considered.

It can be concluded that the proposed control strategy is very robust against measurement errors in the load parameters.
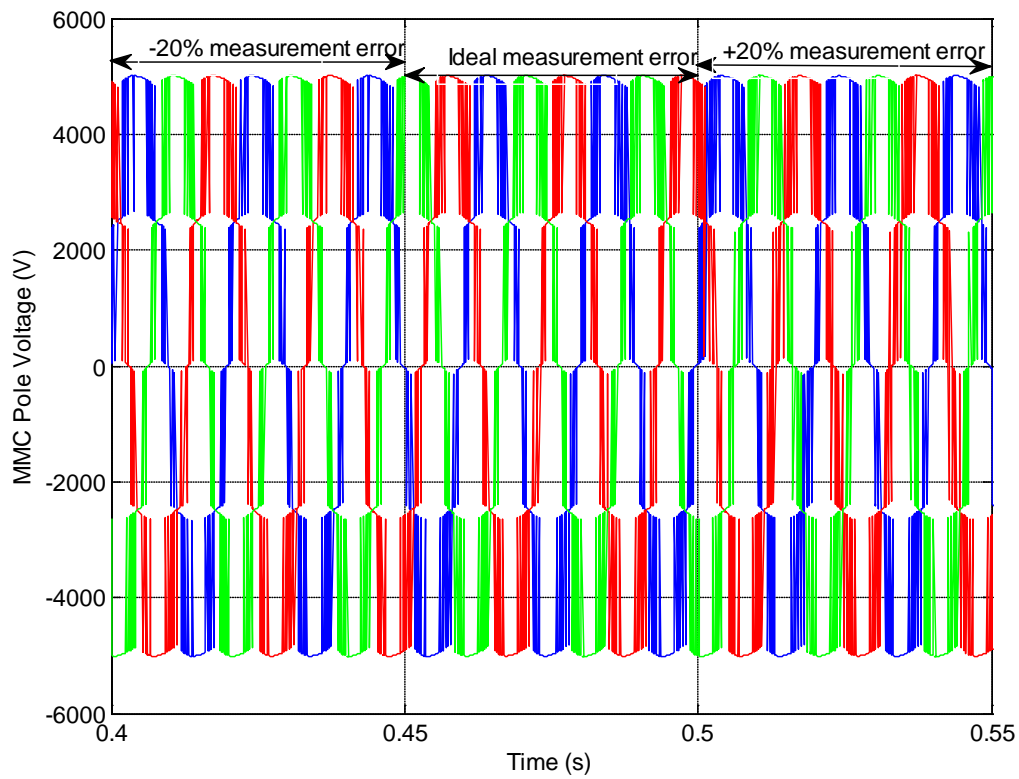
Fig.5.42 The MMC pole voltages when measurement errors are present in load parameters
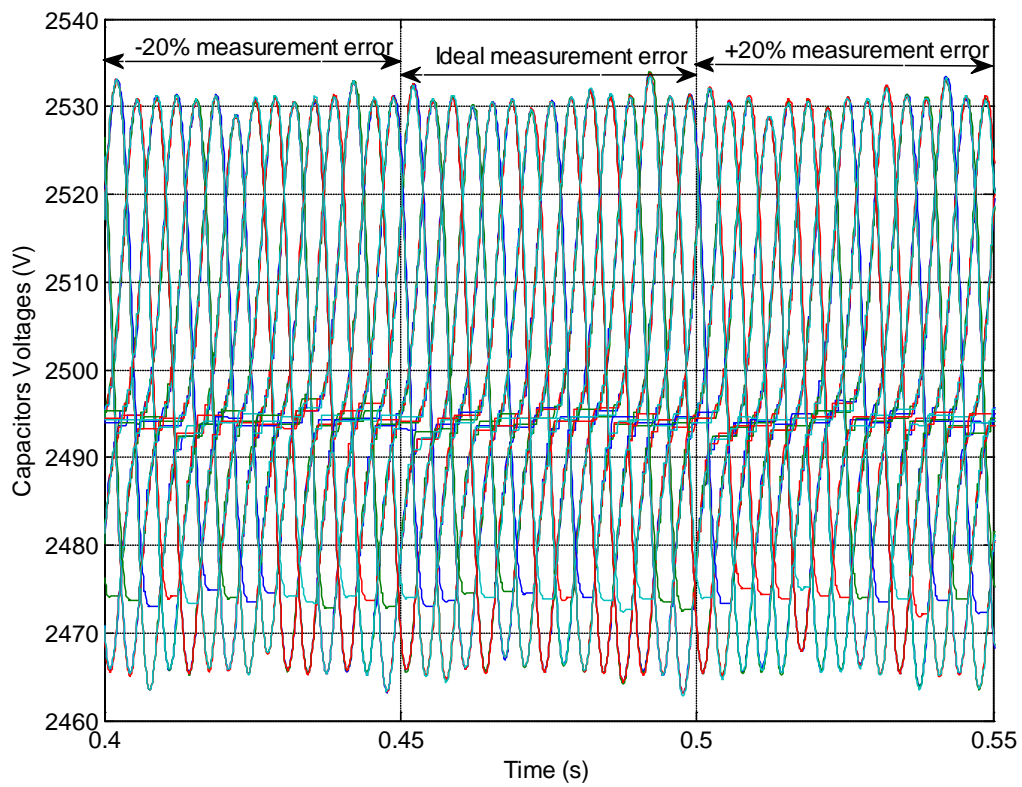

Fig.5.43 The capacitors voltages when measurement errors are present in load parameters

5.5.4 Dynamic performance verification

In this section, the dynamic performance of the FCS-MPC controller is investigated by applying two separate step changes to the dc source and load voltages. In addition, the ¬20% measurement error in load parameters (R and L) has been considered in all the further simulations. The system behavior will be observed specially in transient time duration up to reaching the steady state.

5.5.4.1 Disturbance to DC source voltage

As the MMC can be used in HVDC systems, change in dc line voltage is likely to happen and the controller should be able to provide a smooth and fast transition time to protect the equipment and feed the load properly. Consequently, in this part a +5% step change is applied to the dc source at t=1s (10kV to 10.5kV). The simulation has been done for 2sec.

The most visible change must be seen in capacitor voltages because their reference value is directly dependent to V_{dc}. Fig.5.44 illustrates the capacitor voltages in the transient time. The steady state has been reached after 0.15sec.
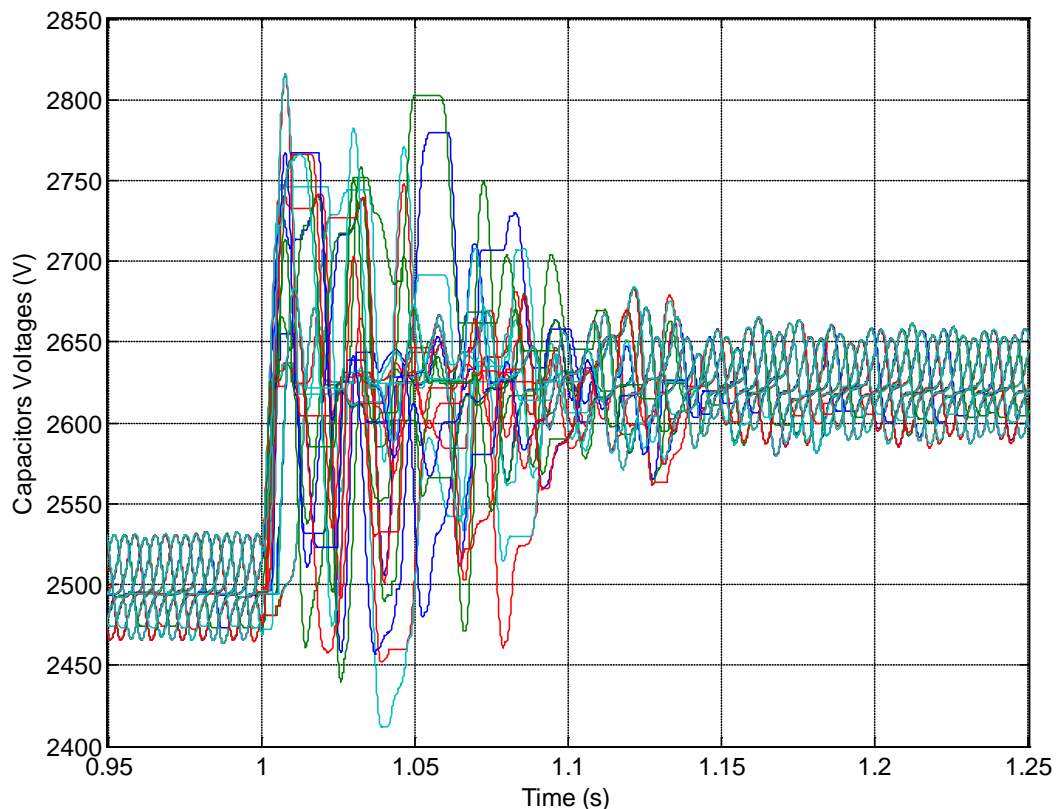

Fig.5.44 The capacitors voltages when the dc voltage source increases 5% at t=1s

The balancing voltage changes from 2500V (=10000/4) to 2625V (=10500/4) as expected. The maximum and minimum values of capacitors voltages in the transient time are 2.8kV and 2.4kV respectively. Therefore, the overvoltage across the capacitors is 300 V in the worst case and the capacitors should be able to tolerate the voltage increase in a short time. In addition, the peak-to-peak value remains almost constant (70V) because the arm currents and the sampling frequency have not been changed.

The load currents have been illustrated in Fig.5.45. As the reference current signals remain constant during the disturbance, there is no change in the load current amplitudes, while the current ripple has slightly increased. This change can be explained by the weighting factors in the cost function. It seems that new weighting factors that are slightly different from current values should be selected to have the ideal performance of the controller.
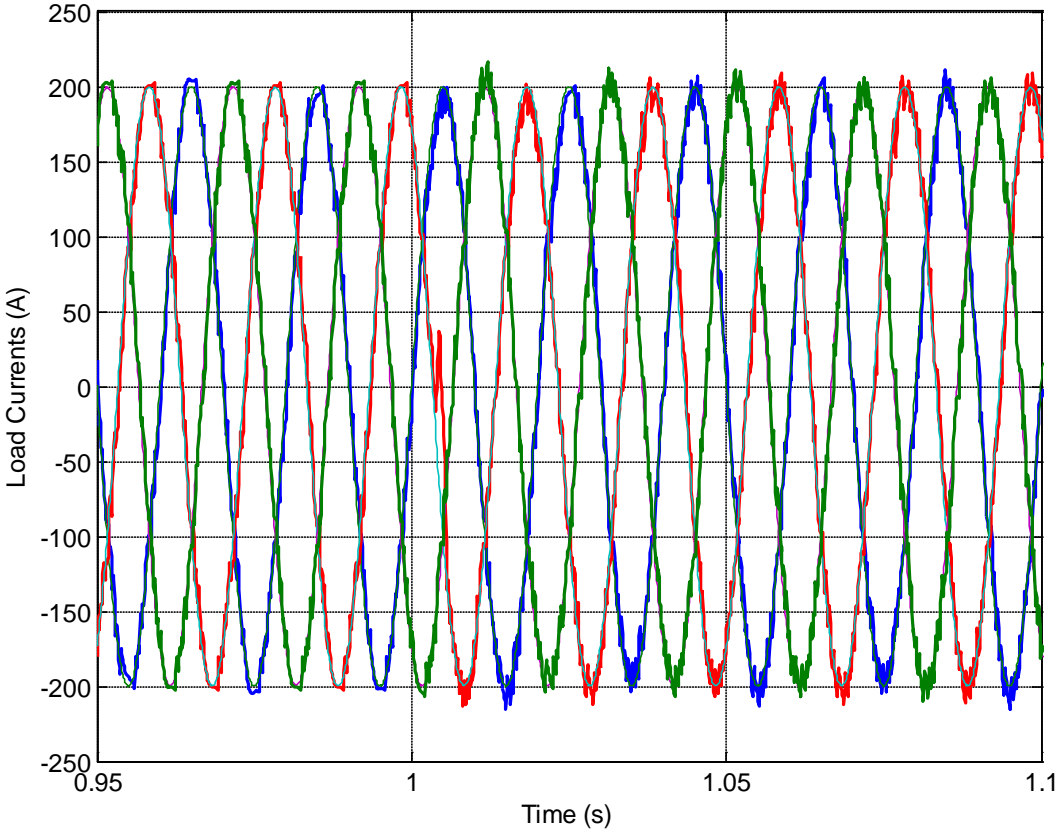

Fig.5.45 The load currents when the dc voltage source increases 5% at t=1 s

The MMC terminal (pole) voltages are the last interesting waveforms in this section. As the dc source value has been changed, the maximum and minimum values ($\pm \frac{V_{dc}}{2}$) will be

71

changed as well as the voltage steps ($\frac{V_{dc}}{4}$) and these changes can be observed from the Fig.5.46.
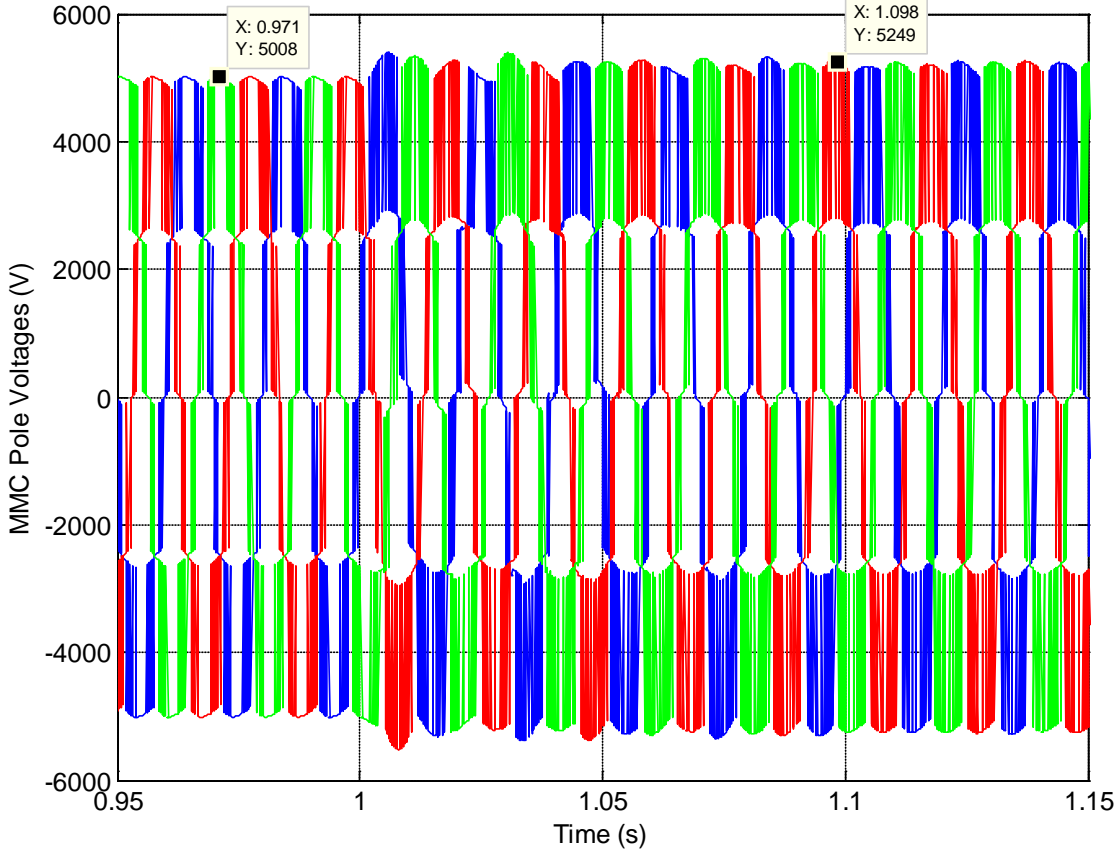
Fig.5.46 The MMC pole voltages when the dc voltage source increases 5% at t=1s

By considering all the above figures, it seems that the designed FCS-MPC controller is able to manage the dc source disturbances if they are in an acceptable range. However, in the case of large changes in dc source voltage level some problems may happen such as excessive arm currents and capacitors voltages. In addition, the weighting factors of the cost function have been selected for MMC normal operation with 10kV as dc source; therefore, they can be inappropriate for the other operating modes very far from the nominal one.

5.5.4.2 Disturbance to load ac source voltage

In this section, the dynamic performance of the controller is verified by applying a step change to the load voltage sources (e_j). In order to do so, they are reduce by 30% at t=1s. The measurement error (¬20%) has also been considered. The other parameters remain the same as before and the simulation has been done for 2sec.

Figures 5.47 and 5.48 show the load currents and pole voltages in the transient time after the step change.
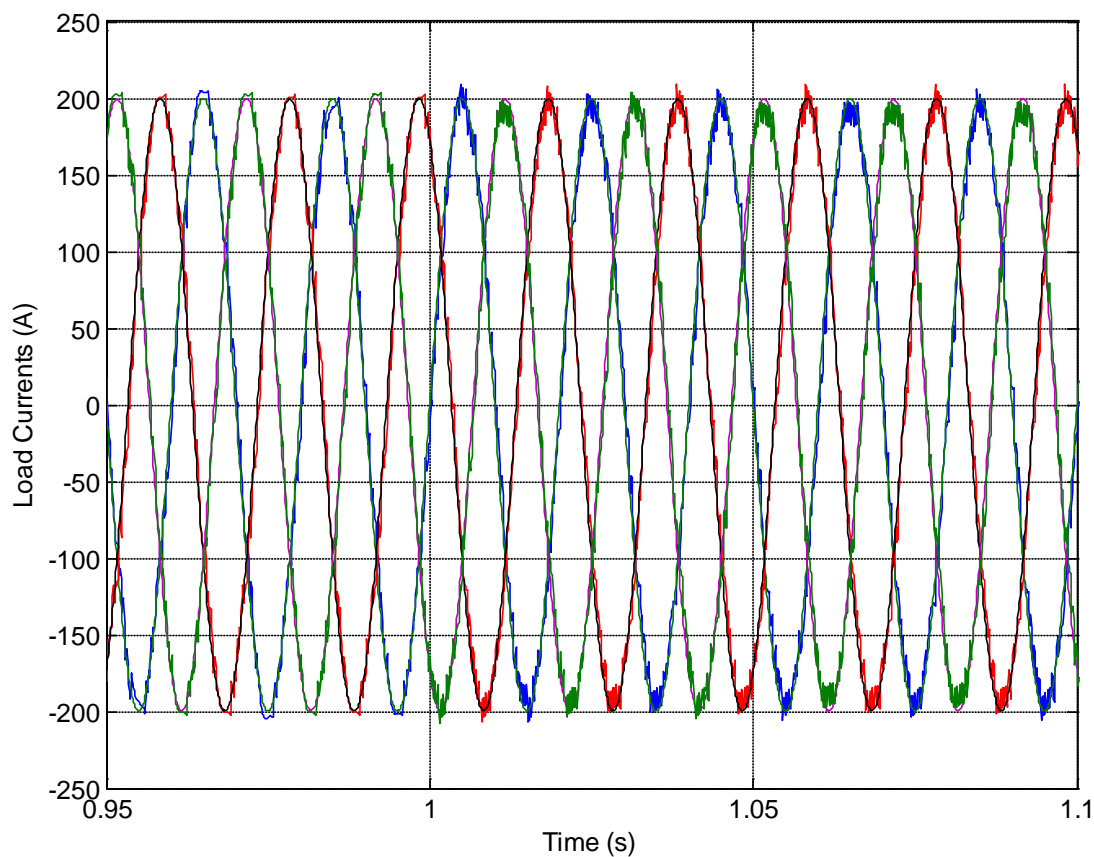
Fig.5.47 The load currents when the load voltage source decreases 30% at t=1s

The load currents have followed their references and no considerable change in their amplitude can be detected. However, it seems that the current ripple has increased after the step change. Again in this case the reason can be explained by the cost function and its weighting factors, because they have been set for the nominal operating mode and they may not be ideally adjusted for the other situations.

Fig.5.48 The pole voltages when the load voltage source decreases 30% at t=1s

The dc source is constant; therefore, the maximum and minimum values of the terminal voltage remain the same as before as wel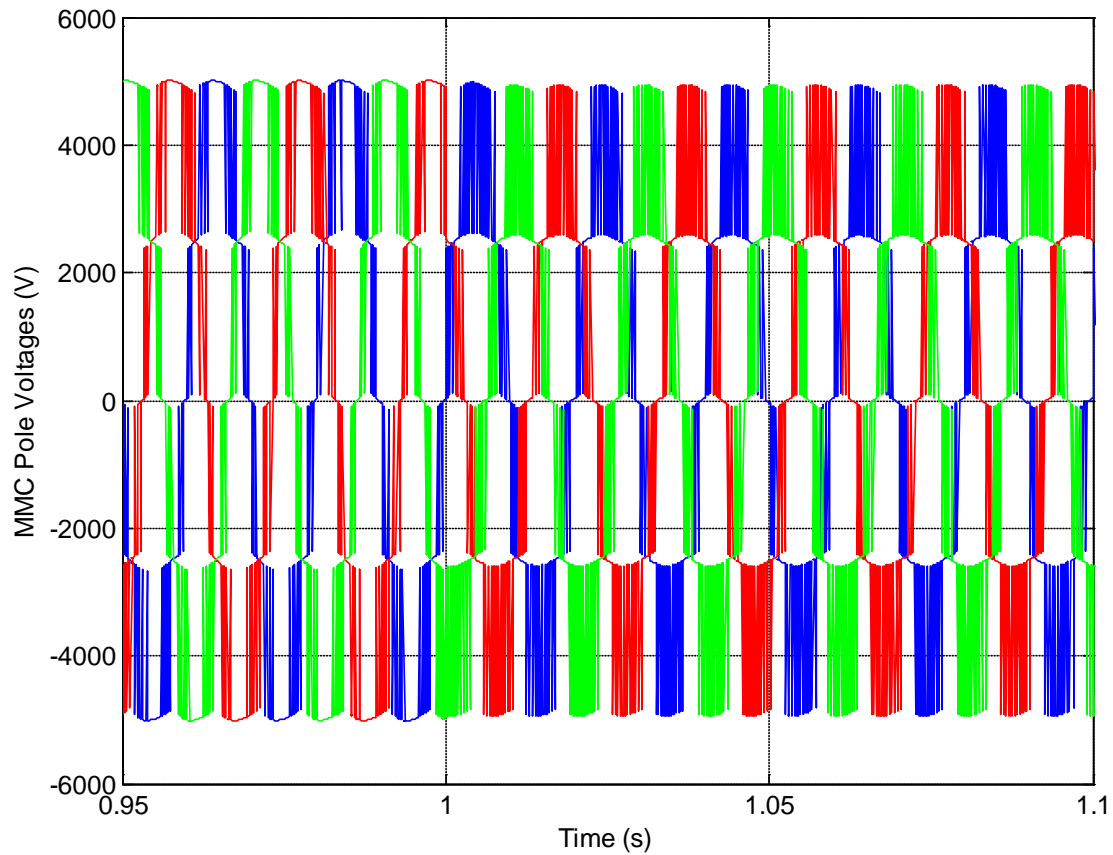l as the voltage steps (2.5kV). In addition, the load currents have followed their references as before. The main component (50Hz) of pole voltages is reduced by almost 30% as a result of a 30% reduction in e_j. The next figure is the frequency spectrum of phase-a terminal voltage before and after the disturbance.

Fig.5.50 shows the capacitors voltages. It can be seen that the transition time is very short and no overshoot or undershoot occurs in this time. In addition, the new steady states values of capacitor voltages have been built around 2.5kV that is the same as before, because it only depends on the dc voltage. Therefore, the controller is able to keep the capacitors voltages smoothly.
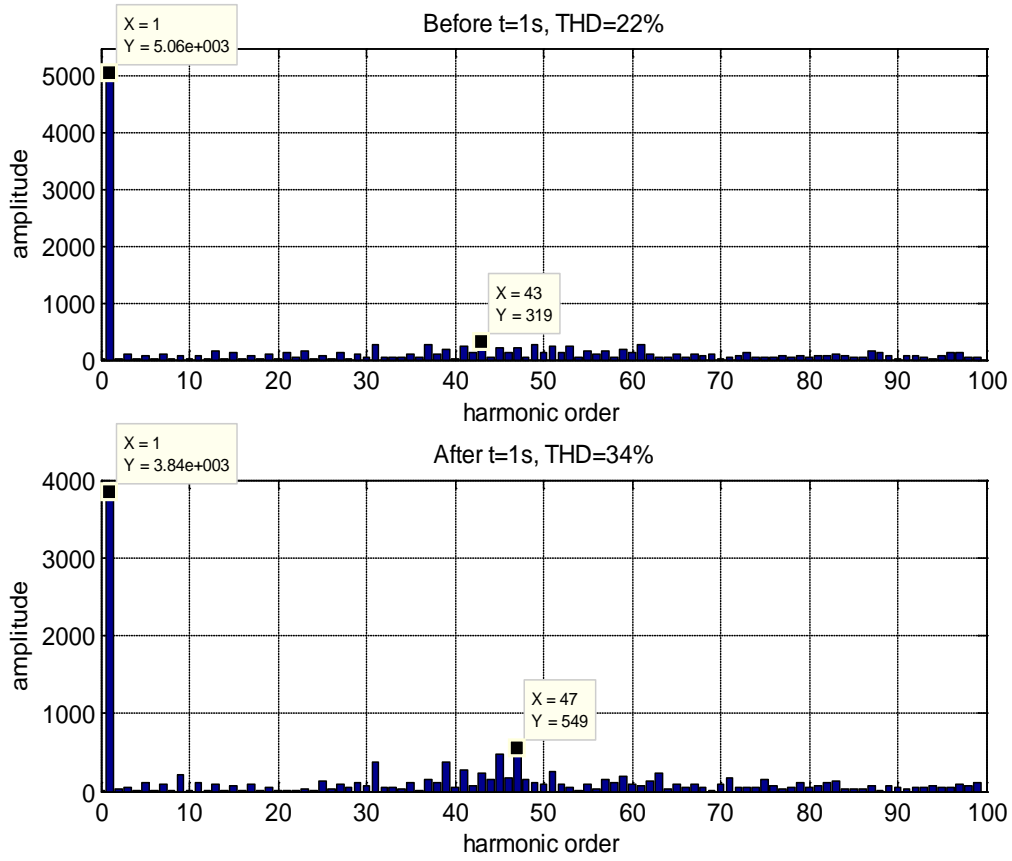
Fig.5.49 The frequency spectrum of phase-a terminal voltage before and after t=1s
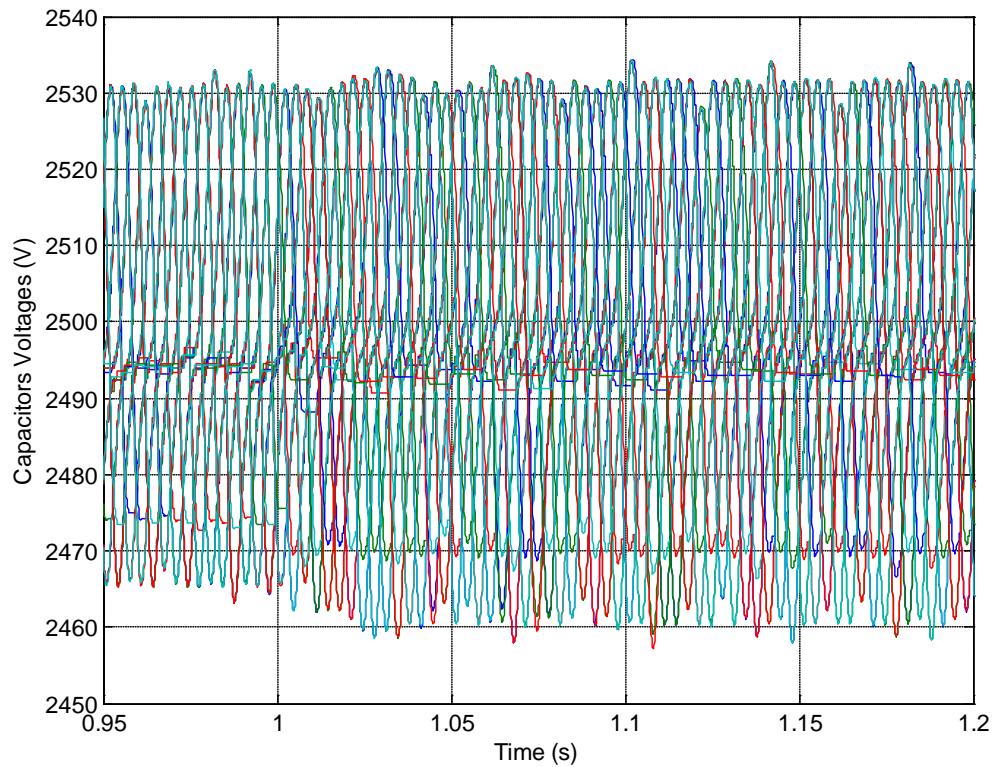

Fig.5.50 The capacitors voltages when the load voltage source decreases 30% at t=1s

75

Chapter 6

Conclusion and future work suggestions

The aim of this study was to verify the applicability of one of Model Predictive Control (MPC) strategies, called Finite Control Set-MPC, to power converters. This goal has been fulfilled by applying this powerful method to control voltage source inverter and modular multilevel converter topologies as two samples. The presented simulation results in chapter 3 and chapter 5 are very good and evident proofs. In this chapter, the overall conclusion will be given and finally a few ideas will be offered for further work on this topic.

6.1 Conclusion

This control method is simple and is able to control different converter topologies and various kinds of variables without the need of additional modulation techniques or internal cascade control loops. FCS-MPC is conceptually very simple yet powerful, since it takes the advantage of the discrete nature of power converters and microprocessors in order to reduce the amount of calculations.

One of the major advantages of this control strategy and probably the greatest distinction with traditional control methods is the flexibility to control different variables as well as system constraints simultaneously. The result of this property would be the increase of controller speed and efficiency. However, some disadvantages have to be mentioned like the larger number of calculations compared to classical controllers. When the system is complicated and there is a large number of switching states, like MMC, high computational power is required to evaluate the cost function at each sampling time. Furthermore, the effectiveness of the control scheme depends not only on the accuracy of the system model, but also to the defined cost function and weighting factors.

In chapter 3, the proposed FCS-MPC controller for VSI topology is successful in forcing the load currents to track their sinusoidal references with small ripple. In addition, all the

discretization methods: forward, backward and midpoint Euler methods have been tested to compare the results. According to the simulation results, it can be concluded that all of them provide acceptable results, while the midpoint Euler provides higher accuracy (less current ripple) and the output currents and terminal voltages have lower harmonics than the other two methods. Hence, it can be the best choice for discretizing the system model. However, the switching frequency is higher in the case of using midpoint Euler which is a disadvantage and leads to higher switching loss.

The main investigation of FCS-MPC method has been performed in chapter 5, where it has been designed for MMC topology which is very complicated than VSI. The load currents have been chosen to be the main controlled variables due to the calculated system model. Moreover, there are two control requirements regarding the MMC operating principles that should be considered: keeping the capacitors voltages balanced around the nominal value and minimizing the circulating currents. The cost function definition has been done based on all these factors by proper weighting factors. According to the simulation results, the FCS-MPC is capable of forcing the load currents to follow their references almost regardless of their shape. In addition, the capacitors voltages can be kept in order and the circulating currents can be minimized only if suitable weighting factors are chosen. Controlling the circulating currents is necessary and it leads to reducing power switches ratings and loss. The performance of the controller is acceptable not only in steady state but also during disturbances. It reacts to system disturbances very fast and keeps the currents and voltages in an acceptable range. The new steady state will be reached accurately and successfully in less than 0.5 sec.

Again in this case, all the Euler discretization methods have been tested to find the best. The controller has good and acceptable performance only with midpoint Euler method in contrast with VSI example. It seems that due to the complexity of the MMC system model, the accuracy of the discretization method plays more important role than the simple example of VSI.

The robustness of the proposed FCS-MPC has been checked by considering ±20% uncertainty to the load parameters measurement. No considerable change has been detected in the system performance; consequently, the proposed FCS-MPC can be counted as a very robust control strategy.

It is reasonable that the increase of sampling frequency will increase the accuracy of prediction and it can improve the performance of the controller. For example, the output current ripple will be reduced and its THD will increase. However, switching frequency is dependent on sampling frequency and the increase of sampling frequency will lead to switching frequency increase which is a disadvantage. Therefore, optimization is the best solution to reach the most appropriate sampling frequency.

6.2 Suggestions for future work

Although the results presented here have demonstrated the effectiveness of the FCS-MPC control strategy for power converters, it could be further developed in a number of ways:

- Implementation of the proposed controller in VSI and MMC topologies and working on the practical challenges that have been ignored in the simulations such as the delay of switches when they are turning on and off.
- Weighting factors values should be able to set dynamically by the controller in order to achieve an optimization in the controller performance in all the situations.
- In this study, the main focus is on the FCS-MPC operating principles and all the reference currents are fixed and there is no dynamic control on them, while an external controller can be designed in order to set the references by for example the use of active and reactive power transfer.
- This powerful control strategy can be applied to the other types of power converters.

References

[1] *Predictive Control in Power Electronics Converters*, Specialization Project, Razieh Nejati Fard, January 2013.

[2] *http://en.wikipedia.org/wiki/Euler_method*

[3] *Predictive Control of Power Converters and Electrical Drives*, First Edition. Jose Rodriguez and Patricio Cortes, 2012 John Wiley & Sons, Ltd.

[4] P. Cortes, M. P. Kazmierkowski, R. M. Kennel, D. E. Quevedo, J. Rodriguez, "Predictive Control of in Power Electronics and Drives", IEEE Transactions on Industrial Electronics, Vol. 55, No. 12, pp. 4312-4324, December 2008.

[5] M.A. Perez, E. Fuentes, and J. Rodríguez, "Predictive current control of ac-ac modular multilevel converters," in Proc. IEEE International Conference on Industrial Technology (ICIT), 14-17 March 2010, Valparaíso, Chile, pp. 1289-1294.

[6] *http://en.wikipedia.org/wiki/Backward_Euler_method*

[7] J. Rodriguez, J. Cortes, R. M. Kennel, M. P. Kazmierkowski, "Model predictive control- a simple and powerful method," IEEE Power Electronics and Motion Control Conference, Chile, 2009.

[8] P. Cortes , J. Rodriguez , R. Vargas and U. Ammann "Cost function-based predictive control for power converters", Proc. 32nd Annu. IEEE IECON, pp.2268 -2273, 2006.

[9] P. Antoniewicz , M. P. Kazmierkowski , P. Cortes , J. Rodriguez and A. Sikorski "Predictive direct power control algorithm for three phase AC/DC converter", Proc. IEEE EUROCON Conf., pp.1530 -1534, 2007.

[10] P. Cortes , J. Rodriguez , D. E. Quevedo and C. Silva "Predictive current control strategy with imposed load current spectrum", IEEE Trans. Power Electron., vol. 23, no. 2, pp.612 -618, 2008.

[11] J. Rodriguez , J. Pontt , P. Correa , P. Lezana and P. Cortes "Predictive power control of an AC/DC/AC converter", Conf. Rec. 40th IEEE IAS Annu. Meeting, vol. 2, pp.934 -939, 2005.

[12] Q. Jiangchao, M. Saeedifard, "Predictive Control of a Three-Phase DC-AC Modular Multilevel Converter", IEEE Energy Conversion Congress and Exposition (ECCE), USA, 2012.

[13] Q. Jiangchao, M. Saeedifard, "Predictive Control of a Modular Multilevel Converter for a Back-to-Back HVDC System", IEEE Transactions on Power Delivery, Vol. 27, No. 3, July 2012, pp. 1538-1547.

[14] *http://en.wikipedia.org/wiki/Midpoint_method*

[15] P. Cortes , S. Kouro , B. La Rocca , R. Vargas , J. Rodriguez , J. Leon , S. Vazquez and L. Franquelo "Guidelines for weighting factors design in model predictive control of power converters and drives", Proc. IEEE Int. Conf. Ind. Technol., pp.1 -7, 2009.

[16] http://en.wikipedia.org/wiki/Total_harmonic_distortion

[17] http://en.wikipedia.org/wiki/Nyquist_frequency

[18] A. Lesnicar and R. Marquardt "An innovative modular multilevel converter topology suitable for a wide power range", Proc. IEEE Bologna PowerTech Conf., pp.1 -6, 2003.

[19] S. Allebrod, R. Hamerski, and R. Marquardt, "New transformerless, scalable modular multilevel converters for HVDC-transmission," in Conf. Rec. IEEE PESC 2008, pp. 174-179.

[20] B. Chuco, E. H. Watanabe, "Back-to-Back HVDC Based on Modular Multilevel Converter", Brazilain Power Electronics Conference (COBEP), 2011 Brazilian, Brazil, 2011.

[21] A. Das, H. Nademi, L. Norum, , "A Method for Charging and Discharging Capacitors in Modular Multilevel Converter," Annual Conference on IEEE Industrial Electronics Society, Australia, 2011.

[22] Rohner, S.; Bernet, S.; Hiller, M.; Sommer, R.; Analysis and Simulation of a 6 kV, 6MVA Modular Multilevel Converter. Industrial Electronics, 2009. IECON '09. 35th Annual Conference of IEEE. 2009, Page(s): 225-230..

[23] M. Saeedifard and R. Iravani "Dynamic performance of a modular multilevel back-to-back HVDC system", IEEE Trans. Power Del., vol. 25, no. 4, pp.2903 -2912, 2010.